

Protein engineering of a sulfotransferase and a monooxygenase for the synthesis of high-value chemicals

Von der Fakultät für Mathematik, Informatik und Naturwissenschaften der RWTH Aachen University zur Erlangung des akademischen Grades einer Doktorin der Naturwissenschaften genehmigte Dissertation

vorgelegt von

Yu Ji

M. Sc. Chemistry

aus

Yangzhou, Jiangsu, P.R. China

Berichter: Univ. -Prof. Dr. rer. nat. Ulrich Schwaneberg

Univ. -Prof. Dr. rer. nat. Lothar Elling

Tag der mündlichen Prüfung: 28.04.2020

Diese Dissertation ist auf den Internetseiten der Universitätsbibliothek verfügbar.

Contents

Publications	IV
Abstract.....	V
1 General introduction	1
1.1 Biocatalysis	1
1.2 Enzyme classes and industrial relevant enzymes	2
1.3 Protein engineering.....	4
1.3.1 Directed evolution	4
1.3.2 KnowVolution	7
1.4 Thesis Objectives.....	9
2 Engineering of aryl sulfotransferase B for application in catechol sulfation	11
2.1 Declaration	11
2.2 State of the art.....	11
2.2.1 Sulfation	11
2.2.2 Function of sulfation.....	12
2.2.3 Chemical sulfation.....	12
2.2.4 Enzymatic sulfation.....	13
2.2.5 Catechols and catechol sulfates	15
2.2.6 Strategies in protein engineering	16
2.2.7 Screening assays for evolution of aryl sulfotransferase.....	17
2.2.8 Objective.....	17
2.3 Material and Methods.....	19
2.3.1 Chemicals and reagents	19
2.3.2 Vectors and strains	19
2.3.3 Generation of an ASTB SeSaM (Sequence Saturation Mutagenesis) library	20
2.3.4 Generation of ASTB OmniChange library	20
2.3.5 Development of <i>p</i> -NPS-4-AAP screening system in 96-well microtiter plates (MTPs).....	21
2.3.6 Expression and purification of ASTB-WT and ASTB variants in flasks	22
2.3.7 Characterization of ASTB-WT and ASTB variants	23
2.3.8 Long-term conversion by ASTB-WT and ASTB variants	23
2.3.9 Product separation by high-performance liquid chromatography-mass spectrometry (HPLC-MS)	23
2.3.10 Nuclear magnetic resonance (NMR) spectroscopy	24
2.3.11 Molecular modeling.....	24
2.4 Results	26
2.4.1 Selection of an aryl sulfotransferase for phenol compounds sulfation.....	26

2.4.2 Selectivity study of aryl sulfotransferase ASTB for catechol sulfation	28
2.4.3 Development of <i>p</i> -NPS-4-AAP screening system	30
2.4.4 Validation of the <i>p</i> -NPS-4-AAP screening system in one round of directed ASTB evolution	34
2.4.5 KnowVolution campaign towards catechols.....	39
2.4.6 Expanding substrate scope	50
2.4.7 Recombination of potential beneficial positions close to catalytic site H350.....	53
2.5 Discussion.....	55
2.6 Conclusion	59
3 Engineering of P450 BM3 toward hydroxylation of surfactant	61
3.1 Declaration.....	61
3.2 State of the art	61
3.2.1 Surfactants.....	61
3.2.2 Cytochrome P450 monooxygenase in biocatalysis.....	63
3.2.3 Protein engineering of P450 BM3.....	65
3.2.4 Objectives	66
3.3 Material and Methods	67
3.3.1 Chemicals and reagents.....	67
3.3.2 OmniChange library generation.....	67
3.3.3 Screening of OmniChange library	69
3.3.4 Long-term conversion in presence of a cofactor regeneration system.....	70
3.3.5 HPLC-MS/MS analysis.....	71
3.3.6 NMR measurement	72
3.3.7 Protein purification of P450 BM3 variants	72
3.3.8 Kinetic Characterization of P450 BM3 variants	73
3.3.9 Surface contact angle measurements	73
3.4 Result and discussion.....	75
3.4.1 OmniChange library generation and diversity estimation.....	75
3.4.2 P450 BM3 variants for CTAB hydroxylation through screening of OmniChange library	77
3.4.3 Product identification of CTAB hydroxylation.....	79
3.4.4 Kinetic characterization of improved enzyme variants.....	81
3.4.5 Surface contact angle measurements	83
3.5 Conclusions.....	83
4 Summary and conclusion	85
5 Appendix.....	88
5.1 List of abbreviations	88
5.2 List of DNA and protein sequences	90

5.3 List of Figures.....	95
5.4 List of Tables.....	97
6 References	98
7 Declaration / Eidesstattliche Erklärung.....	113
8 Author contributions	114
9 Acknowledgement	116
10 Curriculum vitae	118

Publications

Ji, Y., Mertens, A. M., Gertler, C., Fekiri, S., Keser, M., Sauer, D. F., Smith, K. E. C., Schwaneberg, U. (2018). Directed OmniChange evolution converts P450 BM3 into an alkyltrimethylammonium hydroxylase. *Chemistry—A European Journal*, 24(63), 16865-16872.

Ji, Y., Islam, S., Mertens, A. M., Sauer, D. F., Dhoke, G. V., Jakob, F., Schwaneberg, U. (2019). Directed aryl sulfotransferase evolution toward improved sulfation stoichiometry on the example of catechols. *Applied microbiology and biotechnology*, 103(9), 3761-3771.

Ji, Y., Islam, S., Cui, H., Dhoke, G. V., Davari, M. D., Mertens, A. M., Schwaneberg, U. (2020). Loop engineering of aryl sulfotransferase B for improving catalytic performance in regioselective sulfation. *Catalysis Science & Technology*, 10, 2369-2377.

Ji, Y. #, Islam, S. #, Schwaneberg, U. (2020). Regioselective O-Sulfation of high value chemicals by a reengineered aryl sulfotransferase. (#shared first authorship) In preparation.

Ji, Y. #, Cui, H. #, Islam, S., Davari, M. D., Schwaneberg, U. (2020). Stability-guided local region engineering of an aryl sulfotransferase for improving sulfation activity. (#shared first authorship) In preparation.

Contributions to other publications:

Pan, J., **Ji, Y.**, Du, Z., Zhang, J. (2016). Rapid characterization of commercial polysorbate 80 by ultra-high performance supercritical fluid chromatography combined with quadrupole time-of-flight mass spectrometry. *Journal of Chromatography A*, 1465, 190-196. (Not included in thesis)

Wu, X. #, Lin, Y. #, **Ji, Y.**, Zhou, D., Liu, Z., Sun, X. (2020). Insights into the Catalytic Mechanism of Fe-doped LiCoPO₄ for oxygen evolution reaction. *ACS Applied Energy Materials*, 3, 2959-2965. (#shared first authorship) (Not included in thesis)

Zou, Z., **Ji, Y.**, Mate, D. M., Herbst, L. M., Jakob, F., Schwaneberg, U. (2020). Improved thermo-stable sortase A for efficient site-specific protein labeling in flow-based batches. In preparation. (Not included in thesis)

Abstract

The push for sustainability (less waste and less resource use) is a global issue related to environmental, economic, and social concerns. Enzymes as biodegradable catalysts play an important role in the development of sustainable technologies. Enzymatic catalysis, a safer process compared to chemical catalysis occurs usually with high catalytic efficiency and specificity under mild reaction conditions using less hazardous and less toxic chemicals. In this thesis, two different classes of enzymes (transferases and oxidoreductases) were engineered for the detoxification of phenolic compounds and production of biodegradable surfactants, respectively.

Catechols (extensively used in the chemical industry) are abundantly found in the environment and cause human health problems, e.g., vasoconstriction, renal tube degeneration, liver malfunction, and neurodegeneration. Sulfation is an important way for detoxification of xenobiotics and endobiotics including catechols. Metabolites such as catechol sulfates act in our body as important antioxidants and often have anti-inflammatory properties. Moreover, they are used as biomarkers to monitor diseases such as Parkinson's disease, cardiovascular diseases, urinary tract infections, candidemia, and various forms of cancer. Because of their high biological relevance, there is an increasing interest in the synthesis of catechol sulfates. Enzymatic conversion of catechols using aryl sulfotransferase is a synthetically attractive, environmentally-friendly, and sustainable route for regio-/chemoselective sulfation of catechols.

A two-step *p*-NPS-4-AAP screening system for laboratory evolution of aryl sulfotransferase B (ASTB) was developed in 96-well microtiter plates to improve the sulfate transfer efficiency toward catechols. Optimization yielded a coefficient of variation below 15 % for the *p*-NPS-4-AAP screening system. The validation of the established screening system was accomplished by directed aryl sulfotransferase evolution toward 3-chlorocatechol, which yielded the beneficial variant ASTB-M5 (V430A) and showed up to 2.4-fold increased turnover number and a significantly improved sulfate stoichiometry of ASTB-M5 (from 29 % to 58 %). The reengineering of loop12 and loop13 of aryl sulfotransferase B (ASTB) was performed in order to improve the sulfate transfer efficiency of six catechols. The obtained ASTB variants were generated in a KnowVolution campaign using the random mutagenesis method SeSaM and the multi-site saturation method OmniChange. The catalytic activity (k_{cat}) and catalytic efficiency (k_{cat}/K_M) of the final variant ASTB-OM2 (Q191Y/Y218W/L225V) were improved for all six investigated

catechols when compared to ASTB-WT (e.g., 13.6-fold improvement of k_{cat} for 3-bromocatechol). HPLC-MS analysis confirmed the improved sulfate stoichiometry of ASTB-OM2 with a transfer efficiency of up to 94 % for 3-methylcatechol in comparison to 24 % for ASTB-WT. A molecular understanding of the improved sulfation activity of ASTB-OM2 was achieved through molecular docking studies and electron effects of catechol substituents were analyzed by the Hammett plot. The final variant ASTB-OM2 was also applied for the sulfation of important pharmaceutical compounds.

Cetyl-trimethylammonium bromide (CTAB) is a widely used cationic surfactant in nature. Apart from compound expenses, the key parameters for usage of cationic surfactants in the industry are biodegradability and surfactant solubility. CTAB biodegradation requires hydroxylation in the first step, which is rate-limiting and crucial for solubility in water. Nowadays bolaform surfactants (such as hydroxylated CTAB), consist of two hydrophilic groups that are separated by a hydrophobic spacer chain, attracted the interest of industry and academia due to their reduced micelle size and excellent solubilization properties. Enzymatic hydroxylation of CTAB by monooxygenase P450 BM3 is a sustainable route for biodegradable bolaform surfactant hydroxylated CTAB synthesis.

The OmniChange multi-site mutagenesis method was applied to reengineer the P450 BM3 substrate specificity toward the hydroxylation of CTAB by simultaneous mutagenesis of four previously reported positions (R47, Y51, F87, and L188). In total, 1740 clones from the P450 BM3 OmniChange library were screened with the NADPH depletion assay and H_2O_2 detection assay. Several improved P450 BM3 variants were identified and finally, four were kinetically characterized with respect to CTAB hydroxylation based on both performance and coupling efficiency. The P450 BM3 variant P3A8 (R47E/Y51M/F87V/L188E) displayed an initial activity ($64.9 \pm 4.8 \text{ s}^{-1}$, 13.5-fold increased activity compared to wild-type P450 BM3) which is in the range of the specific activity for its natural fatty acid substrate (palmitic acid, $32\text{-}122 \text{ s}^{-1}$) and it showed high coupling efficiency (92.5 %), while wild-type P450 BM3 displayed a very low coupling efficiency (0.5 %). HPLC-MS/MS detection confirmed that P3A8 and P2E7 (R47D/Y51L/F87V/L188A) form 13 and 35 times more 2-hydroxylated CTAB than P450 BM3. In addition, di-hydroxylated CTAB products were detected for all four investigated P450 BM3 variants (up to a yield of 77 %; P3A8).

1 General introduction

1.1 Biocatalysis

Biocatalysis generally refers to the use of enzymes (isolated form or whole-cell format) as catalysts to convert a molecular substrate into a product by decreasing the Gibbs free-energy (ΔG) activation^[1, 2]. Enzymes are proteins which can perform biochemical reactions with high regio-/stereoselectivity under the mild conditions (physiological pH, ambient temperature and pressure) and they have been naturally evolved to perform physiological task to support various forms of life.

The use of enzymes has been seen for thousands of years for the production of food and beverage including bread, cheese, beer, and wine^[3]. The first example of modern biocatalysis was reported by Louis Pasteur in 1858 using microorganism *Penicillium glaucum* for the kinetic resolution of racemic tartaric acid through fermentation^[1, 4]. Afterwards, Buchner proved that cell-free extract instead of living yeast could degrade glucose to ethanol^[5]. Until the late 20th century, the blossom of applications in biocatalysis appeared with the development of DNA technology and high throughput DNA sequencing which allows the recombination of microorganisms and offers enzymes with higher purity and low cost^[3]. In 1984, Zaks demonstrated that lipases have enhanced thermostability in organic solvent instead of water which starting the enzymatic organic synthesis^[6]. As an environmentally friendly (enzymes as nonhazardous and nontoxic substances are produced from renewable resources and are biodegradable) and highly selective technology, the use of biocatalysis has expanded significantly over the last 20 years on chemical synthesis industry, including pharmaceuticals^[7], fine chemicals^[8], food^[9], flavors^[10], leather^[11], textile^[12], and paper production^[3, 13].

The processes of biocatalysis can be classified into three types: resting whole-cell biocatalysis, isolated-enzyme biocatalysis, and immobilized-enzyme biocatalysis^[14, 15]. The resting whole-cell biocatalysis separates the production of biocatalyst step and conversion step in order to replace the fermentation media to suitable reaction media and adjust the cell concentration for efficient conversion^[15]. This process is normally used for synthetic reactions that require cofactors regeneration^[16]. The second type (isolated-enzyme biocatalysis) is designed to avoid substrate diffusional limitations into cells which is beneficial to non-natural substrates and typically used for hydrolytic or isomerization reactions^[16, 17]. As enzyme stabilization under process conditions is an important issue in biocatalysis, immobilized-enzyme biocatalysis is developed (e.g. using anchor peptide for

enzyme immobilization^[18]) and it also brings the benefits for cost-effective enzyme recycling^[19, 20].

Normally enzyme molecules are much larger than substrate molecules and substrate only interacts with a small portion (active site) of enzymes to undergo catalysis. To explain the mechanism of enzyme catalysis, lots of hypotheses were proposed since 1894, including the “key-lock” model from Fisher^[21], “induced fit” theory from Koshland^[22, 23], and “Monod-Wyman-Changeux” proposal^[24]. The “key-lock” theory proposed that the active site has a special geometric shape that is complementary to the geometric shape of the substrate molecule^[21]. The “induced fit” theory assumed that the substrate induces a change in the three-dimensional relationship of the amino acids at the active site which will orient the catalytic groups for the subsequent reaction^[23]. The “Monod-Wyman-Changeux” model supposed that ligand binding causing tertiary changes of proteins that are complementary to ligand structures and multiple conformational states of proteins, including stable “intermediate” will occur^[24, 25]. Numerous computational methods have also been explored to understand the physical basis of the rate acceleration of chemical reactions by enzymes^[26]. In recent years, the advances in techniques have experimental supported the conformational selection scheme of signal transduction which is according to the “Monod-Wyman-Changeux” model^[27].

1.2 Enzyme classes and industrial relevant enzymes

Enzymes are classified into six families according to the type of chemical reaction mechanism by the Nomenclature Committee of the International Union of Biochemistry and Molecular Biology (IUBMB), including oxidoreductases, transferases, hydrolases, lyases, isomerases, and ligases (**Figure 1**)^[28].

(1) Oxidoreductases

Oxidoreductases (e.g. catalases, glycoside oxidases, and laccases) catalyze reactions in which a substrate donates one or more electrons to an electron acceptor, becoming oxidized in the process^[28, 29]. Glucose oxidase (GOx, isolated from *Aspergillus niger*) catalyzes the oxidation of D-glucose to D-gluconolactone with the production of hydrogen peroxide which can be used as anti-bacterial agent for food preservation^[30]. The Bayer-Villiger monooxygenase (BVMO) CDX-003 was used for industrial-scale stereo-selective enzymatic oxidation for the conversion of pyrimetazole to esomeprazole^[31]. Lonza developed a biological oxidation method for the enzymatic oxidation of methyl groups on

aromatic heterocycles^[32]. Turner group developed a process for the industrial production of chiral amines by amonoamine oxidase and commercialized by Ingenza^[33].

(2) Transferases

Transferases (e.g. fructosyltransferases, glucosyltransferases, and sulfotransferases) catalyze reactions in which a chemical group is transferred from a donor substrate to an acceptor substrate^[28, 29]. Transaminases (a homolog of an enzyme from *Arthrobacter sp.*) are used for the synthesis of the chiral amines (e.g. sitagliptin)^[34]. Transglutaminase (isolated from *Streptoverticillium sp.*) forms crosslinks between protein molecules and is widely used in the food industry (especially for noodle production) as texturing agent to improve viscoelastic properties^[35].

(3) Hydrolases

Hydrolases (e.g. amylases, cellulases, lipases, mannanases, pectinases, phytases, proteases, pullulanases, and xylanases) catalyze reactions in which a bond in a substrate is hydrolyzed to produce two fragments^[28, 29]. About 60 years ago, acylases have already been applied for penicillin synthesis^[36, 37]. Badische Anilin-und-Soda-Fabrik (BASF) company developed biocatalytic systems of hydrolases, including lipases for the synthesis of enantiomerically pure alcohols/chiral amines, and nitrilases for the synthesis of amino- and hydroxycarboxylic acids^[16]. Amidases from *P. putida*/*M. neoaurum*/*O. antropii* are used for the synthesis of non-proteinogenic L-amino acids which are important building blocks for pharmaceutical compounds by Royal DSM N.V. (DSM) company^[16, 38]. Proteases as one of the highest volume industrial enzymes have been broadly used from detergent additives to effective therapeutics^[39].

(4) Lyases

Lyases (e.g. pectate lyases, α -acetolactate decarboxylases) catalyze elimination reactions in which a chemical group is removed from a substrate leaving a double bond or rings^[28, 29]. Large-scale manufacturing of enantiomerically cyanohydrins with improved yield and was achieved using hydroxynitrile lyases (HNLs) as a catalyst^[40].

(5) Isomerases

Isomerases (e.g. glucose isomerases, epimerases, mutases, and topoisomerases) catalyze reactions in which a substrate is converted to an isomer^[28, 29]. In industry, glucose isomerases are used for the production of high-fructose corn syrup, by catalyzing the isomerization of D-glucose to D-fructose^[41].

(6) Ligases

Ligases (e.g. argininosuccinate glutathione synthase) catalyze reactions that joining together of two or more molecules coupled to hydrolysis of adenosine triphosphate (ATP) or an analogous molecule^[28, 29]. Glutamylcysteine synthetase and glutathione synthetase can be used for the production of glutathione which highly consumed in pharmaceutical, food additives, and cosmetic industries^[42].

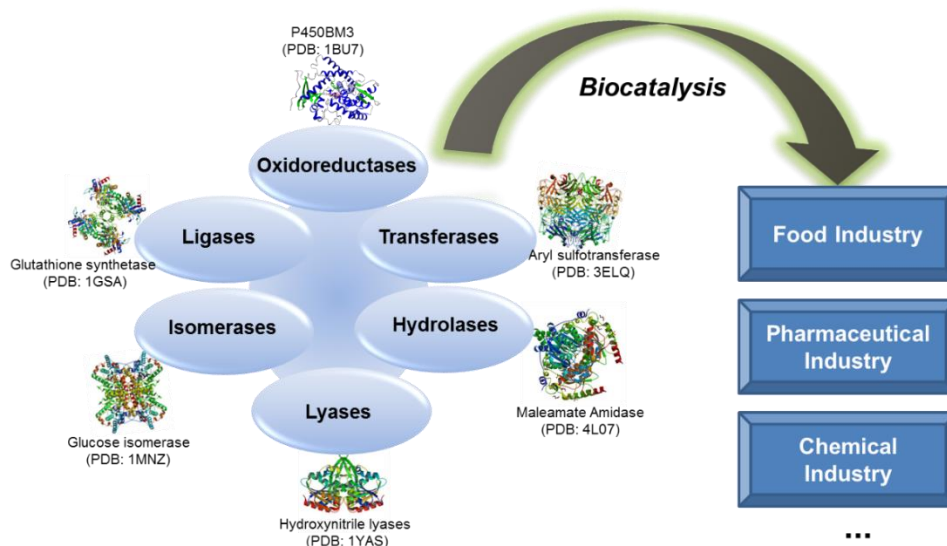


Figure 1. Overview of enzyme classes and industrial relevant enzymes.

1.3 Protein engineering

In Nature, wild-type enzymes are evolved (not designed) to fit their respective substrates within millions of years. In laboratory, enzymes are fast designed and bred using advanced molecular biology technologies^[43]. Protein engineering is a powerful tool to evolve enzymes for different properties, including broader substrate specificity, higher activity, higher selectivity, improved stability, and pH optimum. The developed important proteins enable new applications in broad fields, such as biocatalysis, biosensors, and therapeutic proteins. Therefore, protein engineering enables the transition of synthetic processes from a fossil-based economy to a biobased economy using renewable resources^[44].

1.3.1 Directed evolution

Protein properties can be improved by iterative rounds of the Nobel Prize-winning method “Directed Evolution” which is especially useful for improving properties if reliable structural models are not available or if the properties are rationally not well-understood^[44].

^{45]}. It does not require prior knowledge of such factors as the dimensional structure, conserved sites and catalytic mechanism of the proteins. A classical directed evolution experiment contains the following steps: random mutagenesis (DNA level), screening for improved enzyme variants (protein level), isolating and sequencing of genes that encode improved protein variants, and often iterative cycles of the described steps to obtain excellent catalysts and thermal resistance (**Figure 2**)^[46].

In 1972, the term of “directed evolution” was firstly introduced by Hansche group to evaluate the naturally occurring mutations in enzyme for their effect on the efficiency and activity of acid phosphatase and efficiency of orthophosphate metabolism^[47]. In the 1980s and 1990s, a big breakthrough was obtained-the development of error-prone polymer chain reaction (epPCR, random mutagenesis method) which enable the huge mutant library generated in few hours in the laboratory ^[48-51]. Since 1991, extensive studies were conducted by Arnold group in the laboratory and different enzymes’ properties were altered, e.g. solvent resistance of protase^[52], activity of protase^[53], thermostability of thermitase^[54] and esterase^[55]. In 1997, the first directed evolution campaign towards identification of enantioselective enzyme (lipase from *Pseudomonas aeruginosa*) was explored by Reetz group and Jaeger group^[56].

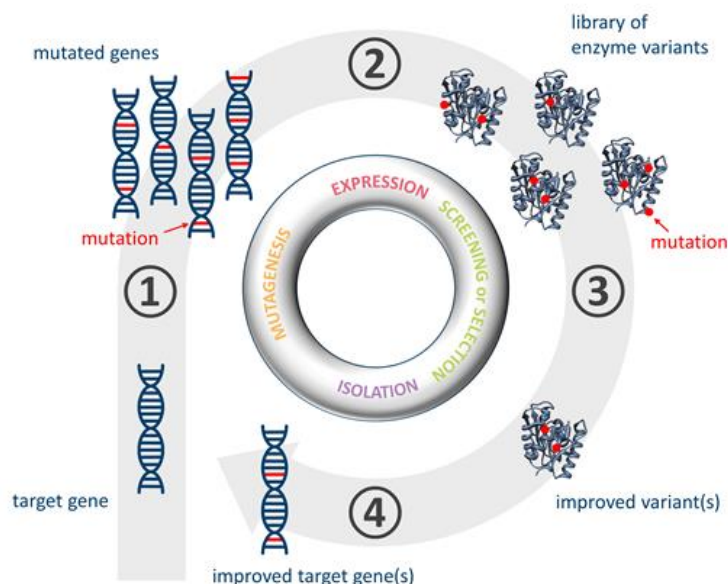


Figure 2. Principles of directed enzyme evolution. Four steps are performed by iteratively in directed evolution: introducing the targeted gene by random mutagenesis; generating a library of protein or enzyme variants; identifying improved variants by high-throughput screening or by selection for a desired property; isolating and sequencing the genes encoding improved variants. The picture was taken from Bornscheuer *et al.*^[44].

The most significant aspects of a successful directed evolution campaign are the quality of generated mutant libraries and the usage of effective screening methods. To introduce random mutations in the gene of interest, a variety of strategies has been implemented in this process, such as epPCR, sequence saturation mutagenesis (SeSaM) and site saturation mutagenesis (SSM, OmniChange). Error-prone PCR (epPCR) is the most common and simplest method for introducing random mutations, but it is limited because only a small fraction of the theoretically possible amino acid exchanges can be achieved by this method^[57]. Sequence saturation mutagenesis (SeSaM) is an alternative method which could not only overcome mutational bias of the employed DNA polymerases but also allows random mutations for a target sequence at every single nucleotide position^[58].

Several approaches have been developed to saturate several positions at the same time, for example OmniChange^[59], which allows simultaneous and efficient saturation of up to five independent codons. The procedure of the OmniChange method comprises four steps^[59], as shown in **Figure 3**. Step 1: Vector and insert generation by standard PCR with phosphorothioated oligonucleotides (PTO) (around 12 on the 5'-end of each primer) containing the degenerated codons; Step 2: Based on a chemical cleavage reaction of phosphorothioate bonds in iodine/ethanol solution, PCR products are cleaved and single-stranded overhangs are generated without additional PCR-amplification and restriction enzymes or ligases (**Figure 3**); Step 3: Assembly of mutated plasmids via complementary DNA hybridization; and Step 4: Transformation and nick repair in *E. coli*. This method does not require a minimum distance between mutated codons and any enzymes for DNA modification (restriction, ligation), is fully sequence and fragment size-independent and generates libraries of high genetic diversity in a single PCR step. In addition, it can be accomplished within one day including transformation.

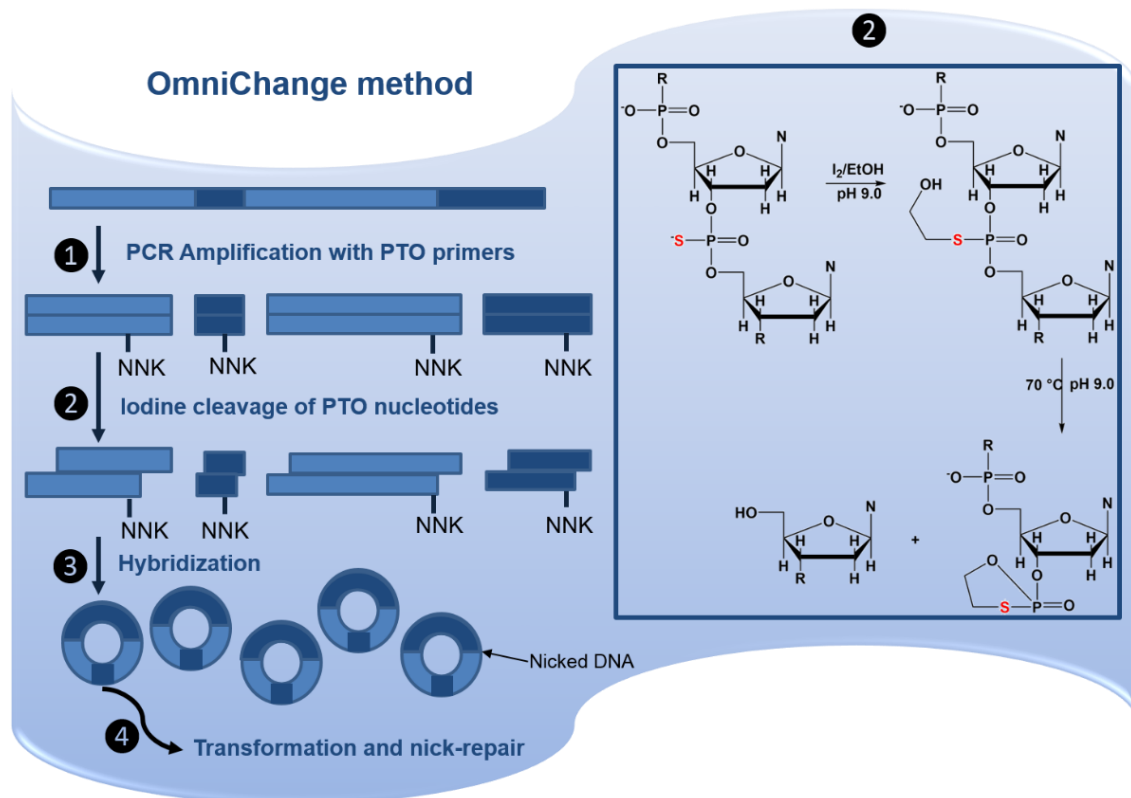


Figure 3. The 4-step strategy for the simultaneous saturation of five independent codons by OmniChange. OmniChange comprises four steps: Step 1. Amplification of five DNA fragments bearing an NNK-saturated codon. Step 2. Chemical cleavage to generate complementary single-stranded 5'-overhangs. Step 3. Hybridization of all fragments to a full circular plasmid containing ten DNA nicks. Step 4. Transformation and nick-repair in *E. coli*^[59].

1.3.2 KnowVolution

To manage the complexity of protein sequence space, a smarter protein engineering strategy termed “KnowVolution” (knowledge gaining directed evolution) was developed by the Schwaneberg group (see **Figure 4**). More than ten successful KnowVolution campaigns have been conducted, including improving thermostability and activity of alkaline protease^[60], thermostability and pH stability of phytase^[61], activity of arginine deiminase^[62], activity of aryl sulfotransferase^[63], activity of cellulase in seawater, activity of glucose oxidase, selectivity of hyaluronic acid synthase^[64], binding strength of anchor peptide LCI^[65], and three of the variants have already been commercialized by industrial partners^[62].

The “KnowVolution” approach requires less screening efforts, less time, and enables a molecular understanding of the targeted properties. The process of the “KnowVolution” strategy contains four iterative phases: identification, determination, selection, and recombination^[62]. In the first phase, potentially beneficial amino acid positions

(approximately 12 positions) are identified in a single round of directed evolution. In the second phase, beneficial amino acid substitutions are determination through screening variants generated by single saturation mutagenesis (SSM) at identified positions from phase 1; a molecular understanding is generated by sequencing and identifying the respective amino acid substitutions and analyzing their chemical properties (charge, size, H-bonds, and hydrophobicity); In phase 3, based on computational (homology) model, beneficial amino acid substitutions from phase 2 are analyzed and clustered in different regions within the three-dimensional (folded) protein. In the last phase, based on the gained knowledge in phase 2 and phase 3, several amino acid positions are recombined through multi-site saturation mutagenesis (e.g. using OmniChange^[59] method) or site-directed mutagenesis to minimize screening efforts and maximize improvements through synergistic substitutions.

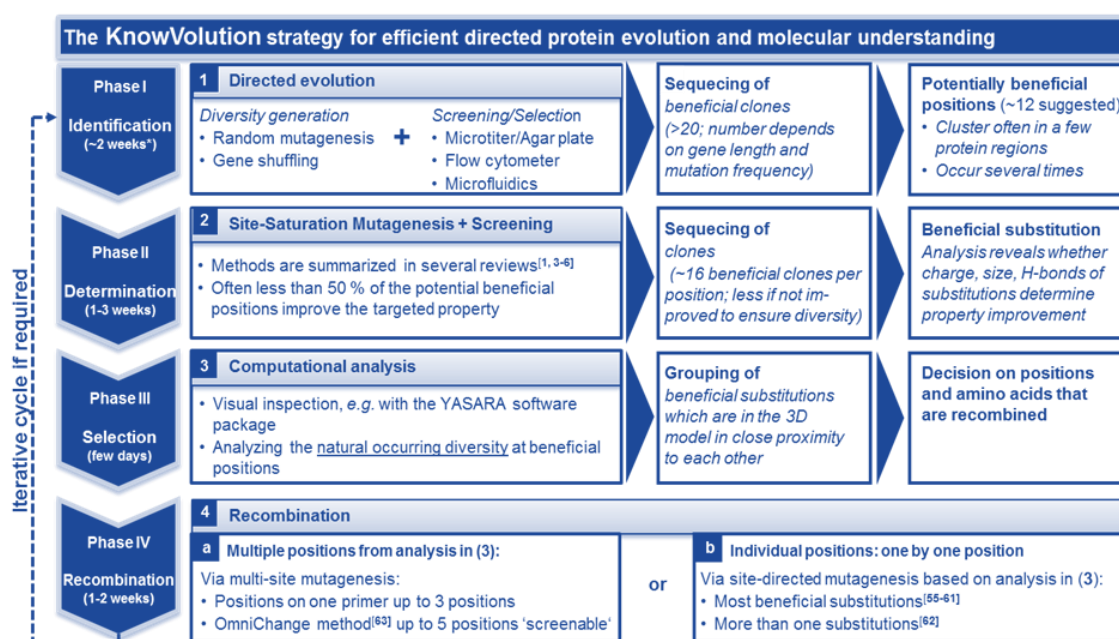


Figure 4. Overview of the KnowVolution strategy which comprises four phases. (I) identification of potentially beneficial amino acid positions, (II) determination of beneficial amino acid positions and substitutions, (III) computational analysis and grouping of amino acid substitution which might interact with each other, and (IV) recombination of beneficial substitutions in a simultaneous or iterative manner. The KnowVolution strategy can also be performed in an iterative manner to further improve targeted enzyme properties. This picture was taken from Cheng *et al.*^[62].

1.4 Thesis Objectives

Catechol sulfates are important compounds with antioxidant and often anti-inflammatory activities. Sulfated catechol can be used as biomarkers in many biological activities (e.g., chronic inflammation). Sulfated compounds are generally synthesized by chemical means using chlorosulfonic acid or sulfur trioxide trimethylamine; the multi-step syntheses require protection/deprotection of chemical groups which often result in low yields and/or titers. Enzymatic synthesis of catechol sulfates using aryl sulfotransferase B is a synthetically attractive and sustainable route to produce monosulfated catechols in single-step reactions. A “green” challenge is the often low stoichiometric transfer efficiency of sulfotransferases and the mediocre specific activities. To address this, the first aim of this dissertation was the engineering of ASTB for selective sulfation of catechols with high sulfate transfer efficiency (**Figure 5**).

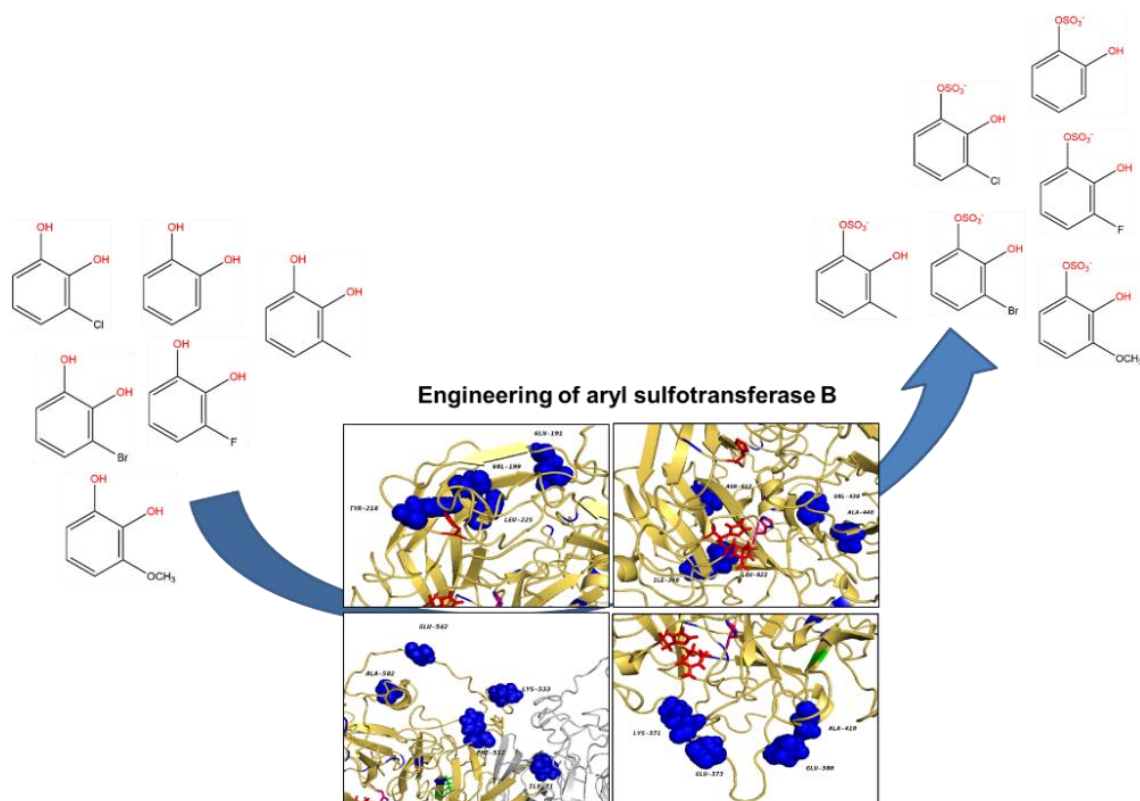


Figure 5. Engineering of aryl sulfotransferase B for chemo- and/or regio sulfation of catechols.

So far, only a few directed evolution campaigns for sulfotransferases engineering were reported and the screening assays relied on *p*-nitrophenol using as product or by-product which leaves a major challenge to use sulfotransferase in biocatalysis with high sulfate transfer efficiency and broader substrate scope. The reliable screening system for high-value substrates aromatic diols, such as catechols are lacking. To achieve this, a two-step

screening system was developed and validated by one round of directed evolution. Then a KnowVolution campaign was conducted and the role of loop12 and loop13 were deeply explored in order to identify beneficial variants with improved the sulfation activity towards six catechols (catechol, 3-methylcatechol, 3-methoxycatechol, 3-fluorocatechol, 3-chlorocatechol, 3-bromocatechol). Furthermore, a molecular docking study and an analysis based on the Hammett equation were applied to rationalize the influence of ring substituents (-F, -Cl, -Br, -CH₃, and -OCH₃) on regioselective sulfation of catechols. This work opens a new biocatalytic route to regioselective sulfation of catechols and flavonoids.

Bolaform surfactants are a novel class of compounds with a wide range of industrial and technical applications. Bolaform surfactants are capable of forming very small micelles (1.0-1.4 nm) and therefore are more effective than contemporary surfactants. However, their production is expensive and involves the use of strong acids and large amounts of solvents. An alternative “green” synthesis route is the direct hydroxylation through monooxygenases as performed in nature. Therefore, the second aim of this dissertation is to engineer the P450 BM3 towards hydroxylation of surfactant CTAB (**Figure 6**). Simultaneous site mutagenesis of four well-known positions (R47, Y51, F87, and L188) was conducted using the OmniChange method. Dramatical improvements were obtained by P450 BM3 variants and di-hydroxylation products of CTAB with bolaform surfactant properties which have excellent solubility have for the first time been produced.

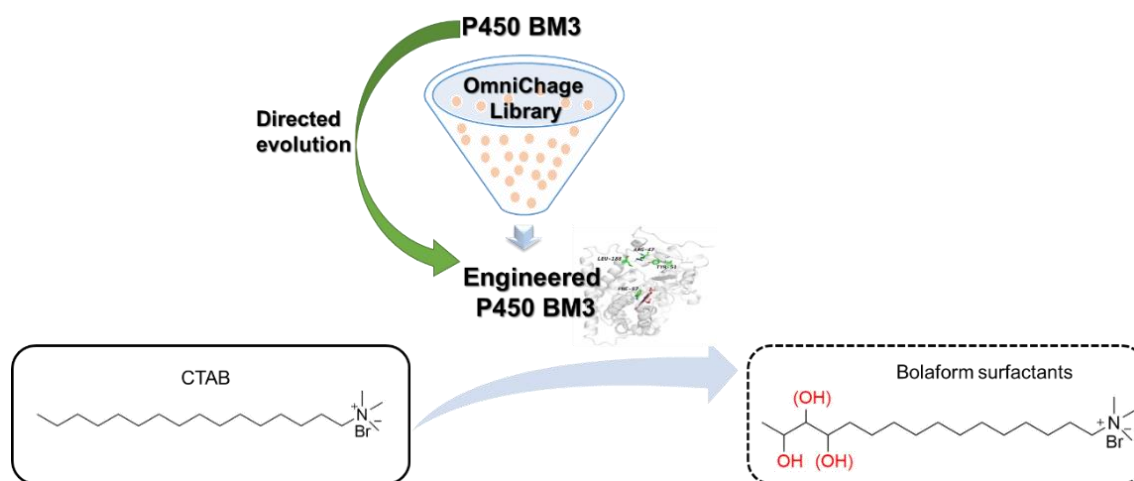


Figure 6. Engineering of P450 BM3 for bolaform surfactants synthesis.

2 Engineering of aryl sulfotransferase B for application in catechol sulfation

2.1 Declaration

Parts of this chapter has been published:

Ji, Y., Islam, S., Mertens, A. M., Sauer, D. F., Dhoke, G. V., Jakob, F., Schwaneberg, U. (2019). Directed aryl sulfotransferase evolution toward improved sulfation stoichiometry on the example of catechols. *Applied microbiology and biotechnology*, 103(9), 3761-3771^[66].

Parts of this chapter has been submitted for publication:

Ji, Y., Islam, S., Cui, H., Dhoke, G. V., Davari, M. D., Mertens, A. M., Schwaneberg, U. (2020). Loop engineering of aryl sulfotransferase B for improving catalytic performance in regioselective sulfation. *Catalysis Science & Technology*, 10, 2369-2377.

2.2 State of the art

2.2.1 Sulfation

Sulfation or sulfurylation (not to be confused with sulfonation, **Figure 7**) in biochemistry is the method for introducing a sulfo group (not a sulfate or sulfonyl group) into another organic molecule, which involves the formation of a C-O-S or C-N-S bond^[67-69]. Unlike sulfonated products with remarkable stability (even after prolonged heat), sulfates are prone to hydrolysis under strong alkaline conditions^[69].

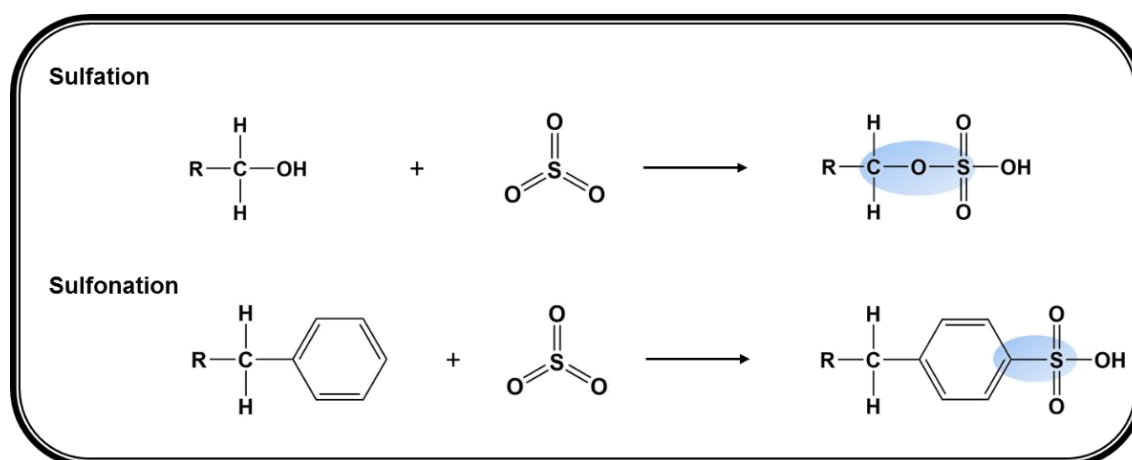


Figure 7. Scheme of sulfation vs. sulfonation.

2.2.2 Function of sulfation

Sulfation exists in all forms of organisms, playing an important role in the metabolism of xenobiotics, hormone regulation, and detoxification of toxic compounds^[70]. Various biomolecules, including steroids and other hormones, carbohydrates, and antibiotics have been identified as substrates of sulfation^[68].

The polar anionic sulfate groups provide unique characteristics to the organic compounds and change physicochemical properties of acceptor molecules, such as charge, size, and especially solubility^[69]. Therefore, aqueous and organic solutions of these sulfates possess many interesting functional properties (including wetting, dispersibility, emulsification, foaming, detergency, interfacial tension reduction, and surface tension reduction), and can be used as wetting aids, dispersants, emulsifiers, foamers, detergents, demulsifiers, corrosion inhibitors, and fluidizers^[69]. Thus, these sulfated compounds are of broad utility and great industrial interest in anionic surfactants^[71], cyclic intermediates, dyes, pigments, medicines, pesticides, sweeteners, lubricant additives, and polymeric specialty chemicals production (e.g. for the pharmaceutical industry: hyaluronic acid derivatives, chondroitin sulfate, and heparin have a global market of about 14 billion US-\$ per year)^[72, 73].

2.2.3 Chemical sulfation

Chemical sulfation has already been used for decades to meet the needs of specific properties and applications by attaching sulfate functional groups to targeted molecules. Some sulfates are synthesized from transformation of natural products, e.g., haliclostano sulfone, mycamine^[74-76]. Sulfuric acid (H_2SO_4) can sulfate alkenes^[77], cycloalkenes^[77], saturated monohydric alcohols^[78], and polyhydric alcohols^[79]. For the sulfation of aliphatic/alicyclic alcohols, phenols, mercaptans, amines, peptides, and oximes, dicyclohexylcarbodiimide (DCC) is added together with sulfuric acid and used as mediator involving the formation of protonated DCC- H_2SO_4 intermediate^[70, 80]. As sulfuric acid has quite strong acidity, complexes of sulfur trioxide (SO_3) with organic bases including pyridine (Py), trimethylamine (NMe_3), and triethylamine (NEt_3), or amides (e.g. dimethylformamide, DMF) which relatively stable at high temperatures and more “user-friendly” are also widely used^[70, 81-84]. A variety of scaffolds containing alcoholic, phenolic, amine, thiol and other functional groups have already been sulfated by those complexes^[70].

⁸²⁻⁸⁶]. In the pharmaceutical/chemical industries, most sulfates are generally synthesized using chlorosulfonic acid or sulfur trioxide trimethylamine^[70, 87, 88].

Chemical sulfation processes often suffer from low chemo- and/or regioselectivity and unwanted side reactions with other functional groups (e.g. dehydration^[70], nonselective sulfation and scaffold degradation)^[89]. The latter demands extensive protection/deprotection strategies in the synthesis that increases the number of synthesis steps and thereby reduces yields and/or titers (insolubility of sulfated molecules in organic solvents)^[90-98].

2.2.4 Enzymatic sulfation

Chemo- and/or regioselective sulfation by enzymes represents an alternative to the aforementioned processes. Enzymatic sulfation occurs usually with high chemo- and/or regioselectivity under mild reaction conditions. The main challenges for enzymatic sulfation processes comprise the comparably low activity of sulfotransferases and inefficient and costly use of sulfate donors. Sulfotransferases (EC 2.8.2.1) catalyze the transfer of a sulfate group (OSO_3^-) from a sulfate donor molecule to an acceptor molecule and can be divided into two classes depending on the type of donor (**Figure 8**)^[68, 99].

The first class contains the so-called PAPS-dependent sulfotransferases in eukaryotic and bacterial cells, which utilize a very expensive sulfate donor called 3'-phosphoadenosine-5'-phosphosulfate (PAPS)^[100]. PAPS-dependent sulfotransferases are reported to regioselectively sulfate proteins, lipids, and polysaccharides as well as xenobiotics, hormones, and neurotransmitters^[68, 101, 102].

The second class comprises mainly bacterial aryl(sulfate) sulfotransferases (ASST) that are PAPS-independent and use more "cost-efficient" phenolic sulfate esters (such as *p*-nitrophenyl sulfate; *p*-NPS^[103]). The bacterial aryl sulfotransferases (e.g., ASST, ASTA, ASTB) were reported to sulfate antibiotics^[104], steroids^[105], flavonoids^[89, 106], and sugars^[107]. For instance, the plant flavonoid quercetin was sulfated regioselectively by ASTA from *Desulfitobacterium hafniense* with yields up to 79 %^[89, 108, 109].

Aryl sulfotransferases isolated from *Eubacterium* A-44, *Enterobacter amnigenus*, and *Aspergillus oryzae* have been shown to react by *ping-pong bi-bi* kinetic mechanisms^[99, 110], which is depicted in **Figure 9**. A crystal structure of the homodimeric ASST from the uropathogenic strain *E. coli* CFT073 in the presence of various sulfate donors showed that the sulfate group is bound transiently to a catalytic histidine residue. This mechanism

resembles the mechanism of trapped intermediate of the phosphohydrolase reaction^[111]; during the transfer of a sulfate donor to a sulfate acceptor molecule by these enzymes, and an activated enzyme sulfo-histidine intermediate is formed.

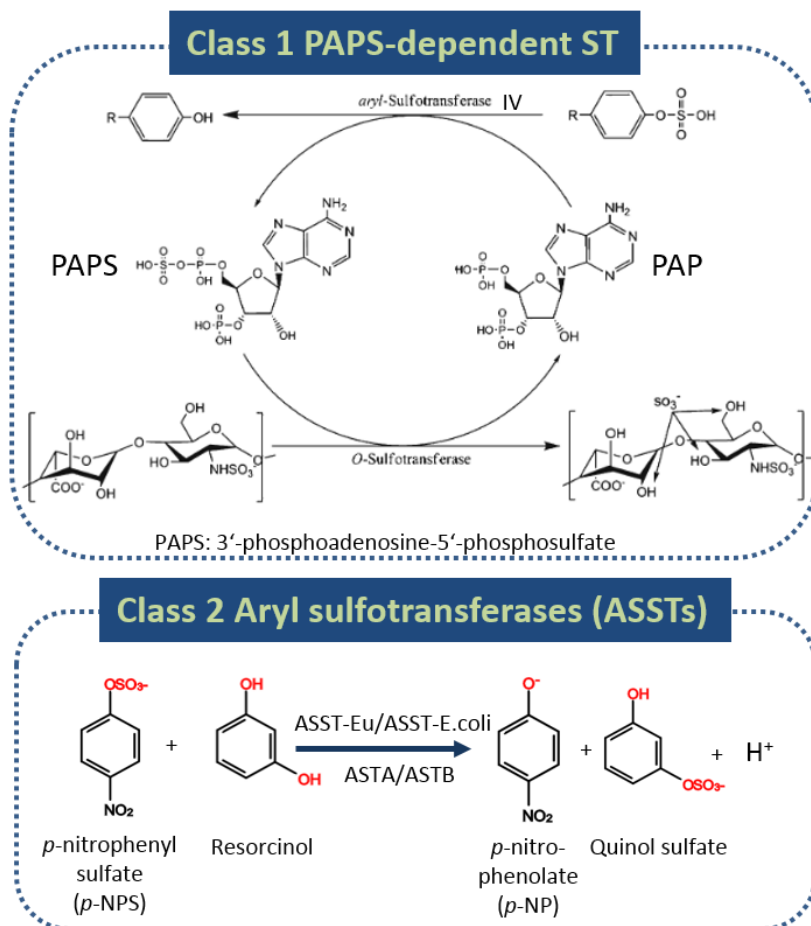


Figure 8. Scheme of PAPS-dependent sulfotransferases and ASST-catalyzed reaction. The figure was adapted from Sterner. *et al.*^[112]

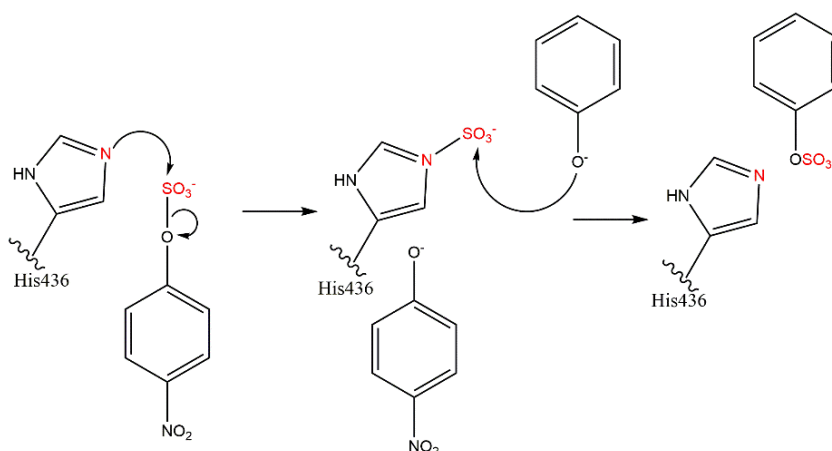


Figure 9. ASST from *Escherichia coli* CFT073 shows a ping-pong bi-bi reaction mechanism.

Dehalorespiring bacterium *Desulfitobacterium hafniense* belongs to the Clostridia and has the ability to dechlorinate halogenated compounds under anaerobic conditions by dehalorespiration. Van der Horst and co-workers^[108] reported cloning and expression of the ASTA gene from *Desulfitobacterium hafniense* and explored its donor and acceptor specificity. Aryl sulfotransferase A (ASTA, genomic sequence: NC_011830.1) sequence codes for a protein of 628 residues corresponding to a molecular mass of 71.4 kDa and shows activity not only towards phenolic substrates but also with aliphatic alcohols (e.g. octanol, glycerol) as sulfate acceptors. A variety of compounds have been tested for their potential as sulfate acceptor for ASTA, and only some of them showed good activity of catalysis. ASTB from *Firmicutes* (630 amino acids) shares a 46 % protein sequence identity with ASTA^[107]. From a commercial point of view, the lower costs and high stability of *p*-NPS (124.5 EUR per g; Sigma-Aldrich) compared to the expensive PAPS (93,000.0 EUR per g; Sigma-Aldrich) makes it attractive to extend the current research on PAPS-independent sulfotransferases.

2.2.5 Catechols and catechol sulfates

Catechols (pyrocatechol or 1,2-dihydroxybenzene) are present in trace amounts in higher plants, such as tobacco, tea, fruit, and some traditional Chinese medicines^[113, 114]. Catechol derivatives (e.g., chlorinated and methylated catechols) are by-products in pulp and oil mills^[115]. They are important chemical intermediates in industry and frequently used as antioxidants or antiseptic in rubbers, hair dyes, pesticides, cosmetics, foods, and pharmaceuticals^[115, 116]. Owing to their widespread use and comparably high toxicity, catechols are abundantly found in the environment and cause human health problems^[117]. For instance, catechol changes erythrocyte morphology with the formation of a few echinocytes at low doses (10 ppm;^[118, 119]) and efficient absorption in the gastrointestinal tract makes catechol even more toxic than phenol (catechol: 50 ppm, phenol: 250 ppm;^[120]). Catechols represent a substance class reported to cause severe human diseases such as vasoconstriction, renal tube degeneration, liver malfunction, cancer, and neurodegenerative diseases^[120-122]. In contrast to catechols, catechol sulfates are not harmful to humans (no toxicity data reported) and are end products of the cellular metabolism of aromatic compounds, involving a combination of gut activity between microbial metabolism and live-kidney functions^[123]. Catechol sulfates have been detected in urine^[124] and plasma (catechol sulfate: 12.2 μ M, 4-methyl catechol sulfate: 0.6 μ M;^[125]).

A recent study reported that the serum level of catechol sulfates in patients with Parkinson's disease is lower than in healthy people, therefore they were identified as a novel biomarker for Parkinson's disease^[123]. Moreover, investigation of obesity-related chronic diseases revealed potential anti-inflammatory activity of catechol monosulfate^[126]. Mycamine (belong to echinocandins) containing a catechol monosulfate group is used to treat invasive fungal infections including candidemia, abscesses, and esophageal candidiasis^[127].

Up to now, the chemo- and/or regioselectivity of bacterial aryl sulfotransferases toward catechols have not been explored and no crystal structures of sulfotransferases other than from *E. coli* CFT073 have been reported.

2.2.6 Strategies in protein engineering

Process and protein engineering are two synergist options to improve product yields and/or titers^[108, 128, 129]. Ron Waver group already conducted substrate modification and investigated new donors to improve the rates of sulfate transfer^[89, 105, 108, 128].

Apart from varying reaction parameters such as enzyme concentration, proposing new donors and acceptor concentration, protein engineering as a useful technique can be used to improve the activity of aryl sulfotransferases towards non-natural acceptors. Protein engineering by directed evolution has due to its broad industrial use^[130-132] been applied in several campaigns to improve sulfotransferases in their activity^[46, 107, 133]. For PAPS-dependent sulfotransferases, several crystal structures (e.g. SULT1A1, SULT1A3) were reported which provides insights in engineering selectivities^[134, 135]. A handful of site-directed mutagenesis campaigns were carried out for PAPS-dependent sulfotransferases in order to improve the enzyme activity^[136-140]. However, for PAPS-independent sulfotransferases only one crystal structure has been solved (*Escherichia coli* CFT073 ASST); the latter PAPS-independent sulfotransferase has a *ping-pong bi-bi* reaction mechanism involving transient sulfation of His-436^[99, 103, 141]. However, many more synthetically important ASSTs (e.g. ASTA, ASTB) are available. The lack of structural information (for instance with the sulfate donor bound to the active site) limits the molecular understanding of ASSTs and therefore rational design can hardly be applied. Directed evolution and KnowVolution campaigns have already been employed for increasing the sulfation activity towards sugars and to improve the thermal resistance of sulfotransferases^[46, 107, 133]. For instance, ASTB variant L446P/V579K led to a 7.6-fold increased specific activity (6.15 U mg⁻¹) towards cellobiose^[107].

2.2.7 Screening assays for evolution of aryl sulfotransferase

To date, no directed evolution campaign or protein engineering attempt with respect to improve the sulfation stoichiometry of an aryl sulfotransferase was reported. The major challenge to conduct successful directed evolution is the development of a robust screening system to identify improved variants^[45]. The *p*-NPS based screening assay quantifies the sulfotransferase activity through the formation of the colorimetric by-product *p*-nitrophenol (*p*-NP) at 405 nm^[107], and it was successfully employed in two reports of directed aryl sulfotransferase evolution campaign^[63, 107]. However, the *p*-NPS screening system does not ensure an efficient stoichiometry of sulfation since the by-product (*p*-NP; yellow color) and not the sulfated product is spectrophotometrically detected. In directed evolution campaigns of other enzymes classes (e.g., monooxygenases), false-positive variants with lower product titers can be selected due to overexpression and/or by-products formation^[142-147]. Coupling efficiency (ratio in % between formed product and consumed cofactor) is therefore one of the key parameters for successfully developing drugs by using for instance P450 monooxygenases^[148]. A similar result can be obtained with aryl sulfotransferase variants which promote only the “hydrolysis” of *p*-NPS (auto-hydrolysis) and/or the sulfation of the catalytic residue (sulfohistidine) of the enzyme without transferring the sulfate group to the target substrate^[46]. Sulfate transfer efficiencies of sulfotransferases range from 1.5 % to 87.1 % in respect to their stoichiometry as previously reported^[107, 149]. The use of 4-AAP for colorimetric detection of phenol compounds is a sensitive way for catechol monosulfate detection^[150-152]. With *p*-position occupied by a nitro group, sulfate donor *p*-NPS and by-product *p*-NP cannot react with 4-AAP^[153] leading toward no false-positive product detection. Catechols also have a very slow reaction rate with 4-AAP due to the competition between two hydroxyl groups, resulting in only a low background of absorbance at 509 nm. Therefore, 4-AAP assay is an ideal screening assay for catechol monosulfate detection in a one-pot reaction system.

2.2.8 Objective

The main goal of this chapter was the engineering of the sulfotransferase ASTB toward the sulfation of catechol compounds. The objectives are divided into five working packages (WP): (1) selection of suitable PAPS-independent sulfotransferases for activity study; (2) investigation of selectivity of aryl sulfotransferase B; (3) generation and screening of mutant libraries of aryl sulfotransferase B towards improved activity using industrially

important compounds; (4) purification and characterization of identified variants including detailed analysis of formed products; (5) kinetic characterization and computational analysis of identified improved variants.

2.3 Material and Methods

2.3.1 Chemicals and reagents

All chemicals used in this research were of analytical grade or higher quality and were purchased from Sigma-Aldrich (Steinheim, Germany), AppliChem (Darmstadt, Germany), ABCR (Karlsruhe, Germany), Carl Roth (Karlsruhe, Germany), and VWR International (Darmstadt, Germany).

Phusion DNA polymerase, DpnI, and dNTPs were obtained from New England Biolabs (Frankfurt, Germany); *Taq* DNA polymerase was produced in-house. PCRs were performed in 0.2 mL thin-walled PCR tubes (Sarstedt Multiply[®]-Pro cup, Nuembrecht, Germany) using a thermal cycler (Eppendorf Mastercycler proS, Hamburg, Germany). DNA was quantified with a NanoDrop photometer (ND-1000, NanoDrop Technologies, Wilmington, DE, USA). Plasmid extraction was achieved by using a commercial kit (QIAGEN QIAprep Spin Miniprep Kit, Hilden, Germany). DNA sequencing was performed at GATC Biotech (Konstanz, Germany) and Eurofins MWG-Operon (Ebersberg, Germany). Analysis of obtained sequencing data was performed using the Clone Manager 9 Professional Edition Software (Scientific & Educational Software, Cary, NC, USA). All kinds of Microtiterplates (flatbottom transparent MTP, black transparent MTP and v-bottom transparent MTP) were purchased from Greiner Bio-One GmbH (Frickenhausen, Germany).

2.3.2 Vectors and strains

The vector pET22b(+) was used for expression of ASTA, ASTB, ASST_*Strepto*, and ASST_*Pseudo* in *Escherichia coli* (*E. coli*).

The vector pET28a(+) was used for expression of ASST_*E.coli* and ASST_*Eu* in *E. coli*.

The *E. coli* strain BL21 Gold (DE3) (Agilent Technologies, Santa Clara, CA) was used for all six sulfotransferases (ASTA, ASTB, ASST_*Strepto*, ASST_*Pseudo*, ASST_*E.coli* and ASST_*Eu*) expression.

Strep-tag II (Ser-Ala-Trp-Ser-His-Pro-Gln-Phe-Glu-Lys) was attached at the C-terminal end of AstA and ASTB genes for purification^[107].

Gene sequences and protein sequences of ASTA-StrepII, ASTB-StrepII, ASST_*Strepto*, ASST_*Pseudo*, ASST_*E.coli*, and ASST_*Eu* can be found in the appendix 5.2.

2.3.3 Generation of an ASTB SeSaM (Sequence Saturation Mutagenesis) library

As previously reported a random mutagenesis library of ASTB (SeSaM-Tv-classic) was used in the directed evolution campaign^[107].

2.3.4 Generation of ASTB OmniChange library

A multi-site saturation mutagenesis library targeting four positions (Q191, V199, Y218, and L225) located in the loop12 and loop13 region was generated by OmniChange method according to published protocol^[59]. The ASTB OmniChange library was generated in four steps: (1) vector and inserts generation with phosphorothiolated oligonucleotides (PTO); (2) chemical DNA-cleavage reaction by iodine ethanol solution; (3) assembly of mutated plasmids via complementary DNA hybridization; (4) transformation and nick repair in *E. coli*^[59].

Step 1: Vector and inserts generation with PTO

First fragment (fragment A, 93 bp) targets position Q191 and V199. Second fragment (fragment B, 3622 bp) contains position Y218 and L225. Third fragment (fragment C, 3627 bp) contains vector backbone. All phosphorothioate oligonucleotide (PTO) primers used in this library generation are listed in **Table 1**. For gene fragment A amplification, the reaction contained 20 ng template-DNA, 0.1 μ M PTO primers (Q191/V199Fw and Q191/V199Rv), 5 U *Taq*/Phusion DNA polymerase (1:2), 1x PfuS buffer, 0.2 mM dNTP mix, and ddH₂O in a total volume of 50 μ L. The PCR was performed as follows: 96°C for 3 min, one cycle; 96°C for 30 s, 60°C for 30 s, 72°C for 30 s, 25 cycles; 72°C, 5 min, one cycle). PTO primers (Y218/L225Fw and Y218/L225Rv, 0.1 μ M each) together with Phusion DNA polymerase (5 U), PfuS buffer (1x), dNTP mix (0.2 mM), template-DNA (20 ng), and ddH₂O in a total volume of 50 μ L were used for amplification of fragment B and the corresponding PCR program was 98°C for 3 min (1 cycle); 98°C for 30 s, 62°C for 1 min, 72°C for 4 min (25 cycles); 72°C for 5 min (1 cycle). The vector backbone (fragment C) was amplified using PTO primers (2148Fw and 2148Rv, 0.1 μ M each) in combination with Phusion DNA polymerase (5 U), PfuS buffer (1x), dNTP mix (0.2 mM), template-DNA (20 ng) by PCR (98°C for 3 min, 1 cycle; 98°C for 30 s, 60°C for 1 min, 72°C for 4 min, 30 cycles; 72°C for 5 min, 1 cycle). The template plasmid DNA was digested by adding DpnI (20 U; 37°C, 12 h) to PCR products. PCR products were purified using the Nucleospin Extract II kit (Macherey Nagel, Dueren, Germany).

Table 1. Sequences and T_m value of primers used for the OmniChange library generation.

PTO primer	Sequence (5'→3')	T_m (°C)*
Q191/V199Fw	catcgtaccgtgNNKAAACCGTATTACAACGTGGGCNNKA TGGAAATGG	68.2
Q191/V199Rv	accgcccggcagACGGTATTCTTTGTAG	65.3
Y218/L225Fw	ctgccgggcggtNNKCATCACGACGCGGTTGAANNKGAA AACGGCAAT	73.5
Y218/L225Rv	ggcgaaacccgaCAGGACTATAAAGATACC	61.4
2148Fw	tcgggtttcgccACCTCTGACTTGAGC	65.8
2148Rv	cacgtacgatgCGACGTATACAGCAGGCGACCATT	68.1

* T_m for degenerate primers have been reported as minimum, mean and maximum value; capital letter: normal nucleotide, small letter: phosphorothioated nucleotide; N=A, C, T, G; K=G, T.

Step 2: Chemical DNA-cleavage reaction

Purified vector backbone fragment C was diluted to $0.04 \text{ pmol } \mu\text{L}^{-1}$ and fragments A, B were diluted to $0.11 \text{ pmol } \mu\text{L}^{-1}$ using distilled deionized water. Subsequently, all fragments (each $4 \text{ } \mu\text{L}$) were cleaved by fresh prepared iodine-ethanol solution ($2 \text{ } \mu\text{L}$) at alkaline conditions as reported before^[59].

Step 3: Assembly of mutated plasmids via complementary DNA hybridization

Cleaved fragment A ($6 \text{ } \mu\text{L}$) was added to the tube containing $6 \text{ } \mu\text{L}$ cleaved vector, then after 5 min incubation, cleaved fragment B ($6 \text{ } \mu\text{L}$) was added in the same tube. All cleaved fragments were assembled by hybridization using a temperature gradient (70°C , 5 min; $-1^\circ\text{C}/10 \text{ s}$, 50 cycles; 20°C , 3 min; 4°C , 5 min).

Step 4: Transformation and nick repair in *E. coli*

Hybridization mix ($10 \text{ } \mu\text{L}$) was transformed into $100 \text{ } \mu\text{L}$ chemically competent *E. coli* BL21-Gold (DE3) cells and plated on LB agar plates supplemented with $50 \text{ } \mu\text{g mL}^{-1}$ ampicillin.

2.3.5 Development of *p*-NPS-4-AAP screening system in 96-well microtiter plates (MTPs)

Variants of ASTB SeSaM and OmniChange libraries were cultivated and cell-free extracts were screened in 96-well MTP as described previously^[107]. In short, The ASTB variants were screened using 3-chlorocatechol as a substrate to identify variants with higher sulfation activity toward catechol compounds compared to ASTB-wildtype (WT). A two-step *p*-NPS-4-AAP MTP based screening assay was developed to select ASTB variants

with high coupling efficiency. A two-step *p*-NPS-4-AAP MTP based screening assay was developed in this study. In the first screening step, each of the MTPs (PS-F-bottom, Greiner Bio-One, Frickenhausen, Germany) contained clarified cell lysate (15 μ L), Tris-HCl buffer (145 μ L, 100 mM, pH 9.0), and 3-chlorocatechol (20 μ L of 1 mM stock, final concentration: 100 μ M). MTPs were incubated at 800 rpm in an MTP shaking device (TiMix, Edmund Bühler GmbH, Hechingen, Germany; room temperature (RT), 5 min) before supplementation of *p*-NPS (20 μ L of 1 mM stock, final concentration 100 μ M). The kinetics of *p*-NP formation were recorded with an MTP reader (wavelength: 405 nm, cycles: 30, kinetic interval: 10 s, RT, Time: 5 min; Tecan Sunrise, Männerdorf, Switzerland). Subsequently in the second step, the reaction was quenched by quenching buffer (20 μ L of 4 M urea in 0.1 M NaOH stock, final concentration 320 mM). After supplementing 4-aminoantipyrine (4-AAP, 15 μ L of 25 mM stock; final concentration: 1.5 mM), potassium peroxodisulfate was added to the reaction (15 μ L of 25 mM stock; final concentration: 1.5 mM). The kinetics of the formed product 1,5-dimethyl-4-(3-sulfo-4-oxocyclohexa-5-chloro-2,5-dienylidenamino)-2-phenyl-1,2-dihydropyrazol-3-one was recorded using a MTP reader (wavelength: 509 nm, cycles: 30, kinetic interval: 10 s, RT, Time: 5 min; Tecan Sunrise). The ASTB SeSaM and OmniChange libraries were screened and re-screened using this two-step *p*-NPS-4-AAP assay.

2.3.6 Expression and purification of ASTB-WT and ASTB variants in flasks

ASTB-WT and ASTB variants were produced in 250 mL Erlenmeyer flasks containing 50 mL TB media supplemented with ampicillin (100 μ g mL⁻¹). The cultures were grown (37°C, 900 rpm, 70 % humidity) until an OD_{600 nm} of 0.6 was reached. Protein expression was induced by adding IPTG (0.1 mM) and the cultures were grown overnight (20°C, 900 rpm, 70 % humidity, 24 h). Cells were harvested by centrifugation (4°C, 11,279 g, 30 min; Sorvall, Thermo Fischer Scientific, Darmstadt, Germany), and cell pellets were frozen at -20 °C before use. Pellets were resuspended in Tris-HCl buffer (100 mM, pH 9.0) and incubated on ice. Lysozyme (1.5 mg mL⁻¹) was added prior to cell disruption via sonication on ice (5 min, 30 s pulse, 70 % amplitude) using ultra sonicator (Vibra-Cell™ Ultrasonic Liquid Processor, VCX 130, Sonics & Materials, Inc., Newtown, CT, USA). The cell lysates were centrifuged (4°C, 11,279 g, 30 min; Sorvall, Thermo Fischer Scientific) and the clarified lysates were used for purification. ASTB-WT and ASTB variants were purified using Strep-Tactin chromatography column (Strep-Tactin

Superflow Plus Cartridge-5 mL, Qiagen, Hilden, Germany) by gravity flow. Eluted protein fractions were collected and analyzed on 10 % sodium dodecyl sulfate-polyacrylamide gel electrophoresis (SDS-PAGE) gels to assess protein purity. ASTB fractions of high purity (around 90 %) were pooled and concentrated by Amicon Centrifugal Filters (50 kDa cut-off; Millipore, Schwalbach, Germany) and the final protein concentrations were determined by Pierce™ BCA protein assay kit (Thermo scientific, Waltham, MA, USA). Protein samples purified to homogeneity were shock-frozen in liquid nitrogen and lyophilized for 8 h in a freeze-dryer (Christ ALPHA 1-2LD plus, Osterode am Harz, Germany).

2.3.7 Characterization of ASTB-WT and ASTB variants

Purified ASTB-WT and ASTB variants were diluted (final concentration of 0.01 μM) in Tris-HCl buffer (100 mM, pH 9.0). Kinetics of ASTB-WT and ASTB variants were determined by measuring the initial rates of *p*-NP formation at various 3-chlorocatechol concentrations (0-1000 μM). All the reactions were performed in five replicates with *p*-NPS as fixed donor (final concentration: 1000 μM) and performed as described for the screening system. The kinetics for other catechol substrates as acceptors (catechol, 3-fluorocatechol, 3-bromocatechol, 3-methylcatechol, 3-methoxycatechol) were also calculated by measuring the initial rates of product formation at various acceptor concentrations (0-1000 μM) with fixed *p*-NPS concentration (1000 μM). Values were obtained by triplicate experiments.

2.3.8 Long-term conversion by ASTB-WT and ASTB variants

Long-term conversion reactions were carried out in Tris-HCl buffer (100 mM, pH 9.0) with 3-chlorocatechol for the later HPLC detection. A reaction mixture of 1 mL was prepared, in which 1 μmol 3-chlorocatechol and 1 μmol *p*-NPS in presence of 1 nmol enzyme were incubated (25°C, 300 rpm, 7 days) using a thermomixer (Eppendorf thermomixer comfort, Hamburg, Germany).

2.3.9 Product separation by high-performance liquid chromatography-mass spectrometry (HPLC-MS)

A high-performance liquid chromatography (HPLC, Nexera X2, Shimadzu Deutschland GmbH, Duisburg, Germany) equipped with a PDA detector and a HPLC (Agilent® HP1100, Waldbronn, Germany) equipped with an ion-trap mass analyzer

(Thermo LTQ Orbitrap™, Waltham, MA, USA) were used for product separation and quantification. The products of investigated sulfation of 3-chlorocatechol were separated (flow rate: 0.4 mL min⁻¹, time: 30 min, injection volume: 5 μL, RT) in analytical scale with a NUCLEODUR® HILIC column (250 × 4.6 mm, 5 μm; MACHEREY-NAGEL, Düren, Germany) using 5 % solvent A (water with 200 mM ammonium acetate (pH 4.3)) and 95 % solvent B (acetonitrile, ACN). Sulfated products were analyzed by ion trap mass analyzer in the negative mode of electrospray ionization (ESI) at a capillary voltage of 3.5 V and a capillary temperature of 350°C. Catechols and products were identified using accurate full scan mode.

2.3.10 Nuclear magnetic resonance (NMR) spectroscopy

A reaction mixture of 3 mL Tris-HCl buffer (100 mM, pH 9.0) containing ASTB-WT/ASTB variants (1 μM, purified enzyme), and 3-chlorocatechol (10 mM) was pre-incubated in 9 mL glass tube, sealed with lid and incubated on an Eppendorf Mix Mate (300 rpm, room temperature; Sigma-Aldrich, Steinheim, Germany) for 5 min. 3-chlorocatechol sulfation by ASTB was induced by adding *p*-NPS (10 mM). The reactions were performed for 12 h. After performing long-term conversion, 3 mL acetonitrile was added and mixed thoroughly, centrifuged (13000 g; 5 min; Eppendorf 5415R centrifuge, Hamburg, Germany) and the sediment was discarded. Subsequently, the samples were shock-frozen in liquid nitrogen and lyophilized (Christ ALPHA 1-2LD plus, 8 h). ¹H-NMR spectra of each sample were recorded on a Bruker Avance III 400 NMR spectrometer (Bruker BioSpin, Germany). Chemical shifts are reported in ppm relative to the residual solvent resonances.

2.3.11 Molecular modeling

The starting structure of the ASTB-WT was taken from our previously published homology model of ASTB^[63]. The structural model of the ASTB-OM2 variant (Q191Y/Y218W/L225V) was constructed in YASARA Structure Version 17.4.1750 employing the YASARA-FoldX plugin^[154] and using the FoldX method^[155]. The starting coordinates for the FoldX in silico mutagenesis were taken from the homology model of ASTB^[63]. A rotamer search, exploring alternative conformations (3 independent runs) of Y191Y/W218/V225 and the surrounding side chains below 6 Å distance from Substituted positions were performed during the FoldX energy minimization using a probability-based

rotamer library. Stability energies were computed with FoldX Suite 4.0^[155] using standard settings.

The protein residues were treated using the AMBER ff9953 whereas the ligand atoms were treated using GAFF^[156, 157] with AM1-BCC partial charges^[158] employing particle mesh Ewald^[159] for long-range electrostatic interactions and a direct force cutoff of 10.5 Å. For molecular docking, a grid box of 12 Å around the active site was generated by selecting catalytic H350 residue. Molecular docking calculations were performed using Autodock4.2 plug-in within YASARA Structure Version 17.4.1750 with a fixed protein backbone. Hundred docking runs were performed and the docking poses were clustered by applying a RMSD cutoff of 0.5 Å and using the default settings provided within the YASARA dock_run macro file.

2.4 Results

This result section is divided into 4 parts. The first part introduces the selection of a suitable PAPS-independent sulfotransferase and sulfate donor for catechol sulfation. The second part reports on the development of the two-step *p*-NPS-4-AAP screening system for the reference compound 3-chlorocatechol. The third part shows the directed evolution campaign toward improved specific activity and sulfate transfer efficiency employing 3-chlorocatechol. The fourth and final part summarizes the results on purified ASTB-WT and the improved variants including their substrate profile.

2.4.1 Selection of an aryl sulfotransferase for phenol compounds sulfation

To select the starting PAPS-independent sulfotransferases, six different PAPS-independent sulfotransferases including aryl sulfotransferase A (ASTA), aryl sulfotransferase B (ASTB), aryl sulfotransferase from *Streptomyces sp.* (ASST_Strepto), aryl sulfotransferase from *Pseudomonas sp.* MK730-62F2 (ASST_Pseudo), aryl sulfotransferase from *Eubacterium A-44* (ASST_Eu), and aryl sulfotransferase from *E. coli* CFT073 (ASST_*E. coli*) were chosen for expression in *E. coli* BL21 (DE3). The expression of ASTA, ASTB, ASST_Strepto, ASST_Pseudo, ASST_Eu, and ASST_*E. coli* in flasks were evaluated by 10 % SDS-PAGE (**Figure 10a**). ASST_Eu showed the highest expression level (intensity of bands at 71.8 kDa), followed by ASTA, ASTB and ASST_*E. coli*. Very faint bands were visible for ASST_Strepto and ASST_Pseudo which is similar to negative control pET28a(+). Therefore, sulfotransferase ASTA, ASTB, ASST_*E. coli*, and ASST_Eu were selected for further activity comparison.

To evaluate the activity of selected four aryl sulfotransferases, resorcinol, the natural acceptor of aryl sulfotransferase was employed as the model substrate and *p*-NPS was used as sulfate donor. The activity of four different aryl sulfotransferases in clarified crude cell extracts was evaluated by *p*-NPS assay^[107]. As is shown in **Figure 10b**, the activity of ASTB toward resorcinol sulfation is the highest among four tested aryl sulfotransferases, which is 1.5-fold, 7.2-fold, 6.2-fold higher than the activity of ASTA, ASST_*E. coli*, and ASST_Eu.

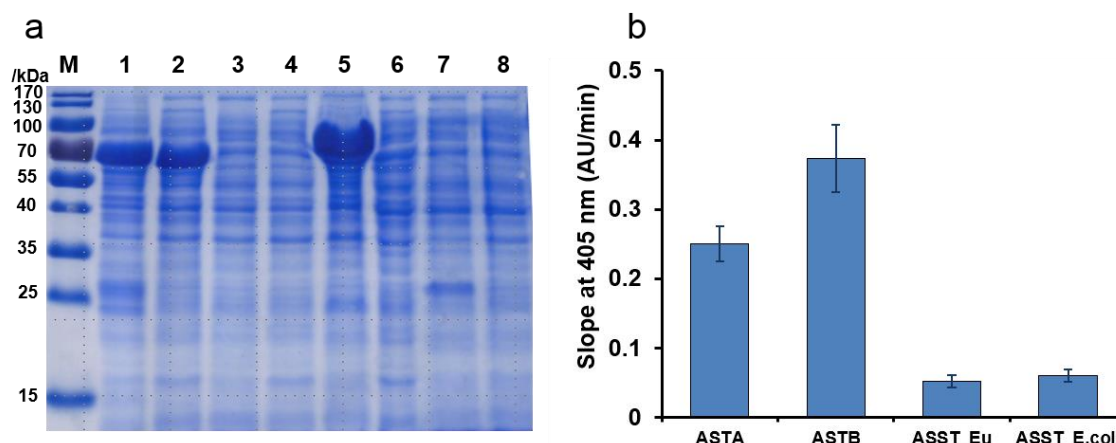


Figure 10. SDS-PAGE analysis of six sulfotransferases and activity comparison. a) SDS-PAGE analysis of six sulfotransferases (M: protein marker; 1: ASTA (molecular weight 74.4 kDa); 2: ASTB (molecular weight 73.2 kDa); 3: ASST_*Strepto* (molecular weight 58.9 kDa); 4: ASST_*Pseudo* (molecular weight 66.4 kDa); 5: ASST_*Eu* (molecular weight 71.8 kDa) 6: ASST_*E. coli* (molecular weight 67.7 kDa), 7: pET22b(+), and 8: pET28a(+)). b) Comparison of activities for ASTB, ASTA, ASST_*Eu*, and ASST_*E. coli* towards resorcinol. 40 μ L crude cell extracts were incubated in MTP with 1 mM resorcinol solution (160 μ L, Tris-HCl buffer pH 9.0, 100 mM). Plates were shaken briefly and 20 μ L *p*-NPS (final conc. 1 mM) was added in Tecan plate reader at 405 nm (room temperature, 15 min) constantly measured the absorbance.

As *p*-NPS assay is based on measuring the by-product formation, the real product formation and sulfation efficiency cannot be monitored by this assay, thus additional analytical technique is required. HPLC-PDA analytical method was established for product detection and the best separation of substrate and product were obtained at room temperature by a C₁₈ column using solvent A (water with 200 mM ammonium acetate (pH 4.3)) and B (ACN) at a flow rate of 0.3 mL min⁻¹. 20 % component B was programmed with a linear gradient to 60 % for 3 min, followed by a linear gradient up to 100 % B in 16 min, and finally return to 20 % B in 1.0 min. The product resorcinol sulfate was observed at 2.7 min (**Figure 11a**) while resorcinol and *p*-nitrophenol (*p*-NP) appeared at 3.4 min and 4.4 min. Among four aryl sulfotransferases, ASTB catalyzed reaction obtained the highest product formation (calculated from peak area, **Figure 11b**). Therefore, considering both results from *p*-NPS assay and HPLC-PDA analysis, ASTB was chosen as the target enzyme for further activity and selectivity study towards phenol compounds.

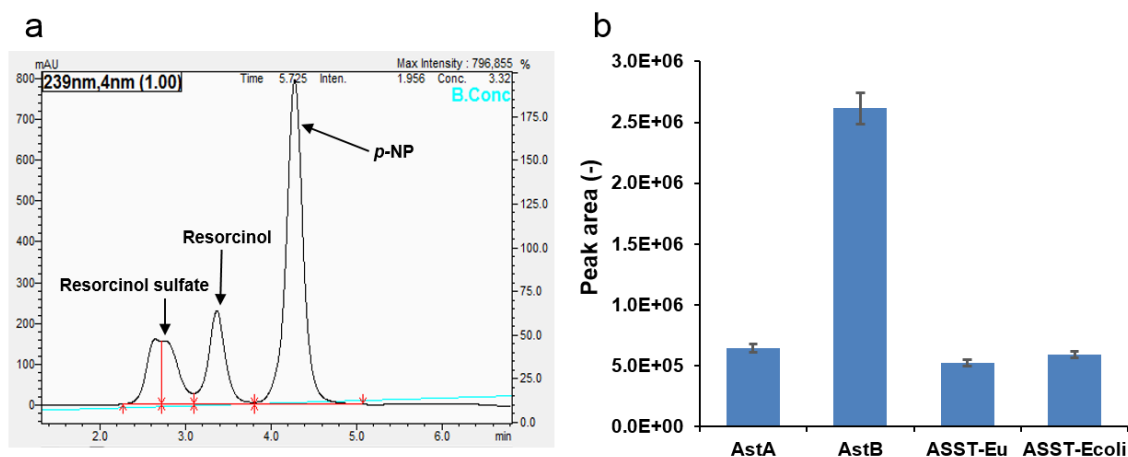


Figure 11. Sulfation efficiency of 4 different aryl sulfotransferases identified by HPLC. a) HPLC-PDA chromatography of resorcinol sulfate (reaction condition: 10 mM resorcinol, 10 mM *p*-NPS, 60 μ L cell crude extract, 12 h reaction; injection volume: 5 μ L). b) Comparison of sulfation product resorcinol sulfate of 4 different aryl sulfotransferases.

2.4.2 Selectivity study of aryl sulfotransferase ASTB for catechol sulfation

As catechol compounds have broad industrial use, simple structure and will most likely easily accepted by ASTB, so that they represent good model compounds for exploring selectivity of sulfotransferases. 3-Chlorocatechol was selected for the characterization of ASTB towards selective sulfation. Theoretically, 3-chlorocatechol can be sulfated at hydroxyl groups by sulfotransferase resulting in three possible products, including 1-chlorocatechol monosulfate, 2-chlorocatechol monosulfate, 1,2-chlorocatechol disulfate (**Figure 12**). For identification of sulfated product formed in conversion by ASTB, MS and NMR were used for determination. After 12h reaction, the reaction mixture was pretreated with ACN and injected to MS. MS determined high abundance at $m/z = 224.6$ (**Figure 13**), which corresponds to the theoretical mass of the monosulfated product ($m/z = 224.0$). Additionally, a negligible amount of 3-chlorocatechol-1,2-disulfate was observed in ASTB catalyzed sulfation reactions at $m/z = 303.9$ (theoretical mass $m/z = 304.0$) as well (**Figure 13**). Then, the structure elucidation of the monosulfated product was performed by $^1\text{H-NMR}$ and a regioselective sulfation by ASTB-WT was determined at 1-hydroxyl group of 3-chlorocatechol confirming the product as 3-chloro-1-catecholsulfate (**Figure 14**).

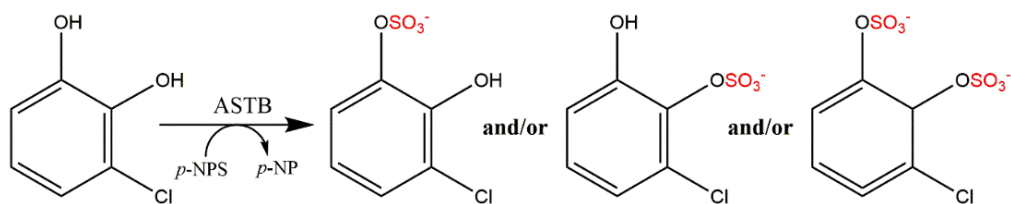


Figure 12. Theoretical sulfation of 3-chlorocatechol catalyzed by aryl sulfotransferase ASTB.

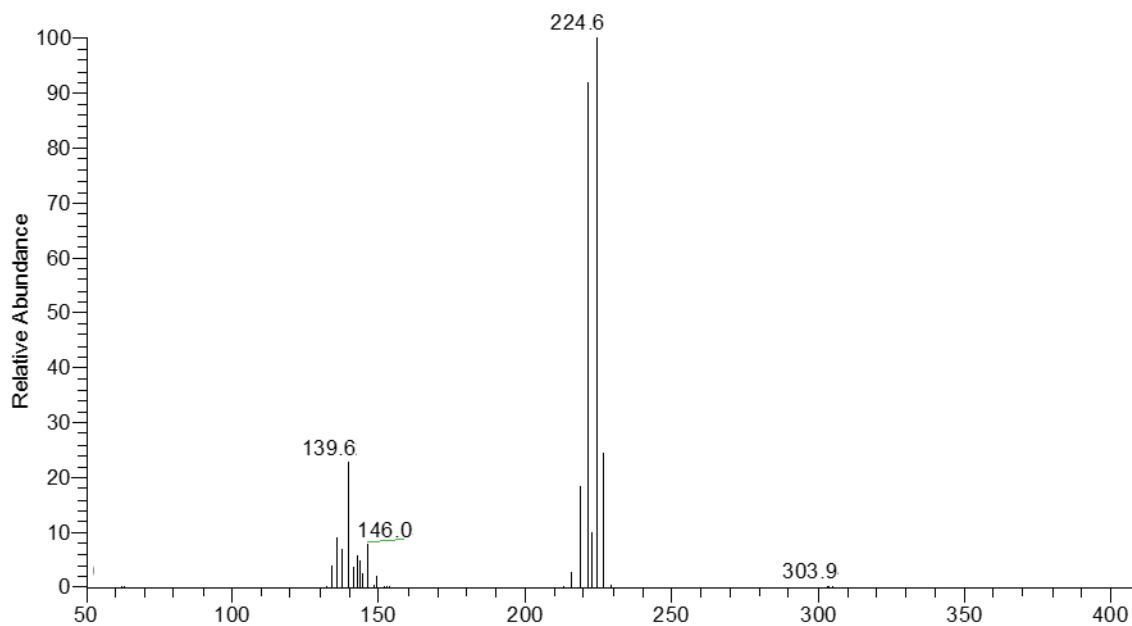


Figure 13. Electrospray ionization mass spectroscopic analysis (negative mode) of enzymatic conversion of 3-chlorocatechol by ASTB.

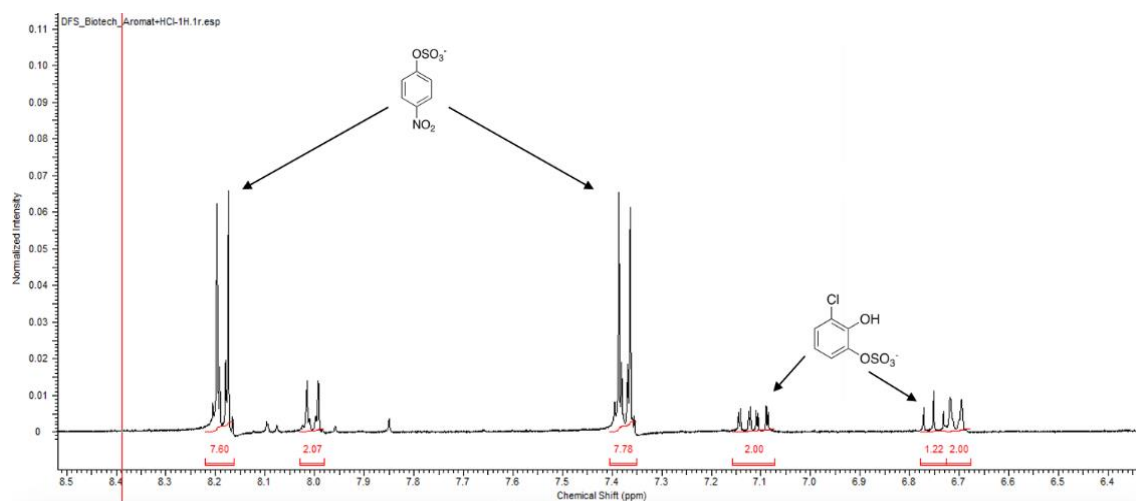


Figure 14. Nuclear magnetic resonance (NMR) spectrum of enzymatic conversion of 3-chlorocatechol by ASTB.

2.4.3 Development of *p*-NPS-4-AAP screening system

The *p*-NPS based screening assay quantifies the sulfotransferase activity through the formation of the colorimetric by-product *p*-nitrophenol (*p*-NP) at 405 nm. However, the *p*-NPS screening system does not ensure an efficient stoichiometry of sulfation since the by-product (*p*-NP; yellow color) and not the sulfated product is spectrophotometrically detected. Aryl sulfotransferase variants could promote only the “hydrolysis” of *p*-NPS (auto-hydrolysis) and/or the sulfation of the catalytic residue (sulfohistidine) of the enzyme without transferring the sulfate group to the target substrate^[46]. Sulfate transfer efficiencies of sulfotransferases range from 1.5 % to 87.1 % with respect to their stoichiometry as previously reported^[107, 149]. In directed evolution campaigns of other enzymes classes (e.g., monooxygenases), false-positive variants with lower product titers can be selected due to overexpression and/or by-products formation^[142-146]. In this work, the well-known *p*-NPS assay, which only allows the determination of the by-product *p*-NP, was expanded to an additional step to determine the sulfated product directly.

2.4.3.1 Principle of *p*-NPS-4-AAP screening system

The principle of the continuous two-step *p*-NPS-4-AAP screening system is shown in **Figure 15**. In the first reaction step, ASTB transfers the sulfate group from *p*-NPS (sulfate donor) to the substrate (3-chlorocatechol; sulfate acceptor) resulting in the product 3-chlorocatechol monosulfate and the by-product *p*-NP. The release of *p*-NP can spectrophotometrically be monitored at 405 nm due to yellow color formation (extinction coefficient, ($\epsilon_{p\text{-NP}}(405\text{ nm}) = 14.7\text{ mM}^{-1}\text{cm}^{-1}$; for 100 mM Tris-HCl, pH 9.0)^[107]. The product 3-chlorocatechol monosulfate reacts in the subsequent step with 4-AAP forming 1,5-dimethyl-4-(3-sulfo-4-oxocyclohexa-5-chloro-2,5-dienylideno)-2-phenyl-1,2-dihydropyrazol-3-one, which appears as dark red color (**Figure 15**) and can be quantified spectrophotometrically at 509 nm.

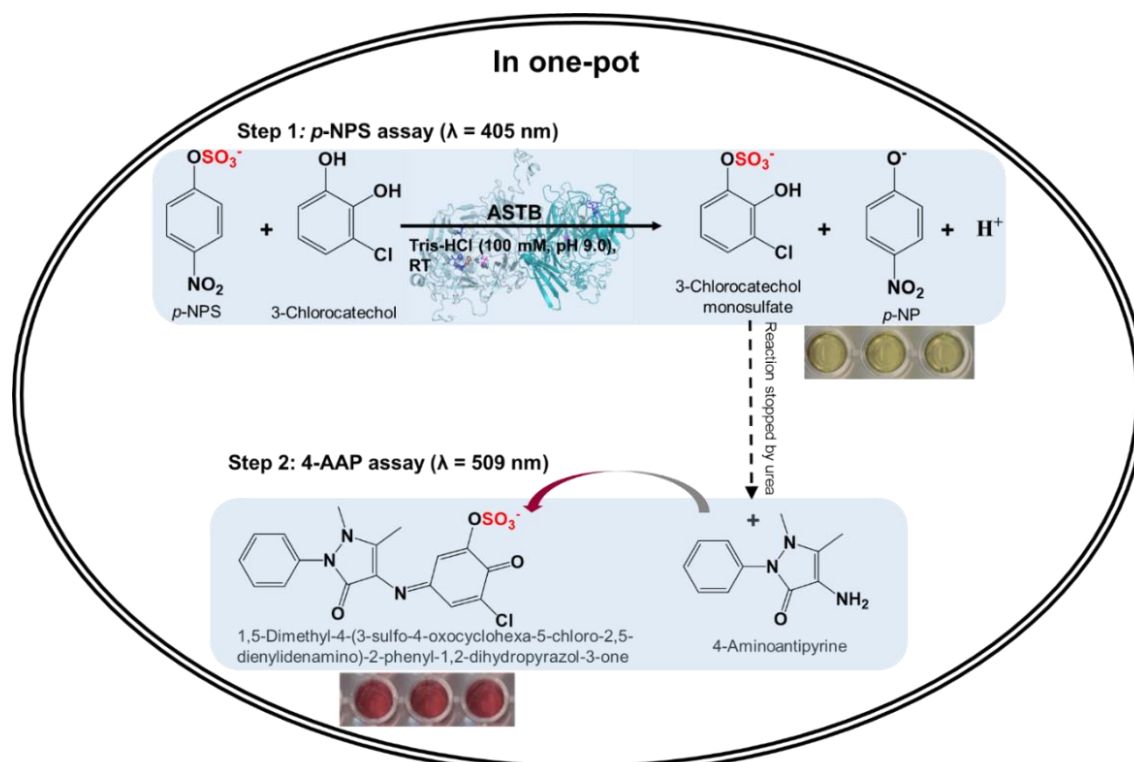


Figure 15. Principle of the two-step *p*-NPS-4-AAP screening system. ASTB catalyzes the sulfation of 3-chlorocatechol forming 3-chlorocatechol monosulfate and the yellow by-product *p*-NP (monitored at 405 nm). The product 3-chlorocatechol monosulfate is quantified in a one-pot reaction with 4-aminoantipyrine through formation of the red compound 1,5-dimethyl-4-(3-sulfo-4-oxocyclohexa-5-chloro-2,5-dienylideneamino)-2-phenyl-1,2-dihydropyrazol-3-one which can be detected at 509 nm. Figure is adopted from Ji *et al.*^[66].

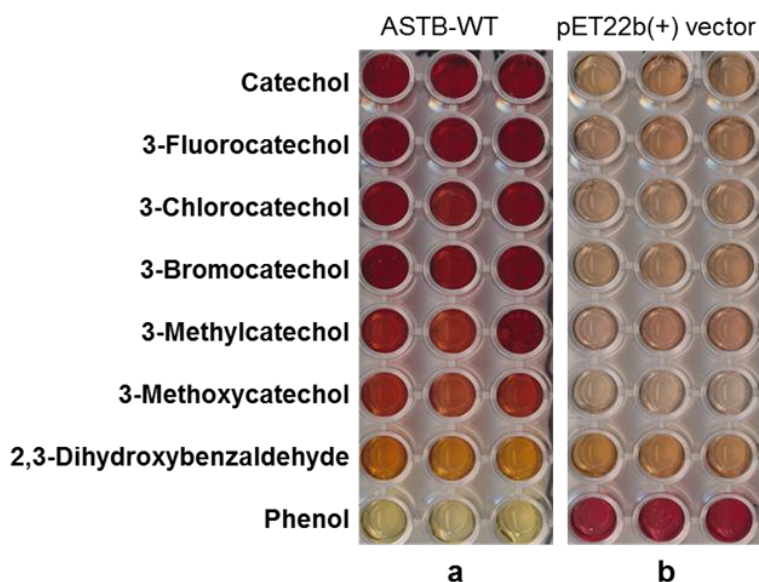


Figure 16. Sulfation of catechols and phenol catalyzed by ASTB-WT followed by treating with 4-AAP : a) ASTB-WT; b) negative control (pET22b (+) vector). Reaction conditions: 1 mM catechol (catechol derivative) or phenol, 1 mM *p*-NPS, 320 mM urea, 1.5 mM 4-AAP, 1.5 mM potassium peroxodisulfate, and 30 μL clarified cell lysate (ASTB or pET22b (+) vector). Figure is taken from Ji *et al.*^[66].

2.4.3.2 Optimization of *p*-NPS-4-AAP screening system

The reaction parameters of the *p*-NPS-4-AAP screening system were optimized step by step (pH value, volume of cell free extract, and linear detection range) in order to reduce the background and to obtain a reliable coefficient of variation (CV; in 96-well MTPs) that ensures a successful directed evolution campaign.

In order to determine the background activity, the interference of 3-chlorocatechol within the *p*-NPS-4-AAP screening system at pH 9.0 was investigated (**Figure 17a** & **Figure 17b**). In absence of ASTB, low absorbance values were observed at 509 nm in the negative control (3-chlorocatechol, *p*-NPS, and 4-AAP; see **Figure 17a**). Afterwards, the reaction was carried out in MTP plates and measured at 509 nm which confirmed the low background absorbance at 509 nm (**Figure 17b**).

To optimize the CV of the *p*-NPS-4-AAP screening system, the pH ranges from pH 8.0 to pH 10.5 was explored (**Figure 17c**). For the first reaction step (*p*-NPS assay), the highest activity was obtained at pH 9.0 and the ASTB activity was terminated through urea treatment (4 M urea in 0.1 M NaOH). In the second step, the reaction solution of the first step was directly used for the 4-AAP assay and the highest activity was observed at pH 9.5. The pH value of pH 9.0 was finally selected for the two-step screening procedure in one-pot due to a lower background (empty vector) of *p*-NPS-4-AAP assay compared to all investigated pH values (**Figure 17c**).

In addition, varied volumes of clarified cell lysate (5-30 μ L) were analyzed for both reaction steps and 15 μ L was finally selected for the screening (**Figure 17d**). The linear detection range of the two-step *p*-NPS-4-AAP screening system was determined for the acceptor molecule 3-chlorocatechol (from 0 to 600 μ M; **Figure 17e**) and the lower detection limit of the *p*-NPS-4-AAP screening system is 15 μ M. In order to have a sufficient dynamic range to detect improved variants, concentration of 100 μ M 3-chlorocatechol was chosen.

Based on the optimized parameters, the coefficient of variation was determined for each reaction step with 100 μ M *p*-NPS, 100 μ M 3-chlorocatechol, 1.5 mM 4-AAP, and 15 μ L clarified cell lysate at pH 9.0. The true CV of both steps was determined by subtracting the background activity (96 identical ASTB-WT clones vs. 96 identical “empty vectors” as negative control). The true CV of the *p*-NPS assay (black circle) is 12.3 % (first step; determined by measuring the slope of *p*-NP formation in 96-well format at 405 nm); the true CV of the 4-AAP assay (white circle) is 14.5 % (second step; determined by measuring the slope of 3-chlorocatechol monosulfate formation in 96-well format at

509 nm) (see **Figure 17f**). Optimization yielded a coefficient of variation below 15 % for the two-step screening system (*p*-NPS-4-AAP).

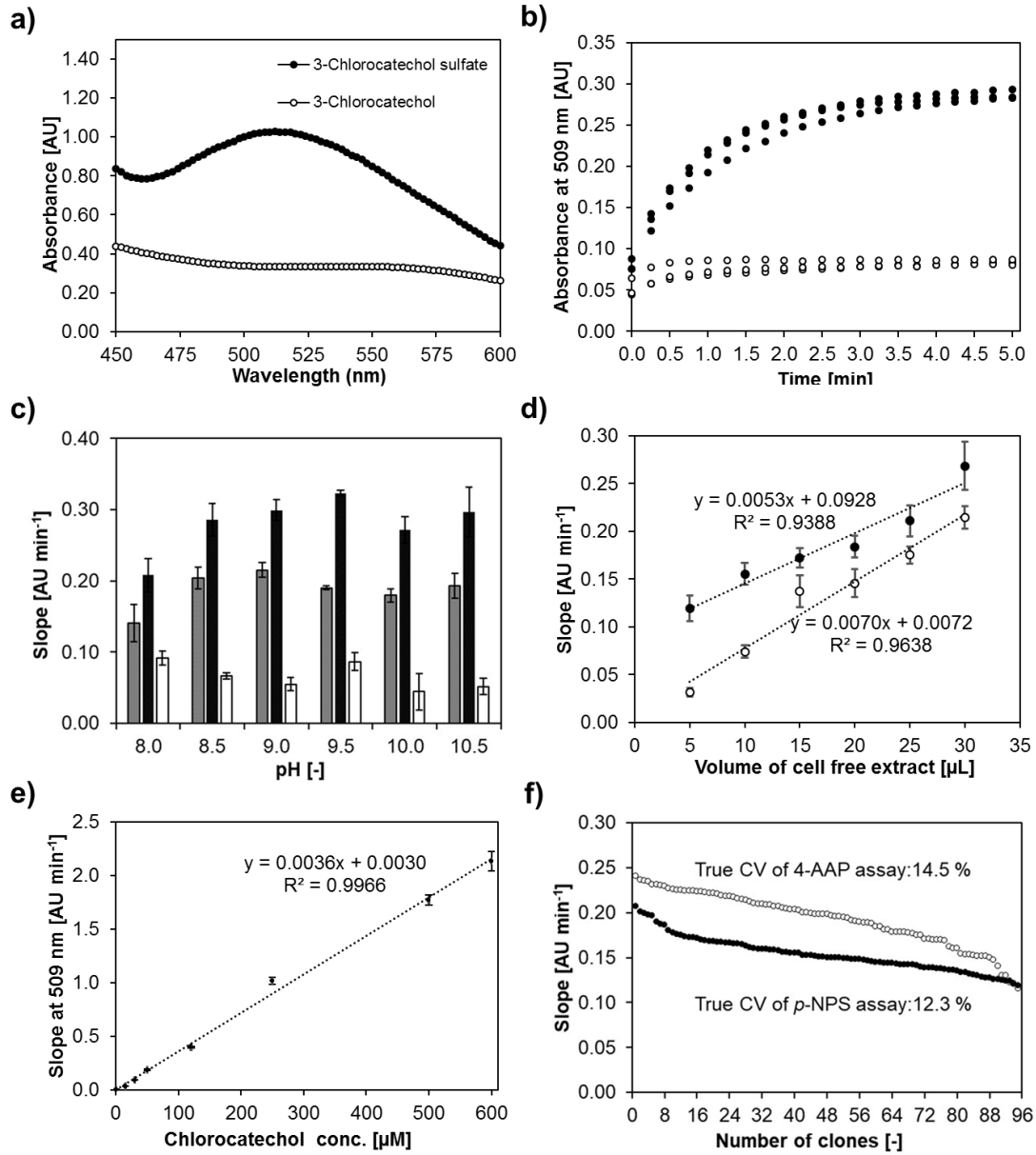


Figure 17. Optimization of important parameters and the coefficient of variation determination. a) Absorption of 3-chlorocatechol sulfate catalyzed by ASTB followed by treating with 4-AAP (solid circle) and absorption of 3-chlorocatechol, *p*-NPS, empty vector mixture treated with 4-AAP (hollow circle). Reaction conditions: 1 mM 3-chlorocatechol, 1 mM *p*-NPS, 320 mM urea, 1.5 mM 4-AAP, 1.5 mM potassium peroxodisulfate, and 30 μ L clarified cell lysate (ASTB or pET22b (+) vector); b) Kinetic of the ASTB catalyzed two-step reaction with 3-chlorocatechol as substrate and quantification of the produced 3-chlorocatechol sulfate after quenching the ASTB reaction through urea supplementation. Quantification of the produced 3-chlorocatechol sulfate is achieved with 4-AAP (solid circle). 3-chlorocatechol shows a low absorbance with 4-AAP (hollow circle) at 509 nm in MTP plates. Reactions were carried out using 15 μ L clarified cell lysate (ASTB-WT or pET22b (+)), 100 μ M 3-chlorocatechol, 100 μ M *p*-NPS, 320 mM urea, 1.5 mM 4-AAP, and 1.5 mM of potassium peroxodisulfate in the Tris-HCl buffer (100 mM; pH 9); c) Activity of ASTB-WT and pET22b (+) vector in 100 mM Tris-HCl from pH 8.0 to pH 10.5. Grey bar: increase in *p*-NP formation catalyzed by ASTB-WT measured at 405 nm (*p*-NPS assay-first reaction step); Black

bar: quantification of 3-chlorocatechol monosulfate (product of the first step) through reaction with 4-AAP measured at 509 nm (4-AAP assay-second reaction step); White bar: background between 3-chlorocatechol (supplemented with pET22b (+) vector and *p*-NPS) and 4-AAP measured at 509 nm; d) ASTB activities at varied amounts of clarified cell lysate [5- 30 μ L]. White circle: Slope measured at 405 nm; Black circle: slope measured at 509 nm. Each measurement represents a mean value of five measurements; e) Determination of the linear detection range of the continuous *p*-NPS-4-AAP screening system. Reactions were performed using 0-1000 μ M 3-chlorocatechol, 1000 μ M *p*-NPS and 15 μ L clarified cell lysate, 320 mM urea, 1.5 mM potassium peroxodisulfate, and 1.5 mM 4-AAP in total 250 μ L reaction volume. Reported values are the average of measurements in triplicates; f) Determining the true coefficient of variation (CV) of the *p*-NPS-4-AAP screening system. The true CV of *p*-NPS assay (first reaction step) was determined by measuring the slope of *p*-NP formation in 96-well format (black circles). The true CV of the 4-AAP assay (second reaction step) was determined by measuring the slope of 3-chlorocatechol monosulfate formation in 96-well format (white circles). Obtained slopes are plotted in descending order.

2.4.4 Validation of the *p*-NPS-4-AAP screening system in one round of directed ASTB evolution

The developed *p*-NPS-4-AAP screening system was validated in one round of directed ASTB evolution by screening a random mutagenesis library of ASTB toward improved specific activity and sulfate transfer efficiency employing 3-chlorocatechol.

2.4.4.1 Screening of ASTB SeSaM library

In total, 1,760 clones from SeSaM library (ASTB-SeSaM library^[63]) expressed in *E.coli* BL21 Gold (DE3) were screened for improved ASTB activity toward 3-chlorocatechol. In order to find improved ASTB variants compared to ASTB-WT, the following formula was used:

$$\text{Improvement [fold]} = \frac{\frac{\text{Slope}(\text{Variant})_{509 \text{ nm}} - \text{Slope}(\text{EV})_{509 \text{ nm}}}{\text{Slope}(\text{WT})_{509 \text{ nm}} - \text{Slope}(\text{EV})_{509 \text{ nm}}}}{\frac{\text{Slope}(\text{Variant})_{405 \text{ nm}} - \text{Slope}(\text{EV})_{405 \text{ nm}}}{\text{Slope}(\text{WT})_{405 \text{ nm}} - \text{Slope}(\text{EV})_{405 \text{ nm}}}}$$

Where, $\text{Slope}(\text{Variant})_{(509 \text{ nm})}$ is the reaction rate of 3-chlorocatechol monosulfate produced by ASTB variant and measured at 509 nm, and $\text{Slope}(\text{WT})_{(509 \text{ nm})}$ is the reaction rate of 3-chlorocatechol monosulfate produced by ASTB-WT and measured at 509 nm, and $\text{Slope}(\text{EV})_{(509 \text{ nm})}$ is the background of the reaction between chlorocatechol monosulfate and 4-AAP measured at 509 nm (using empty vector pET22b(+) as control); $\text{Slope}(\text{Variant})_{(405 \text{ nm})}$ is the formation rate of *p*-NP catalyzed by ASTB variant and measured at 405 nm, and $\text{Slope}(\text{WT})_{(405 \text{ nm})}$ is the formation rate of *p*-NP catalyzed by ASTB-WT and measured at 405 nm, and $\text{Slope}(\text{EV})_{(405 \text{ nm})}$ is the background of *p*-NP formation measured at 405 nm (using empty vector pET22b(+) as control).

In total, 234 variants (13 %) were identified with a higher 3-chlorocatechol sulfation activity compared to ASTB-WT (>1.1-fold) under screening conditions. 1526 (87 %) of the ASTB variants displayed similar or less activity compared to ASTB-WT (≤ 1.1 -fold). The identified 234 variants were rescreened in four replicates to determine the 23 most promising ASTB variants (≥ 1.3 -fold) with increased 3-chlorocatechol sulfation activity (

Table 2). Finally, variant ASTB-M5 (V430A) was randomly chosen for further characterization.

Table 2. Sequencing results of beneficial ASTB variants from Phase 1 (obtained after the screening of the SeSaM library). All ASTB variants had an activity improvement in the range of 1.3-1.6.

No.	ASTB variant	Substitution
1	ASTB-M1	L225Q
2	ASTB-M2	K533E
3	ASTB-M3	N612D
4	ASTB-M4	F22S; L622Q
5	ASTB-M5	V430A
6	ASTB-M6	Q191R; T393I
7	ASTB-M7	V199A; K371E
8	ASTB-M8	Y218H; E373G
9	ASTB-M9	I71T
10	ASTB-M10	I398V
11	ASTB-M11	R552H
12	ASTB-M12	R600C
13	ASTB-M13	A448V; E542G
14	ASTB-M14	F512L; A582V
15	ASTB-M15	E380G; A410V; F551L

2.4.4.2 Characterization of ASTB-WT and ASTB-M5

In order to validate that the *p*-NPS-4-AAP screening system is capable to identify ASTB variants with improved specific activity and transfer efficiency, the ASTB-M5 (ASTB-V430A) was purified, subjected to kinetic studies and compared to ASTB-WT. Kinetic parameters (k_{cat} and K_M values) of ASTB-WT and ASTB-M5 were determined by measuring initial *p*-NP formation rate and using the Michaelis-Menten model (**Figure 18**). The turnover number ($k_{cat} = 41 \pm 2 \text{ s}^{-1}$) and catalytic efficiency ($k_{cat}/K_M = 0.41 \mu\text{M}^{-1} \text{ s}^{-1}$) of ASTB-M5 were 2.4 and 2.3 times improved compared to ASTB-WT ($k_{cat} = 17 \pm 2 \text{ s}^{-1}$, $k_{cat}/K_M = 0.18 \mu\text{M}^{-1} \text{ s}^{-1}$).

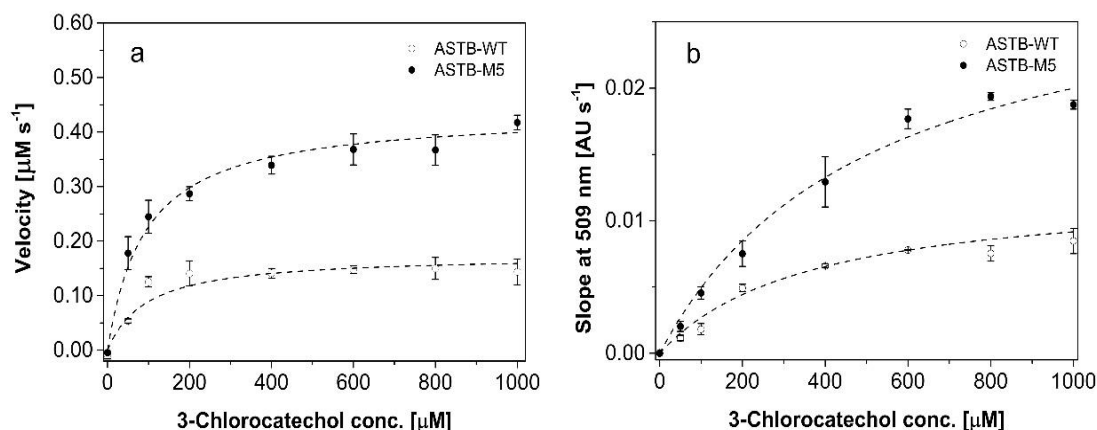


Figure 18. Kinetic curves of ASTB-WT and ASTB-M5. a) Kinetic curves of ASTB-WT (white circles) and ASTB-M5 (black circles) measured at 405 nm; b) rate of product formation from catalyzed by ASTB-WT (white circles) and ASTB-M5 (black circles) determined at 509 nm.

2.4.4.3 Product identification of 3-chlorocatechol sulfation

Enzymatic long-term conversions of purified ASTB-WT and ASTB-M5 (V430A) were investigated by HPLC-PDA/MS and regioselectivity was determined by NMR. Reaction components were separated via a HILIC column and detected by PDA/MS. **Figure 19** shows the retention time of sulfate donor *p*-NPS (11.6 min), product monosulfated 3-chlorocatechol (13.2 min), by-product *p*-NP (16.9 min), and sulfate acceptor 3-chlorocatechol (18.0 min). Based on the HPLC-PDA/MS analysis, ASTB-M5 achieved a conversion of 17 % while ASTB-WT was able to sulfate only 6 % of 3-chlorocatechol after 12 h (calculated by peak area at 13.2 min, **Figure 19**). After a reaction period of 7 days, ASTB-M5 achieved a conversion of 58 % while ASTB-WT was able to sulfate 29 % of 3-chlorocatechol, indicating a 2.0-fold increased conversion of ASTB-M5 compared to ASTB-WT. ESI-MS measurement of ASTB-M5 sulfation identified a high abundance at $m/z = 224.4$ (**Figure 20**), which corresponds to the theoretical mass of the monosulfated product ($m/z = 224.0$). No double sulfation product was observed in MS.

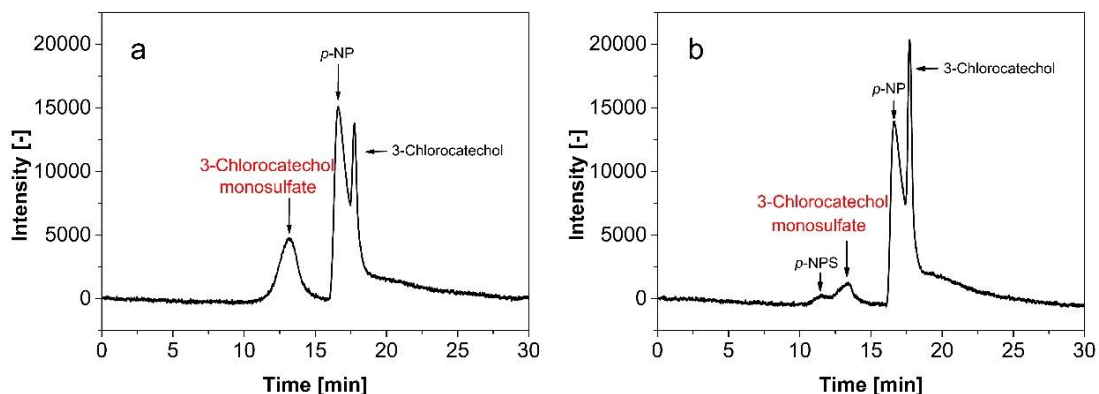


Figure 19. HPLC chromatography of 3-chlorocatechol conversion after 12 h by a) ASTB-M5 and by b) ASTB-WT. Peaks were identified at 280 nm by a PDA detector: 11.6 min *p*-NPS, 13.2 min 3-chlorocatechol-monosulfate, 16.9 min *p*-NP, and 18.0 min 3-chlorocatechol.

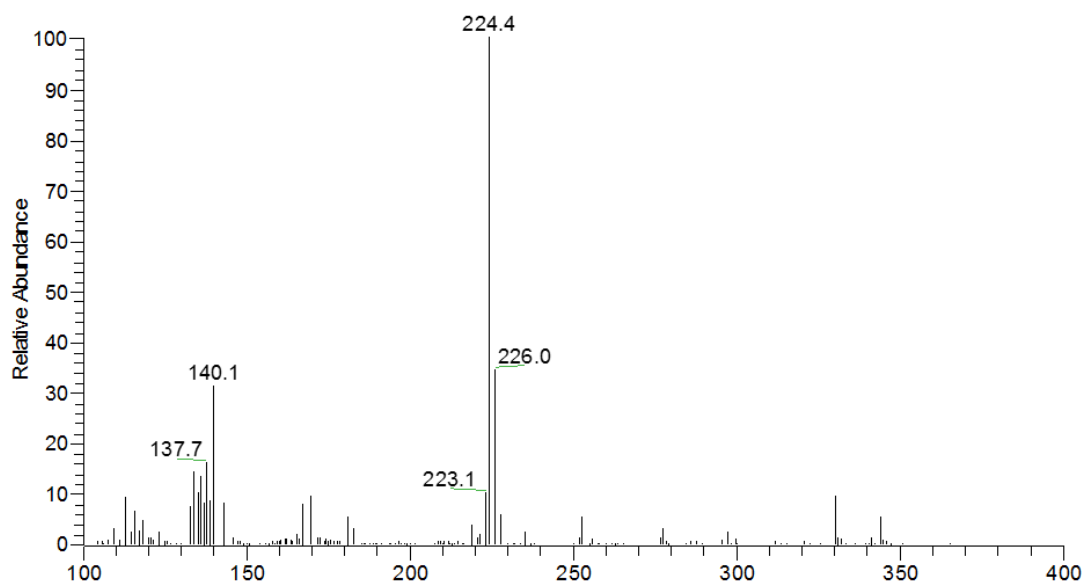


Figure 20. Electrospray ionization mass spectroscopic analysis of 3-chlorocatechol. (negative mode) of enzymatic conversion of 3-chlorocatechol by ASTB-M5 (3-chlorocatechol monosulfate: $m/z=224.4$, theoretical mass: $m/z=224.0$).

2.4.4.4 Broadening the substrate scope of ASTB toward other catechols

Five additional catechols (catechol, 3-methylcatechol, 3-methoxycatechol, 3-fluorocatechol, and 3-bromocatechol) were investigated to explore the substrate profile of ASTB-M5 and answer the question whether the activity of ASTB-M5 is also improved toward other catechols (**Table 3**). As a general trend, ASTB-M5 exhibits higher catalytic efficiency toward all investigated catechols. The turnover number (k_{cat}) of ASTB-M5 was improved between 2.4 and 4.5 times depending on the selected catechol (**Table 3**). The highest improvement of k_{cat} value (4.5-fold) achieved by ASTB-M5 was determined for 3-fluorocatechol as acceptor (ASTB-M5: $107 \pm 8 \text{ s}^{-1}$ and ASTB-WT: $24 \pm 2 \text{ s}^{-1}$). The highest

improvement (2.3-fold) in catalytic efficiency achieved by ASTB-M5 was also observed for 3-fluorocatechol as acceptor (ASTB-M5: $0.41 \mu\text{M}^{-1} \text{s}^{-1}$ and ASTB-WT: $0.18 \mu\text{M}^{-1} \text{s}^{-1}$). The product quantification for all five catechols was carried out by HPLC-MS. In all conversions only monosulfated catechols were obtained (**Figure 21**). Among the additional five selected catechols, the “highest” improvements in conversion were achieved for catechol (1.7-fold; ASTB-M5: $43 \pm 6 \%$ and ASTB-WT: $25 \pm 1 \%$, **Table 4**).

Table 3. Substrate profile and kinetic characterization of six converted catechols by ASTB-WT and ASTB-M5.

Acceptors	ASTB-WT			ASTB-M5		
	k_{cat} [s ⁻¹]	K_M [μM]	k_{cat}/K_M [$\mu\text{M}^{-1} \text{s}^{-1}$]	k_{cat} [s ⁻¹]	K_M [μM]	k_{cat}/K_M [$\mu\text{M}^{-1} \text{s}^{-1}$]
Catechol	46 ± 2	52 ± 13	0.88	169 ± 13	132 ± 17	1.28
3-Methylcatechol	51 ± 3	106 ± 18	0.48	197 ± 11	269 ± 35	0.73
3-Methoxycatechol	40 ± 4	255 ± 12	0.16	108 ± 3	412 ± 25	0.26
3-Fluorocatechol	24 ± 2	131 ± 6	0.18	107 ± 8	257 ± 6	0.42
3-Chlorocatechol	17 ± 2	95 ± 2	0.18	41 ± 2	101 ± 2	0.41
3-Bromocatechol	11 ± 1	55 ± 4	0.20	34 ± 1	137 ± 3	0.25

Table 4. ASTB-WT and ASTB-M5 catalyzed conversions of six catechols.

Acceptors	Conversion (%)*		Improvement [fold]
	ASTB-WT	ASTB-M5	
Catechol	25 ± 1	43 ± 6	1.7
3-Methylcatechol	25 ± 2	31 ± 4	1.2
3-Methoxycatechol	23 ± 1	32 ± 2	1.4
3-Fluorocatechol	18 ± 4	29 ± 1	1.6
3-Chlorocatechol	29 ± 1	58 ± 1	2.0
3-Bromocatechol	31 ± 2	48 ± 7	1.5

*Conversion was determined with 10 mM catechols, 1 mM *p*-NPS, and 1 μM ASTB-WT/ASTB-M5 after 7 days' reaction. Values were obtained by triplicate experiments.

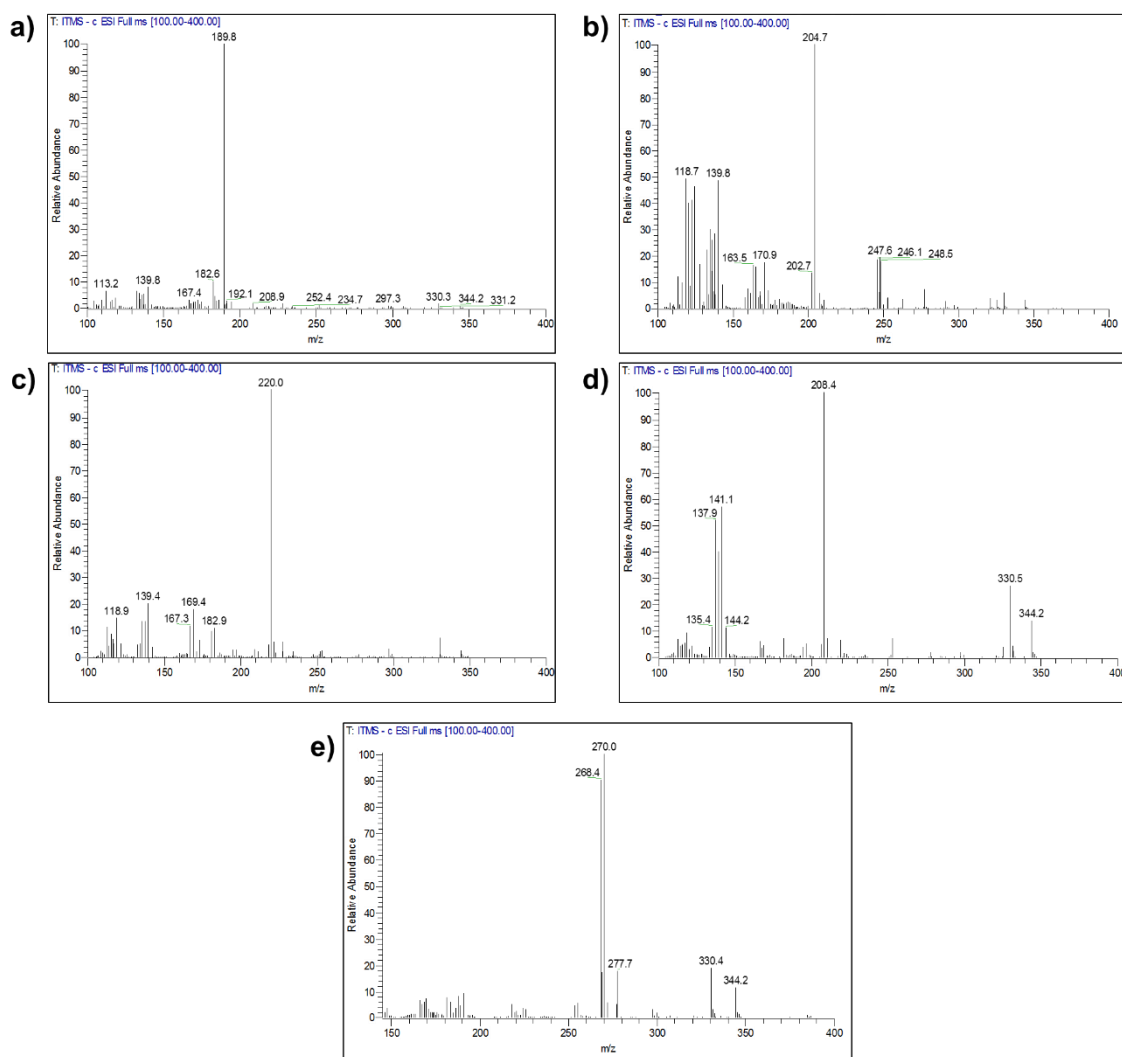


Figure 21. Electrospray ionization mass spectroscopic analysis. a) electrospray ionization mass spectroscopic analysis (negative mode) of enzymatic conversion of catechol by ASTB-M5 (catechol monosulfate: $m/z=189.8$; theoretical mass: $m/z=190.0$). The Mass spectrum of ASTB-WT is nearly identical to ASTB-M5; b) electrospray ionization mass spectroscopic analysis (negative mode) of enzymatic conversion of catechol by ASTB-M5 (3-methylcatechol monosulfate: $m/z=204.7$; theoretical mass: $m/z=204.0$). The Mass spectrum of ASTB-WT is nearly identical to ASTB-M5; c) electrospray ionization mass spectroscopic analysis (negative mode) of enzymatic conversion of 3-methoxycatechol by ASTB-M5 (3-methoxycatechol monosulfate: $m/z=220.0$; theoretical mass: $m/z=220.0$). The Mass spectrum of ASTB-WT is nearly identical to ASTB-M5; d) electrospray ionization mass spectroscopic analysis (negative mode) of enzymatic conversion of 3-fluorocatechol by ASTB-M5 (3-fluorocatechol monosulfate: $m/z=208.4$; theoretical mass: $m/z=208.0$). The Mass spectrum of ASTB-WT is nearly identical to ASTB-M5; e) electrospray ionization mass spectroscopic analysis (negative mode) of enzymatic conversion of 3-bromocatechol by ASTB-M5 (3-bromocatechol monosulfate: $m/z=268.4$; theoretical mass: $m/z=268.0$). The Mass spectrum of ASTB-WT is nearly identical to ASTB-M5.

2.4.5 KnowVolution campaign towards catechols

Screening of an ASTB-SeSaM library identified novel and beneficial substitutions and structural analysis revealed that the loop region of ASTB surrounding the conserved residue H220 (one of four active site residues) might have an important role in the catalytic

performance of ASTB. A KnowVolution campaign comprised of four phases was pursued to confirm the role of loop12 and loop13 and to identify key amino acid positions (**Figure 22**).

2.4.5.1 Identification of potential beneficial positions

A random mutagenesis ASTB-SeSaM library was screened (1760 clones) using the developed *p*-NPS-4-AAP screening system to ensure an excellent sulfation stoichiometry as previously reported^[66]. Fifteen variants with an improved 3-chlorocatechol sulfation activity (≥ 1.3 -fold) were sequenced. In total, 23 positions were identified that potentially improve ASTB activity (**Table 5**). In a dimeric structural model of ASTB, the positions H220, H283, R301, and H350 were identified as active site residues^[63]. These positions can be classified into four groups (**Figure 22& Figure 23**): (1) positions in loop region close to the active site residue H220 (loop12: Q191 and V199; loop13: Y218 and L225); (2) positions close to catalytic center H350 (T393, I398, V430, A448, N612, L622); (3) positions in loop22 and loop24 regions (loop22: K371, E373, and E380; loop24: A410); and (4) positions in the dimer interface (I71, F512, K533, E542, and A582).

Table 5. Sequencing results of beneficial ASTB variants from Phase 1 (obtained after the screening of the SeSaM library). All ASTB variants had an activity improvement in the range of 1.3-1.6.

No.	ASTB variant	Substitution
1	ASTB-M1	L225Q
2	ASTB-M2	K533E
3	ASTB-M3	N612D
4	ASTB-M4	F22S; L622Q
5	ASTB-M5	V430A
6	ASTB-M6	Q191R; T393I
7	ASTB-M7	V199A; K371E
8	ASTB-M8	Y218H; E373G
9	ASTB-M9	I71T
10	ASTB-M10	I398V
11	ASTB-M11	R552H
12	ASTB-M12	R600C
13	ASTB-M13	A448V; E542G
14	ASTB-M14	F512L; A582V
15	ASTB-M15	E380G; A410V; F551L

elements are given as α -helices (α), β -sheets (β), loop (l). The sequence number of α -helices, β -sheets, and loop are named by continuous letter more than 3.

2.4.5.2 Determination of beneficial variants

Four positions (191, 199, 218, and 225) in loop12 and loop13 close to active site residue H220 were selected for mutagenesis and each position was saturated by site-saturation mutagenesis (SSM, NNK codon). After screening these four SSM libraries (library size: 188 variants each), all of them were identified as beneficial positions with up to 2.4-fold improvement (Q191L: 1.6-fold, V199S: 2.4-fold, Y218A: 2.2-fold, L225V: 2.4-fold, **Table 6**). Among them, the substitutions Q191R, V199A, and Y218H were also identified by screening the SeSaM library.

Table 6. Beneficial positions and substitutions with improved sulfation activity.

Position	Substitutions	Improvement
Q191	Q191L	1.6
	Q191R	1.1
V199	V199S	2.4
	V199A	1.5
Y218	Y218A	2.2
	Y218H	1.1
L225	L225V	2.4
	L225K	1.8

2.4.5.3 Selection of beneficial positions

Based on the former generated dimeric structural model of ASTB-WT, molecular docking of 3-chlorocatechol and evolutionary conservation analysis of residues in ASTB were performed. In docking study, positions T145, P146, L147, Y184, L182, G180, L183, R181, V197, Y218, and E243 were suggested as beneficial positions around the active site (**Figure 24a**). The positions G180, H219, H220, D221, S234, E243, H283, N284, N285, A286, R301, H350, and Y416 are conserved and are therefore excluded from mutagenesis studies (**Figure 24b**). Interestingly, the beneficial position Y218 located in loop13 was identified in the experimental as well as docking studies (**Figure 22& Figure 24a**). The importance of the loop region engineering has been reported for other enzymes, e.g., the multi-site substitution A285P/A310R/A312E/A318G in loopL1 of laccase lcc2 from *T. versicolor* obtained 8.4-fold increased laccase activity in EMIM EtSO₄^[145, 160-164].

Therefore, Q191, V199, Y218, and L225 were selected for a multiple-site saturation study to investigate the synergistic effects.

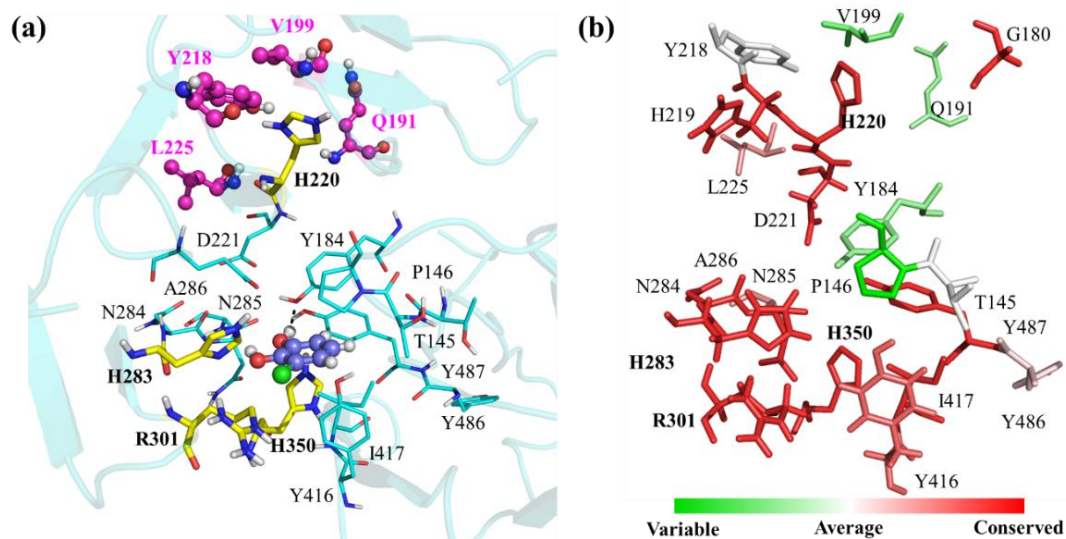


Figure 24. Molecular docking study and conservation analysis. a) Molecular docking pose of 3-chlorocatechol using the dimeric structural model of ASTB^[63]. Monomers are highlighted in green and cyan. In a zoomed view of the active site, catalytic histidine (H350) and key residues (H220, H283, and R301) forming together the active site are shown in yellow sticks and labeled with bold letters. Hydrogen bond between 3-chlorocatechol and Y184 is highlighted with a tiny black dotted line. 3-Chlorocatechol is shown as ball and stick whereas other residues in the active site apart from catalytic residues are shown in cyan. The experimentally and rationally selected positions (Q191, V199, Y218, and L225) are highlighted in magenta as ball and sticks representation. b) Evolutionary conservation analysis of active site residues of ASTB was performed using the ConSurf online server. Amino acid conservation scores are shown using the color-coding bar (1-9 scale) in which highly variable and highly conserved residues are shown in turquoise and maroon, respectively.

2.4.5.4 Recombination of beneficial positions

2.4.5.4.1 Generation of ASTB OmniChange library

Simultaneous multiple site saturation mutagenesis of positions Q191, V199, Y218, and L225 of ASTB was performed by the OmniChange method^[59]. In this approach, ASTB OmniChange library was generated by using ASTB-WT plasmid as template and simultaneous saturation of selected four target positions was performed as explained in section 2.3.4. In the first step, totally three DNA fragments (Fragment A; Fragment B; Fragment C) was generated by PCR amplification for introducing NNK-saturated codon in four targeted positions. Fragment A covers positions Q191 and L199 (93 bp) were verified on 2 % agarose gel; fragment B includes position Y218 (3622 bp), fragment contains position L225 (3627 bp) were verified on 1 % agarose gel (**Figure 25**). Then, these three PCR products were purified, cleaved and assembled. Finally, the hybridization mix was transformed into *E. coli* BL21 Gold (DE3) cells and 1760 clones were saved as ASTB

OmniChange library. Verification of the correct assembly was performed by colony PCR and sequencing of nine randomly picked colonies (**Table 7**). Sequencing results show that all picked and sequenced ASTB variants were unique.

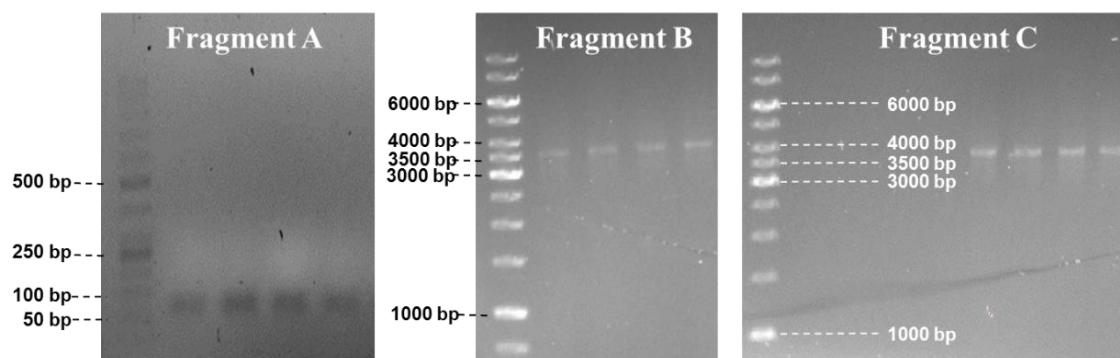


Figure 25. Agarose gel analysis of DNA fragments for ASTB OmniChange library generation. Fragment A (93 bp): contains positions Q191 and L199; Fragment B (3622 bp): contains position Y218; fragment C (3627 bp): contains positions L225.

Table 7. Sequencing results of nine randomly picked clones from the ASTB OmniChange library.

	Q191	V199	Y218	L225
Clone 1	W (CAG→TGG)	P (GTT→CCT)	G (TAT→GGG)	Q (CTG→CAG)
Clone 2	E (CAG→GAG)	V (GTT→GTT)	F (TAT→TTT)	R (CTG→CGG)
Clone 3	R (CAG→CGG)	L (GTT→CTG)	Stop (TAT→TAG)	N (CTG→AAT)
Clone 4	R (CAG→CGG)	V (GTT→GTG)	L (TAT→TTG)	L (CTG→CTT)
Clone 5	Q (CAG→CAG)	V (GTT→CTT)	M (TAT→ATG)	Q (CTG→CTG)
Clone 6	G (CAG→GGT)	V (GTT→CTG)	Y (TAT→TAT)	L (CTG→TTA)
Clone 7	H (CAG→CAT)	C (GTT→TGT)	L (TAT→TTG)	L (CTG→CTG)
Clone 8	M (CAG→ATG)	W (GTT→TGG)	Y (TAT→TAT)	L (CTG→CTG)
Clone 9	Q (CAG→CAG)	V (GTT→CTT)	Y (TAT→TAT)	L (CTG→CTT)

2.4.5.4.2 Screening of ASTB OmniChange library

In total 1760 clones were screened through the two-step *p*-NPS-4-AAP screening system using 3-chlorocatechol as substrate and 145 active clones (≥ 1.1 -fold, 8 % active) were rescreened toward improved catechol sulfation activity. Amino acid substitutions of the 10 “best” ASTB variants with ≥ 1.5 times higher activity compared to ASTB-WT are shown in **Table 8**.

Substitutions in position 191 showed a strong preference toward a positively charged or hydrophobic amino acid (2×R, 1×H; 2×W, 2×Y, 1×L, 1×A). At position 199 a strong preference toward the hydrophobic amino acid L was observed (occurred four times). At position 218 a strong preference toward a substitution to tryptophan (occurred three times) was observed which is only encoded by a single codon. Position 225 showed no preference in respect to chemical properties of side chains (e.g. 1×V, 1×R, 1×C, 1×Q). Interestingly, substitution V199R resulted in significantly increased sulfation activity (see comparison ASTB-OM1 (Q191R/V199R/Y218L) and ASTB-OM10 (Q191R/V199C/Y218L) in **Table 8**). Finally, the top three ASTB variants (ASTB-OM1, ASTB-OM2, and ASTB-OM3) were chosen for further characterization.

Table 8. Sequencing results of the ten most beneficial ASTB variants found after rescreening of the OmniChange library.

ASTB variant	Substitution				Improvement*
	Q191	V199	Y218	L225	
ASTB-OM1	R	R	L	-	2.6
ASTB-OM2	Y	-	W	V	2.9
ASTB-OM3	A	Y	-	-	3.5
ASTB-OM4	W	L	H	R	2.3
ASTB-OM5	Y	S	F	-	1.8
ASTB-OM6	L	-	W	-	1.7
ASTB-OM7	W	L	-	C	1.5
ASTB-OM8	G	L	F	-	1.5
ASTB-OM9	H	L	W	Q	1.5
ASTB-OM10	R	C	L	-	1.5

*Improvement was calculated using a previously reported equation^[66].

2.4.5.5 Characterization of ASTB-WT and ASTB-OM1/ASTB-OM2/ASTB-OM3

The three most beneficial ASTB variants (ASTB-OM1 (Q191R/V199R/Y218L), ASTB-OM2 (Q191Y/Y218W/L225V), and ASTB-OM3 (Q191A/V199Y)) were produced and purified for kinetic characterization (**Table 9**). Kinetic parameters such as catalytic activity (k_{cat}), Michaelis Menten constant (K_M), and catalytic efficiency (k_{cat}/K_M) were calculated based on initial *p*-NP formation rate at varying substrate concentrations. The kinetic constants of ASTB variants and ASTB-WT for sulfation of 3-chlorocatechol are shown in **Table 9**. All three ASTB variants had enhanced k_{cat} values and improved catalytic efficiencies for 3-chlorocatechol sulfation. For instance, ASTB-OM3 reached an initial k_{cat} value of 202 s^{-1} , which is 12 times faster than ASTB-WT (17 s^{-1}). Among all the variants, ASTB-OM2 obtained the highest catalytic efficiency ($0.82 \mu\text{M}^{-1} \text{ s}^{-1}$) which was 4.6-fold improved compared to ASTB-WT.

Table 9. Kinetic characterization of 3-chlorocatechol by ASTB-WT and variants.

ASTB variant	k_{cat} [s ⁻¹]	K_M [μM]	k_{cat}/K_M [μM ⁻¹ s ⁻¹]
ASTB-WT	17 ± 2	95 ± 2	0.18
ASTB-OM1	136 ± 11	257 ± 63	0.53
ASTB-OM2	179 ± 7	217 ± 32	0.82
ASTB-OM3	202 ± 6	570 ± 53	0.35

ASTB-OM2 was finally selected for conversions studies with six catechols due to its process robustness. Apart from 3-chlorocatechol, five additional catechols (catechol, 3-methylcatechol, 3-methoxycatechol, 3-fluorocatechol, and 3-bromocatechol) were investigated with ASTB-WT and ASTB-OM2 to determine the general applicability of the identified substitutions. Variant ASTB-OM2 proved to be faster than ASTB-WT for all six investigated substrates; k_{cat} improvements ranged from 6.1 to 13.6-fold (**Table 10**). More than 10 times increased k_{cat} values were observed in case of catechol and halogenated catechols (3-fluorocatechol, 3-chlorocatechol, and 3-bromocatechol; 11.7-fold, 10.1-fold, 10.5-fold, and 13.6-fold respectively).

Table 10. Kinetic characterization of ASTB-WT and ASTB-OM2 for six converted catechols to explore their substrate profile and general importance of the identified substitutions.

Acceptors	ASTB-WT			ASTB-OM2		
	k_{cat} [s ⁻¹]	K_M [μM]	k_{cat}/K_M [μM ⁻¹ s ⁻¹]	k_{cat} [s ⁻¹]	K_M [μM]	k_{cat}/K_M [μM ⁻¹ s ⁻¹]
Catechol	46 ± 2	52 ± 13	0.88	538 ± 18	306 ± 35	1.80
3-Methylcatechol	51 ± 3	106 ± 18	0.48	421 ± 12	272 ± 24	1.50
3-Methoxycatechol	40 ± 4	255 ± 12	0.16	243 ± 12	422 ± 77	0.58
3-Fluorocatechol	24 ± 2	131 ± 6	0.18	242 ± 9	455 ± 47	0.52
3-Chlorocatechol	17 ± 2	95 ± 2	0.18	179 ± 7	217 ± 32	0.82
3-Bromocatechol	11 ± 1	55 ± 4	0.20	150 ± 7	137 ± 27	1.10

2.4.5.6 Analysis of catechol sulfation by the Hammett equation

To evaluate the effect of electrophilic aromatic substitutions on the reaction rate, the Hammett equation was applied^[165-167]. In **Figure 26**, nonlinear Hammett plots consisting of two intersecting straight trend lines were observed for both ASTB-WT and variant ASTB-OM2. Linear correlations of the logarithmic ratios of rate constants $\log(k/k_0)$ with Hammett σ -values were obtained for these four trend lines (k represent the k_{cat} value of catechol derivatives, k_0 is the k_{cat} value of catechol). Both enzymes exhibit negative slopes (substitution constant for ASTB-WT: $\rho_1 = -0.57$, $\rho_2 = -5.83$; and for ASTB-OM2: $\rho_1 = -0.57$, $\rho_2 = -3.70$, respectively).

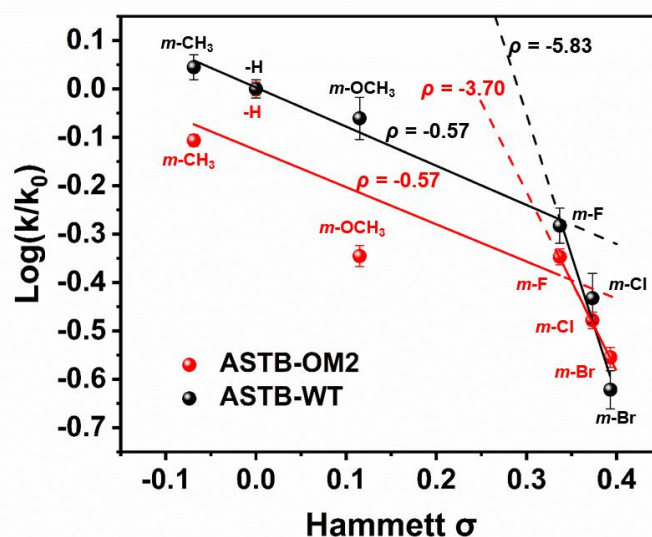


Figure 26. Hammett plots for the sulfation reaction of meta- substituted catechol (ASTB-WT : $y_1 = -0.57x_1 + 0.01$, $R^2 = 0.99$ / $y_2 = -5.83x_2 + 1.69$, $R^2 = 0.95$; ASTB-OM2: $y_1 = -0.57x_1 - 0.19$, $R^2 = 0.71$ / $y_2 = -3.70x_2 + 1.70$, $R^2 = 0.99$).

2.4.5.7 Determination of sulfated products in 24 h conversions to improve the sulfate transfer stoichiometry

Conversions of purified ASTB-WT and ASTB-OM2 toward catechols were determined by HPLC-MS (See **Figure 27**) analysis. After a reaction period of 24 h, ASTB-OM2 achieved sulfate transfer efficiency of 40-94 % to all six catechols while ASTB-WT reached between 16-53 %, (**Table 11**). The “highest” improvements in sulfate stoichiometry were achieved for 3-methylcatechol (3.9-fold; ASTB-OM2: 94 ± 3 % vs. ASTB-WT: 24 ± 2 %, **Table 12**).

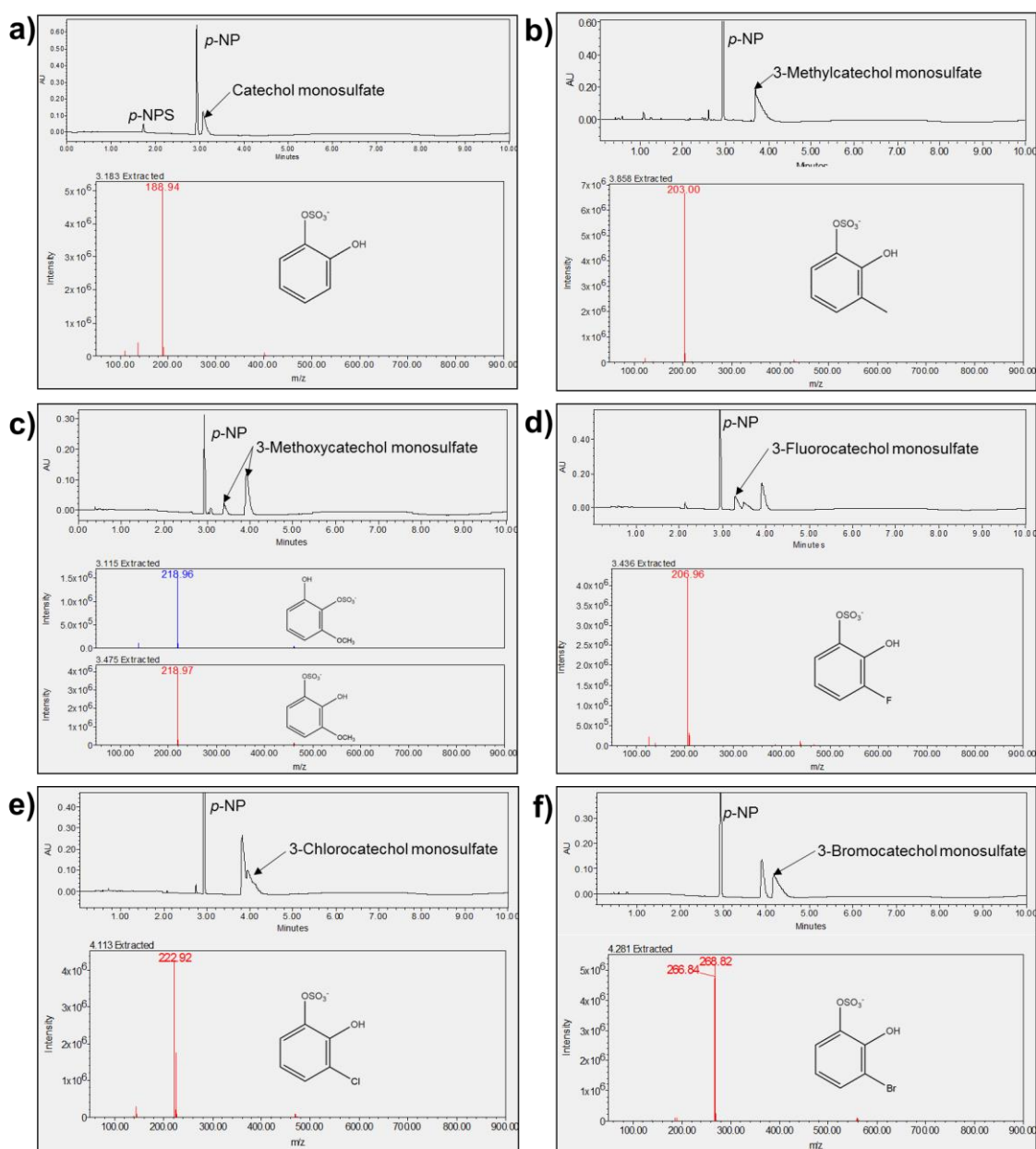


Figure 27. HPLC-MS analysis of enzymatic sulfation of catechols. a) HPLC-MS analysis of enzymatic sulfation of catechol by ASTB-OM2 (negative mode: catechol monosulfate: $m/z=188.9$; theoretical mass: $m/z=189.0$); b) HPLC-MS analysis of enzymatic sulfation of 3-methylcatechol by ASTB-OM2 (negative mode: 3-methylcatechol monosulfate: $m/z=203.0$; theoretical mass: $m/z=$

203.0); c) HPLC-MS analysis of enzymatic sulfation of 3-methoxycatechol by ASTB-OM2 (negative mode: 3-methoxycatechol monosulfate: $m/z=219.0$; theoretical mass: $m/z=219.0$); d) HPLC-MS analysis of enzymatic sulfation of 3-fluorocatechol by ASTB-OM2 (negative mode: 3-fluorocatechol monosulfate: $m/z=207.0$; theoretical mass: $m/z=207.0$); e) HPLC-MS analysis of enzymatic sulfation of 3-chlorocatechol by ASTB-OM2 (negative mode: 3-chlorocatechol monosulfate: $m/z=222.9$, theoretical mass: $m/z=223.0$); f) HPLC-MS analysis of enzymatic sulfation of 3-bromocatechol by ASTB-OM2 (negative mode: 3-bromocatechol monosulfate: $m/z=266.8/268.8$; theoretical mass: $m/z=267.0/269.0$).

In all conversions catalyzed by ASTB-OM2, the HPLC-MS data shows that only monosulfated catechols and no disulfated products were obtained in case of 3-methylcatechol, 3-fluorocatechol, 3-chlorocatechol, and 3-bromocatechol (always the 1-hydroxyl group). The latter was also previously reported for 3-chloro-1-catecholsulfate by $^1\text{H-NMR}$ analysis^[66]. However, one exception is 3-methoxycatechol which shows a ratio of 84:16 for sulfation of the 1-hydroxyl group over the 2-hydroxyl group.

Table 11. Results on sulfation stoichiometry of ASTB-WT and ASTB-OM2 for six catechols. Conversions are calculated from the amount of sulfated catechols in respect to employed *p*-NPS.

Acceptors	Sulfate transfer efficiency (%)	
	ASTB-WT ^[66]	ASTB-OM2
Catechol	27 ± 2	82 ± 2
3-Methylcatechol	24 ± 2	94 ± 3
3-Methoxycatechol	16 ± 2	40 ± 2
3-Fluorocatechol	53 ± 2	92 ± 4
3-Chlorocatechol	47 ± 3	73 ± 4
3-Bromocatechol	45 ± 2	70 ± 2

In all conversions, 1 mM catechols, 1 mM *p*-NPS, and 1 μM ASTBWT/ASTB-OM2 was used (dissolved in 100 mM Tris-HCl buffer, pH 9.0). The conversions were performed at room temperature and sulfate transfer efficiency was determined after 24 h reaction time. Sulfate transfer efficiencies were calculated from the amount of sulfated catechols with respect to the employed *p*-NPS. The reported values and deviations correspond to the average values of triplicates

2.4.5.8 Computational analysis

Molecular docking studies of 3-chlorocatechol were carried out to understand the influence of substitutions on the catalytically competent docking poses of the catechols (acceptor) in the binding pocket of ASTB. Studies revealed that the 3-chlorocatechol binds close to the catalytic residue H350 as shown in **Figure 24a**. 3-Chlorocatechol forms a hydrogen bond with the Y184 residue and interacts further with the residues (T145, P146,

Y184, D221, A286, Y285, N284, Y416, I417, Y486 and Y487) (**Figure 24a**). These residues are located in the vicinity of the catechol substrates and can partially provide hydrophobic interactions.

Variant ASTB-OM2 shows higher binding energies (approx. -2.17 to -4.09 kcal mol⁻¹; **Table 12**) for all six catechol substrates when compared to wild type (WT) (around -0.15 to -3.22 kcal mol⁻¹). The observed trend in binding energies of 3-substituted catechol has the following order: 3-methylcatechol > 3-fluorocatechol > 3-methylcatechol > 3-chlorocatechol > 3-bromocatechol. The observed trend in binding energies of 3-substituted catechol with ASTB-OM2 has the following order: catechol > 3-fluorocatechol > 3-methoxycatechol > 3-methylcatechol > 3-chlorocatechol > 3-bromocatechol, while the observed trend in binding energies of 3-substituted catechols with ASTB-WT has a different order: catechol > 3-fluorocatechol > 3-methylcatechol > 3-chlorocatechol > 3-methoxycatechol > 3-bromocatechol. The molecular docking using substrates in catalytically competent docking poses can be correlated with catalytic efficiency of enzymes and shows a similar trend in improvement (**Table 10** and **Table 12**).

Table 12. Binding energies determined by molecular docking of all six catechol substrates within the binding pocket of ASTB-WT and ASTB-OM2.

Acceptors	Binding energy (kcal mol ⁻¹)	
	ASTB-WT	ASTB OM2
Catechol	-3.22	-4.09
3-Methylcatechol	-2.09	-2.42
3-Methoxycatechol	-0.61	-3.06
3-Fluorocatechol	-3.12	-3.42
3-Chlorocatechol	-1.62	-2.38
3-Bromocatechol	-0.15	-2.17

2.4.6 Expanding substrate scope

The substrate scope was expanded to pharmaceutically important compounds, such as catechol amines^[168-170], flavonoids^[171-173], steroids^[172], and phenolic carboxylic acid derivatives^[174]. Their sulfated form have already been detected as metabolites and always correlated to specific functions^[172]. Totally seven compounds including dopamine, (-)-

epinephrine, quercetin, taxifolin, (-)-epicatechin, resveratrol, and tanshinol (**Figure 28**) was selected for sulfation using ASTB-WT and variant ASTB-OM2 as a catalyst.

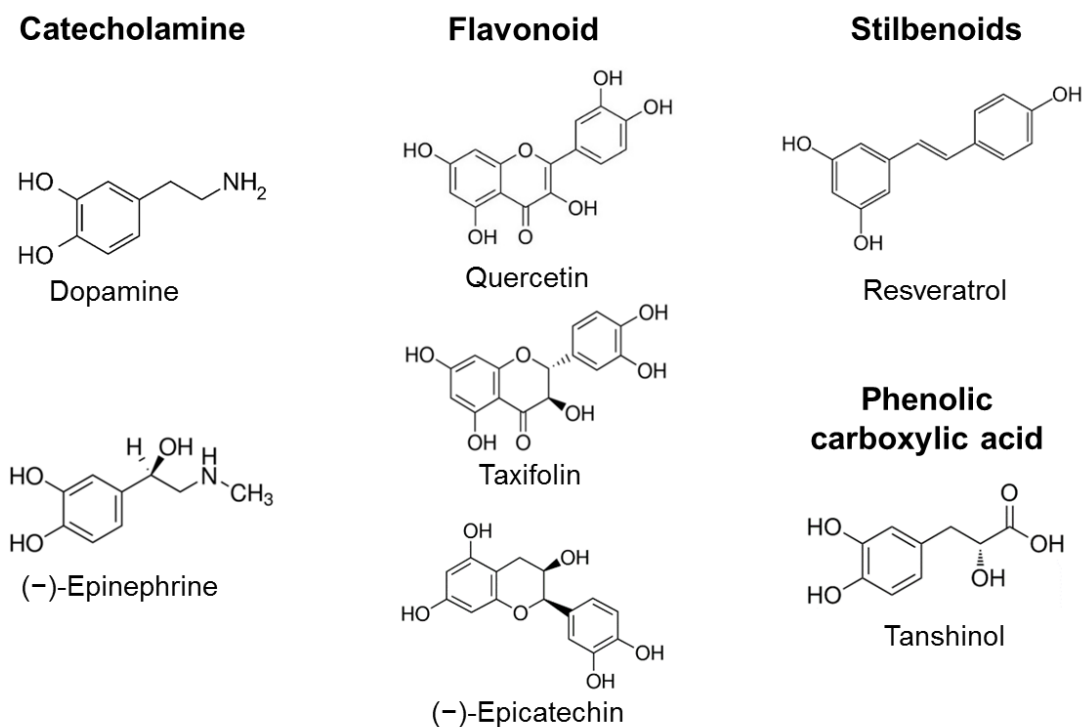


Figure 28. Chemical structure of 7 selected compounds for sulfation study.

MS measurement (**Figure 29**) shows that 5 of them obtained mono sulfation using ASTB-WT/ASTB-OM2 after 24 hour conversion (10 mM substrate, 0.1 μ M enzyme, 10 mM *p*-NPS in Tris-HCl buffer (pH 9)), including dopamine ($m/z= 232.1$, see **Figure 29a**), (-)-epinephrine ($m/z= 262.3$, see **Figure 29b**), tanshinol ($m/z= 276.9$, see **Figure 29c**), taxifolin ($m/z= 383.4$, see **Figure 29d**), and quercetin ($m/z= 381.1$, see **Figure 29e**). All three positions from resveratrol were sulfated and no product formation of (-)-epicatechin was observed from MS analysis.

Among all the mono sulfation reactions, dopamine, tanshinol, taxifolin, and quercetin obtained improved conversions from ASTB-OM2 compared to ASTB-WT, ranging from 2.0-10.0-fold (**Table 13**). The obvious difference after reaction for 24h can be observed in the example of quercetin (**Figure 29f**) and the solubility of quercetin was dramatically improved by introducing a $-SO_3$ group using catalyst ASTB-OM2. Moreover, the kinetic parameters of ASTB-OM2 towards dopamine sulfation was detected with 5.9-fold improvement compared to ASTB-WT (**Table 14**). These results demonstrate the successful engineering of ASTB toward catechol derivatives and variant ASTB-OM2 can be a good candidate for tanshinol sulfation (75 % conversion).

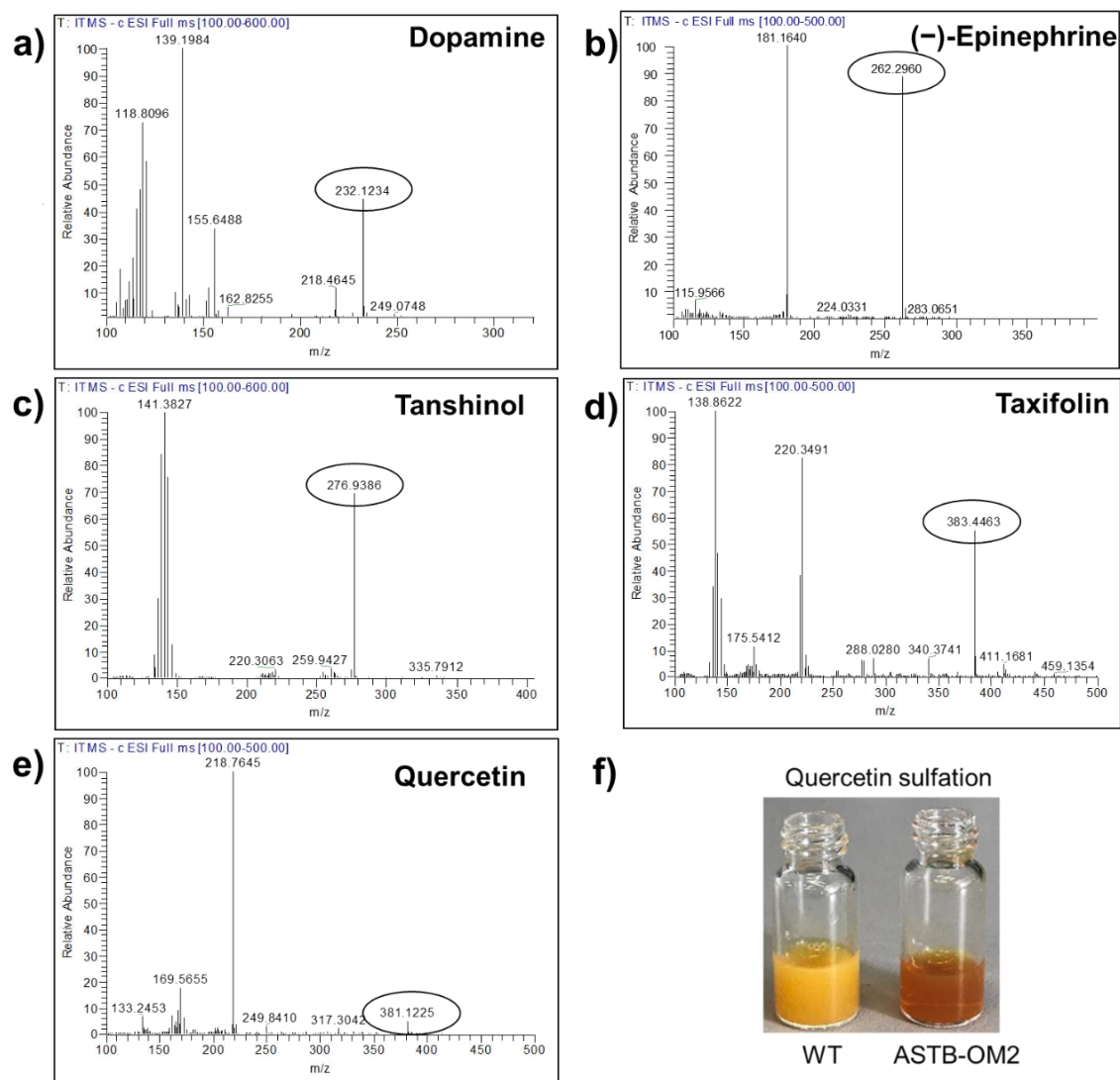


Figure 29. Electrospray ionization mass spectrometry analysis of enzymatic conversion of other compounds. a) Electrospray ionization mass spectrometry analysis (negative mode) of enzymatic conversion of dopamine by ASTB-OM2 (dopamine monosulfate: $m/z=232.1$; theoretical mass: $m/z=232.2$). The Mass spectrum of ASTB-WT is nearly identical to ASTB-OM2; b) electrospray ionization mass spectrometry analysis (negative mode) of enzymatic conversion of (-)-epinephrine by ASTB-OM2 ((-)-epinephrine monosulfate: $m/z=262.3$; theoretical mass: $m/z=262.2$). The Mass spectrum of ASTB-WT is nearly identical to ASTB-OM2; c) electrospray ionization mass spectrometry analysis (negative mode) of enzymatic conversion of tanshinol by ASTB-OM2 (tanshinol monosulfate: $m/z=276.9$; theoretical mass: $m/z=277.2$). The Mass spectrum of ASTB-WT is nearly identical to ASTB-OM2; d) electrospray ionization mass spectrometry analysis (negative mode) of enzymatic conversion of taxifolin by ASTB-OM2 (taxifolin monosulfate: $m/z=383.4$; theoretical mass: $m/z=383.2$). The Mass spectrum of ASTB-WT is nearly identical to ASTB-OM2; e) electrospray ionization mass spectrometry analysis (negative mode) of enzymatic conversion of quercetin by ASTB-OM2 (quercetin monosulfate: $m/z=381.1$; theoretical mass: $m/z=381.2$). The Mass spectrum of ASTB-WT is nearly identical to ASTB-OM2; f) Photo of reaction solution (catalyzed by ASTB-WT/ASTB-OM2) after 24 h reaction.

Table 13. Results on sulfation stoichiometry of ASTB-WT and ASTB-OM2 for dopamine, tanshinol, taxifolin, and quercetin after 24 h. Conversions are calculated from the amount of sulfated catechols in respect to employed *p*-NPS.

Acceptors	Conversions (%)		Improvement [fold]
	ASTB-WT	ASTB-OM2	
Dopamine	2	20	10.0
Tanshinol	33	75	2.3
Taxifolin	12	24	2.0
Quercetin	21	65	3.1

Table 14. Kinetic characterization of ASTB-WT and ASTB-OM2 for dopamine.

Acceptor	ASTB-WT			ASTB-OM2			Improvement of k_{cat} [fold]
	k_{cat} [s^{-1}]	K_M [μM]	k_{cat}/K_M [$M^{-1} s^{-1}$]	k_{cat} [s^{-1}]	K_M [μM]	k_{cat}/K_M [$M^{-1} s^{-1}$]	
Dopamine	18 ± 1	140 ± 34	1.3×10^5	107 ± 7	412 ± 93	2.6×10^5	5.9

2.4.7 Recombination of potential beneficial positions close to catalytic site H350

Previous random SeSaM library screening resulted in six potential beneficial positions (I398, V430, A448, E542, N612, and L622) close to the catalytic center H350 (**Figure 30**). The recombination of beneficial positions always yields variants with higher activity than single point mutations. Catalytic activity is closely related to enzyme thermostability^[175], therefore the relative changes in folding free energy ($\Delta\Delta G^{fold}$) become an important index for enzyme evolvability/performance prediction^[176]. FoldX^[155, 177] as a popular webtool was used here for guidance the recombination of single point mutations and the energy difference between the variants and WT was calculated (**Table 15**).

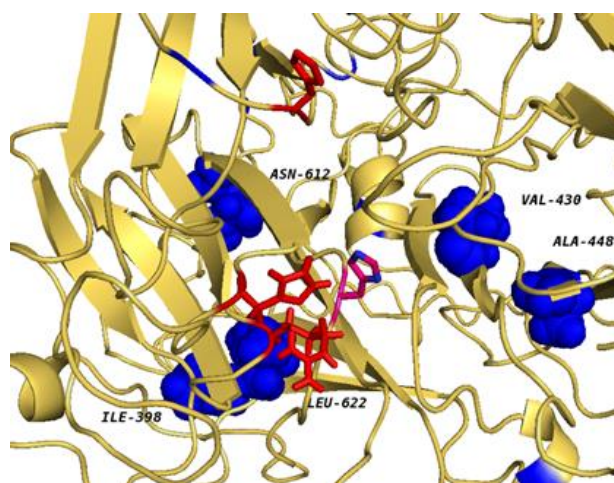
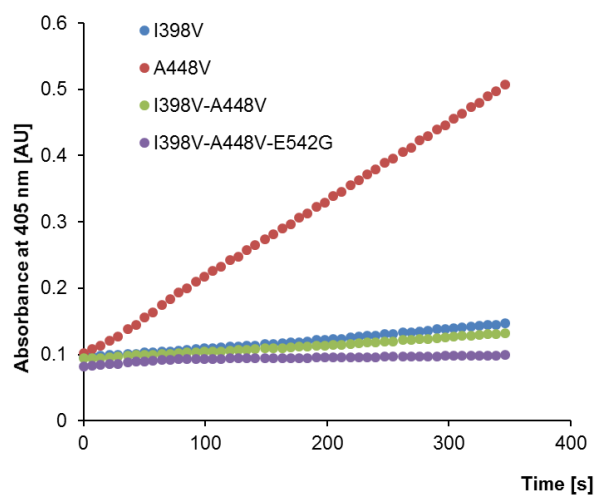
**Figure 30. Six potential beneficial positions (I398, V430, A448, E542, N612, and L622) close to the catalytic center H350.**

Table 15. $\Delta\Delta G$ calculation of recombination of beneficial substitutions.

Substitutions	$\Delta\Delta G^{\text{fold}}$
I398V	-1.5618
V430A	-0.3849
A448V	-3.3266
E542G	-0.6468
N612D	0.4006
L622Q	4.0892
I398V/A448V	-1.1700
I398V/E542G	-0.3849
I398V/N612D	0.7849
A448V/V430A	-0.0517
A448V/E542G	-1.5084
A448V/L622Q	2.8198
N612D/L622Q	4.4898
I398V/A448V/E542G	-1.5618
I398V/A448V/N612D	-0.7646
I398V/E542G/N612D	-1.5084
I398V/N612D/V430A	1.4448
I398V/N612D/V430A/E542G	1.1101

The lowest energy difference was obtained by variant A448V (-3.33) and substitutions I398V, I398V/A448V, I398V/A448V/E542G also observed low $\Delta\Delta G^{\text{fold}}$ value (-1.56, -1.17, -0.38). Therefore these four substitutions (I398V, A448V, I398V/A448V, and I398V/A448V/E542G) are selected for variant generation and purification. Obvious activity differences were seen from the *p*-NPS assay using 3-chlorocatechol as substrate (**Figure 31**) and variant A448V showed the highest activity. The kinetics of variant A448V was also determined and the k_{cat} value was 24 s^{-1} (1.5-fold improvement).

**Figure 31. Activity comparison of four ASTB variants (I398V, A448V, I398V/A448V, and I398V/A448V/E542G).**

2.5 Discussion

Catechols are primary pollutants in wastewater and can result in skin and respiratory tract irritation and highly toxic for human cell lines^[117]. They have been proven to cause DNA damage, vascular collapse, and even death^[118, 119, 122]. Sulfation is an important biological function for detoxification of catechols. Sulfated catechols are for instance known metabolites in human plasma and urine and have potential antioxidant and anti-inflammatory activity^[123-125, 178-180]. Sulfated catechol can be used as biomarkers in many biological activities (e.g. chronic inflammation)^[125, 126, 181]. Sulfated compounds are generally synthesized by chemical means using chlorosulfonic acid or sulfur trioxide trimethylamine; the multi-step syntheses require protection/deprotection strategies which often result in low yields and/or titers^[89]. As chemoselective sulfation is very challenging and often employs organic solvents (tetrachloromethane, 1,2-dichloroethane^[70]), enzymatic synthesis of catechol sulfates using bacterial sulfotransferase ASTB is a synthetically attractive and sustainable route to produce monosulfated catechols in single-step reactions^[66]. Here we report the first synthetic access to chemo- and regioselectively sulfated catechols through the aryl sulfotransferase ASTB from *D. hafniense*. A “green” challenge is the often low stoichiometric transfer efficiency of sulfotransferases and the mediocre specific activities.

A reliable screening system with direct detection of the desired sulfated product is needed to tailor sulfotransferase properties to synthetic demands. Here, a two-step *p*-NPS-4-AAP screening system was established for directed ASTB evolution toward catechols (e.g., 3-chlorocatechol) in 96-well MTP format to tailor ASTB properties. Mainly two screening assays were applied until now in MTP-format for directed PAPS-dependent sulfotransferase evolution (e.g., SULT1A1/SULT1E1) toward *p*-nitrophenol (*p*-NP; colorimetric) and 3-cyano-7-hydroxycoumarin (3CyC; fluorometric;^[46]). Both screening systems quantify sulfotransferase activity through the consumption of the substrate. In order to ensure successful directed evolution campaigns, product-based screening systems are highly desirable as outlined in the introduction^[182]. The developed two-step one-pot assay (*p*-NPS-4-AAP) was validated as product-based screening system in a directed ASTB evolution campaign. Compared to the one-step *p*-NPS assay^[107], an extra step with 4-AAP reaction step was applied. Optimization of the screening parameters comprised background activity, optimum pH value, volume of clarified cell lysate, and linear detection range. Finally, true CVs below 15 % were achieved for the two-step one-pot screening system.

Screening systems with CVs below 15 % are routinely employed in successful direction evolution campaigns^[107, 152]. A single round of evolution yielded ten ASTB variants with improved 3-chlorocatechol sulfation activity (ASTB-M1 to ASTB-M5). The randomly chosen variant ASTB-M5 among the improved ones possesses an amino acid substitution from valine to alanine at position 430 (see **Table 2**).

Turnover number (k_{cat}) and catalytic efficiency (k_{cat}/K_M) of ASTB-M5 showed up to 2.4-fold and 2.3-fold improvement compared to ASTB-WT toward 3-chlorocatechol. The following HPLC-PDA/MS analysis further confirmed the 2.0-fold improved sulfation transfer efficiency of variant ASTB-M5 with a conversion of 58 % (ASTB-WT: 29 %). These findings validate that the *p*-NPS-4-AAP screening system identifies ASTB variants with higher sulfation activity and improved sulfation stoichiometry. MS and NMR data confirmed the excellent chemo- and regioselectivity of ASTB-M5 toward 3-chlorocatechol-1-monosulfate, while ASTB-WT forms both 3-chlorocatechol-1-monosulfate as the main product and 3-chlorocatechol-1,2-disulfate in negligible amounts (see **Figure 13** & **Figure 20**). An aryl sulfotransferase from *Haliangium ochraceum* using PAPS as sulfate donor was reported for sulfation of catechol as well^[100]. However, both hydroxyl-groups of the catechol were sulfated yielding a product mixture of catechol monosulfate and catechol disulfate^[100]. This indicates that reengineering of aryl sulfotransferase using *p*-NPS-4-AAP screening system is able to yield variants with chemo- and regioselectivity. In order to explore the general importance of the substitution V430A, five additional catechols (catechol, 3-methylcatechol, 3-methoxycatechol, 3-fluorocatechol, 3-chlorocatechol, 3-bromocatechol) were investigated. As a general trend, ASTB-M5 showed improved turnover number (k_{cat}) for all six catechols. The highest improvement of k_{cat} value and k_{cat}/K_M value of ASTB-M5 were obtained using 3-fluorocatechol indicating 4.5- and 2.2-fold improvement compared to ASTB-WT, respectively (see **Table 3**). HPLC analysis revealed that the conversion of catechol sulfates catalyzed by ASTB-M5 can reach from 29 % (3-fluorocatechol) to 58 % (3-chlorocatechol) (see **Table 4**).

The coupling efficiency of product formation to *p*-NPS consumption was determined by HPLC analysis for the ASTB-WT and variant ASTB-M5 (**Table 16**). ASTB-M5 had an improved coupling efficiency compared to the WT for all six investigated compounds. Furthermore, the computational analysis showed that the targeted position V430 is located close to the substrate-binding pocket of ASTB. A dimeric structural model of ASTB was reported and the H220, H283, H350, and R301 were identified as the catalytic and active site residues^[63]. The substitution of valine with alanine in ASTB-M5 variant introduces

side-chain flexibility of Y423 and R490 residues near to the binding pocket as shown in **Figure 32**. Specifically, the V430A substitution in ASTB-M5 variant reduces steric crowding and allows structural rearrangement of Y423 and R490 residues which might influence substrate accessibility and thereby increases the catalytic activity of ASTB-M5 variant.

Table 16. Coupling efficiency determined from ASTB-WT and ASTB-M5.

Acceptors	Enzyme	Sulfated products conc. (mM)	<i>p</i> -nitrophenolate conc. (mM)	Coupling efficiency (%)
Catechol	WT	0.20	0.33	59
	ASTB-M5	0.31	0.35	89
3-Fluorocatechol	WT	0.16	0.37	42
	ASTB-M5	0.22	0.45	50
3-Chlorocatechol	WT	0.16	0.30	53
	ASTB-M5	0.30	0.38	80
3-Bromocatechol	WT	0.23	0.38	61
	ASTB-M5	0.31	0.41	76
3-Methylcatechol	WT	0.18	0.22	79
	ASTB-M5	0.21	0.24	87
3-Methoxycatechol	WT	0.12	0.34	35
	ASTB-M5	0.17	0.34	49

Reaction condition: 10 mM substrate, 1 mM *p*-NPS; and 1 μ M enzyme in 1 mL reaction mixture. The concentration of sulfated products and para-nitrophenolate was determined by HPLC.

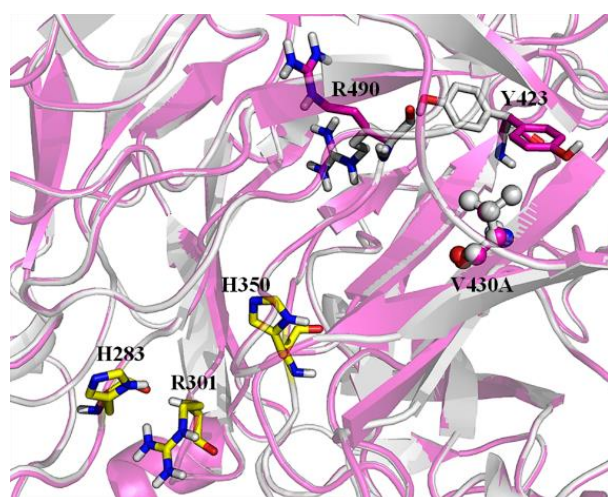


Figure 32. A 3D-structural alignment of ASTB-WT (white cartoon) and the improved ASTB-M5 variant (magenta cartoon). The residues in close to the binding pocket are shown as sticks whereas the catalytic residues (H350, H283, and R301) are shown with yellow sticks.

The importance of the loop region engineering has been reported for other enzymes, e.g., the multi-site substitution A285P/A310R/A312E/A318G in loopL1 of laccase lcc2 from *T. versicolor* obtained 8.4-fold increased laccase activity in EMIM EtSO₄^[145, 160-164]. Loop engineering of loop12 and loop13 is an efficient way to improve the sulfate transfer efficiency of ASTB. Here OmniChange method was applied for investigating the synergy effect of four positions (Q191/V199/Y218/L225) in loop12& loop13. The k_{cat} values of ASTB-OM2 (Q191Y/Y218W/L225V) were improved from 6.1 to 13.6-fold compared to ASTB-WT for all six catechol (catechol, 3-methylcatechol, 3-methoxycatechol, 3-fluorocatechol, 3-chlorocatechol, and 3-bromocatechol). It might be a general trend that simultaneous substitutions in loop12 and loop13 boost the sulfation activities on a broad range of catechols and that the proposed strategy (combination of computational analysis and multi-site saturation mutagenesis) is efficient in minimizing experimental efforts and yields highly improved ASTB variants.

The HPLC-MS analysis revealed that on top of the k_{cat} values, the stoichiometry of catechol sulfation catalyzed by ASTB-OM2 is between 40 %-94 %, whereas ASTB-WT shows the stoichiometry of catechol sulfation between 16 %-53 % (see **Table 11**). The sulfation transfer efficiency was overall stimulated with up to 3.9-fold improvement (here 3-methylcatechol; ASTB-WT: 24 % and ASTB-OM2: 94 %), making ASTB-OM2 a very efficient catalyst for regioselective sulfating substituted catechols and optimization of reaction conditions will very likely achieve conversion rates up to 90 % for sulfation of substituted catechols by ASTB-OM2. The four positions (Q191, V199, Y218, and L225) in loop12& loop13 proved to highly influence specific activity and stoichiometry of sulfate transfer by kinetic characterization of variants ASTB-OM1, ASTB-OM2, and ASTB-OM3 (**Table 9**).

In both enzymes (ASTB-OM2 and ASTB-WT), the halogenated catechols (150-242 s⁻¹ for ASTB-OM2 and 11-24 s⁻¹ for ASTB-WT) are converted slower than catechol itself (538 s⁻¹ for ASTB-OM2 and 46 s⁻¹ for ASTB-WT), 3-methoxycatechol (243 s⁻¹ for ASTB-OM2 and 40 s⁻¹ for ASTB-WT), and 3-methylcatechol (421 s⁻¹ for ASTB-OM2 and 51 s⁻¹ for ASTB-WT) (**Table 10**). Electronic properties and steric demand of substituents (-OCH₃, -CH₃, -H, -F, -Cl, -Br) have a significant influence on the sulfation (see **Table 12& Figure 26**). The negative reaction constant values (ρ) obtained from the Hammett equation revealed that the electron-donating capability of catechol substituents increases the k_{cat} by stabilizing the transition state of the nucleophilic attack of phenolate oxygen to the sulfur in the proposed ping-pong bi-bi mechanism^[141]. Halogen groups are weakly electron-

withdrawing groups that reduce the nucleophilicity of the phenolate oxygen that likely decreases the reaction rate.

To the best of our knowledge, ASTB-OM2 is by far the fastest aryl sulfotransferase for sulfation of catechols ($k_{\text{cat}}=538 \pm 18 \text{ s}^{-1}$) and for phenolic compounds. The highest k_{cat} values for sulfation of phenols that we found in the literature were an aryl sulfotransferase from *E. coli* CFT073 (49 s^{-1} , using phenol as substrate). No data is available on the sulfation of catechols by PAPS-dependent sulfotransferases; however, for estrogen specificity activities up to 23500 s^{-1} were reported for mouse estrogen sulfotransferase (EST)^[138, 183, 184].

2.6 Conclusion

In this work, a screening assay for directed ASTB evolution was established and ASTB was engineered for the selective sulfation of catechol compounds. As a starting point for engineering, 3-chlorocatechol was selected as substrate. Surprisingly, ASTB-WT was able to sulfate catechols with nearly identical chemoselectivity which is in contradiction with previously reported catechol metabolites exceed from our body. To achieve the goal of identifying beneficial variants with improved sulfate transfer efficiency, a successful two-step *p*-NPS-4-AAP screening system towards catechols was developed and validated. Firstly, the *p*-NPS assay is applied by determining the colorimetric by-product *p*-nitrophenol which shows the consumption of sulfate donor. Then, the sulfated product, 3-chlorocatechol-1-monosulfate, is quantified by the 4-aminoantipyrine (4-AAP) assay which shows the production of 3-chlorocatechol-1-monosulfate. Therefore, sulfate transfer efficiency can be detected by comparison of product formation with *p*-NPS consumption. Important parameters of the *p*-NPS-4-AAP screening assay, including pH value, volume of cell free extract, and linear detection range were optimized in order to achieve a reliable coefficient of variation (below 15 %) in MTP form. A random library (sequence saturation mutagenesis (SeSaM) library) of ASTB was screened. Finally, a beneficial variant (ASTB-M5) was purified and characterized. Variant ASTB-M5 has an improved catalytic performance towards sulfation of catechol compounds (k_{cat} up to $197 \pm 11 \text{ s}^{-1}$, in the case of 3-methylcatechol), high coupling efficiency (up to 89 %, in the case of catechol) and selectivity (>99 %) to produce catechol sulfates. The substrate profile of ASTB-M5 was subsequently determined by investigating five additional catechols (catechol, 3-

methylcatechol, 3-methoxycatechol, 3-fluorocatechol, 3-chlorocatechol, 3-bromocatechol).

KnowVolution campaign was conducted for further exploring the variants with higher improved activity towards chemo- and regio selective sulfation of catechols and catechol derivatives. One round of directed evolution yielded some potential beneficial positions which can be classified into four groups: positions in loop region close to the active site residue H220 (Q191, V199, Y218, and L225); positions close to catalytic center H350 (T393, I398, V430, A448, N612, L622); (3) positions in loop22 and loop24 regions (K371, E373, E380, A410); and positions in the dimer interface (I71, F512, K533, E542, and A582). Meanwhile, a homology model was generated based on the known ASST protein structure (PDB: 3ETS) and the residue Y218 found in directed evolution was also recommended from molecular docking study and conservation analysis as possible beneficial position. This indicates the potential importance of loop region near the active site H220 of ASTB. Therefore, four SSM libraries at position Q191, V199, Y218, and L225 in loop12 and loop13 were generated and screened. All of these four positions are beneficial with the improvement ranges from 1.1-2.4-fold. The moderate improvements of these variants could be attributed to individual saturation of these positions and no synergetic effect was explored. OmniChange as a robust method for simultaneous multi-site saturation mutagenesis was applied to obtain variants with higher improvement. After screening the ASTB OmniChange library, the final variant ASTB-OM2 (Q191Y/Y218W/L225V) was identified with up to 13.6-fold improved k_{cat} value (in the case of 3-bromocatechol) compared to ASTB-WT. Moreover, variant ASTB-OM2 also enables the improved sulfation activity towards other compounds, including dopamine, tanshinol, taxfolin, and quercetin, and the maximum conversion was achieved with tanshinol (75 %).

3 Engineering of P450 BM3 toward hydroxylation of surfactant

3.1 Declaration

Parts of this chapter has been published:

Ji, Y., Mertens, A. M., Gertler, C., Fekiri, S., Keser, M., Sauer, D. F., Smith, K. E. C., Schwaneberg, U. (2018). Directed OmniChange evolution converts P450 BM3 into an alkyltrimethylammonium hydroxylase. *Chemistry-A European Journal*, 24(63), 16865-16872^[147].

3.2 State of the art

3.2.1 Surfactants

Surfactants (adopted from term *surface-active agent*) are substances that capable of lowering surface or interfacial tension between two immiscible phases and acting as detergents, foaming agents, emulsifiers, wetting agents, and dispersants^[185]. They can be classified into several types: non-ionic surfactant, anionic surfactant, cationic surfactant and zwitterionic surfactant. Cationic surfactants are frequently used in laundry industry^[186, 187], nano- materials synthesis^[188], and drug delivery^[189]. Among these, cetyltrimethylammonium bromide (CTAB) is one of the most ubiquitous surfactants which is used in hair conditioners, in the synthesis of nanoparticles (e.g. mesoporous silica nanoparticles, gold nanoparticles) and for electrode modification^[188, 190-192]. Apart from compound expenses, the key parameters for use of cationic surfactants in industry are biodegradability and surfactant solubility^[193, 194]. Recently, bolaform surfactants attracted the interest of industry and academia due to their reduced micelle size and excellent solubilization properties^[195-199]. In detail, bolaform surfactants, such as hydroxyl quaternary ammonium compounds, consist of two hydrophilic groups that are separated by a hydrophobic spacer chain. By “double anchoring”, the radius of the micelle size is drastically reduced (~50 %) with low aggregation numbers (N=5-18), compared to the corresponding non-hydroxylated (conventional) surfactant (**Figure 33**). As a result, bolaform surfactants can generate microporous silicates with smaller pore sizes^[200, 201], polystyrene-b-poly(2-vinylpyridine) copolymer particles with axially stacked lamellae structure^[202], anisotropic gold nanoparticles with flexible shape^[203, 204], and improve gene delivery efficacy^[205]. For instance, 16-hydroxy cetyl-trimethylammonium bromide (16-hydroxy-CTAB) was applied in super-microporous silicate templating reactions which

resulted in highly ordered silicate materials^[201]. 11-hydroxy undecyl-trimethylammonium bromide modified gold nanoparticles are used for inhibition of chymotrypsin by electrostatic binding^[206]. CTAB is relatively persistent to biodegradation and thus can be found abundantly in the environment (7.7 mg mL^{-1})^[207]. Hydroxylation of CTAB is the first step of CTAB biodegradation and hydroxylated CTAB surfactants are not reported in the environment due to rapid degradation^[187].

16-hydroxy-CTAB can be chemically synthesized in three steps: (1) ring-opening bromination of hexadecanolide (non-polar lactone) via a nucleophilic attack of bromide; (2) borane reduction of 15-bromohexadecanoic acid; (3) quaternization of 16-bromohexadecanol^[208]. However, the current synthesis method use expensive hexadecanolide, strong acids (sulphuric acid, hydrobromic acid and hydrochloric acid), extensive amounts of toxic solvents (e.g. tetrahydrofuran, hexane, and dichloromethane) and result in moderate yields of around 50 %^[208, 209]. Chemical routes to subterminal hydroxylated CTAB have to the best of our knowledge not been reported yet. Double hydroxylated CTAB products are very challenging to synthesize because of the required chemoselectivity for subterminal hydroxylation. Nevertheless, production of double hydroxylated CTAB products could be worthwhile due to a higher polarity of bolaform surfactants that could result in further reduced micellar sizes and therefore improved solubilisation power.

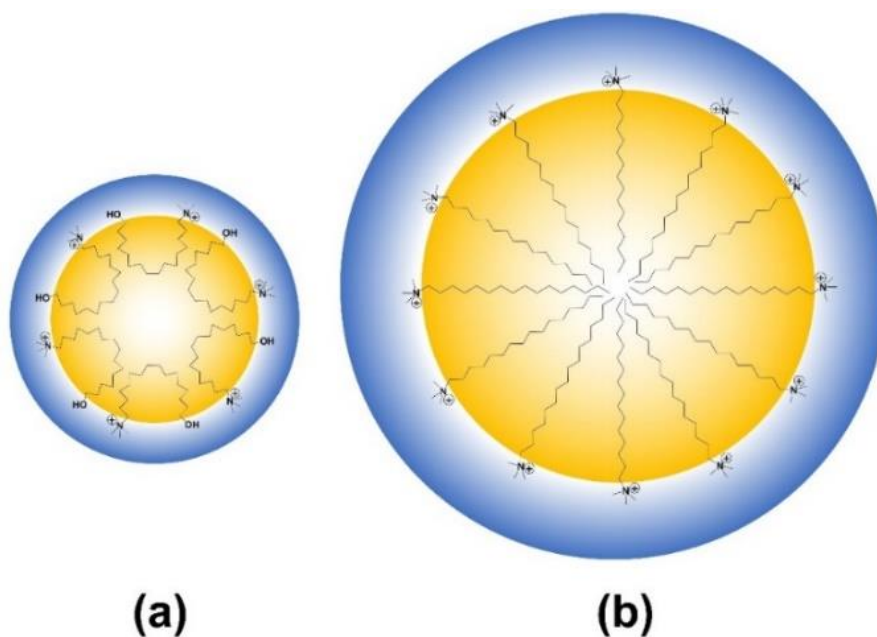


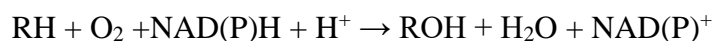
Figure 33. Micelle model formed by the bolaform surfactant : (a) 16-hydroxy-CTAB; (b) conventional CTAB. The figure was taken from Ji *et al.*^[147].

3.2.2 Cytochrome P450 monooxygenase in biocatalysis

Cytochrome P450 monooxygenases (CYPs or P450s) are heme-iron containing oxidoreductases (EC 1.14.14.1) that catalyze the oxidation of endogenous and exogenous substrates with a high degree of regio- and stereoselectivity^[143]. They are ubiquitous in nature (more than 300, 000 sequences) and present in many species, ranging from simple organisms (bacteria, yeast, fungi) to complex organisms (insects, plants and mammals)^[210].

In 1958, the first time P450 spectrum was reported by Klingenberg who identified that after treating rat liver microsomes with reducing agent sodium dithionite and addition of carbon monoxide (CO), an orange-yellow pigment was observed with an UV absorbance at 450 nm^[211]. Later, it was demonstrated that the absorbance at 450 nm was caused by the bound between reduced heme iron and CO (the coordination state)^[212] and the item “P450” is widely used for describing this superfamily of enzymes^[212].

Various difficult oxidative reactions including hydroxylation, epoxidation, heteroatom oxygenation, dealkylation, sulfoxidation, was reported using P450s as catalyst^[143]. The ability of introducing molecular oxygen into non-activated carbon at ambient temperature, in aqueous solutions and by using oxygen as oxidant makes P450s highly attractive for chemical synthesis^[213, 214]. Their catalytic function is the reductive cleavage of molecular oxygen to form an hydroxylated product (ROH) with water (H₂O) and the general reaction catalyzed by P450s is as follows:



The catalytic cycle of P450s was already reported by Whitehouse *et al.*^[143] and it was divided to nine states (**Figure 34**). Firstly, the ferric state (Fe³⁺) was risen from low-spin (resting state, State I) to high-spin (State II) caused by the binding of substrate to the active site; then, cofactor NAD(P)H transferred a single electron to the haem iron by the electron transfer systems, reducing the ferric state (Fe³⁺) to the ferrous state (Fe²⁺, State III); afterwards, with the binding of oxygen, the reduced haem iron resulting an oxy-complex (State IV); after that a second electron from the cofactor was transferred, yielding a peroxy-complex (State V); therefore, two successive protonations occur (a hydroperoxy adduct which was named “Compound 0” (State VI) and a highly active ferryl species named “Compound I” (State VII)); compound I which is the active unit in most P450 oxidations could abstract the H-atom from the substrate molecule and formed State VIII; finally, the ·OH radical was rebound to the substrate portion, resulting the release of hydroxylated product and the heme iron returns to the pentaferrous state (State IX)^[143].

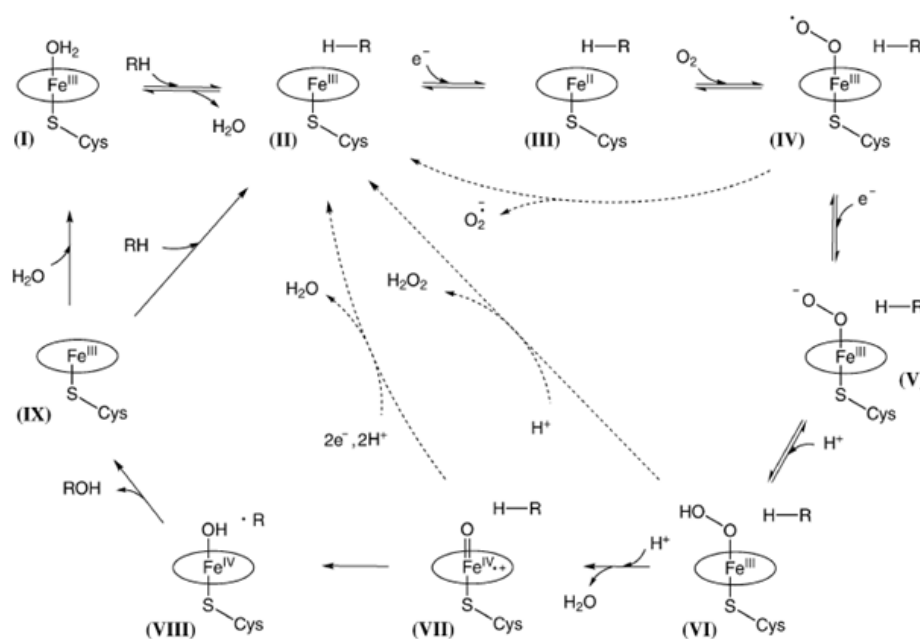


Figure 34. Cytochrome P450 monooxygenases catalytic cycle. The figure was taken from Whitehouse *et al.*^[143].

In many studies it was observed that the oxidized cofactor amount could not produce a stoichiometric amount of product due to uncoupling reactions^[145, 215, 216]. Uncoupling reactions in the P450s catalytic circle were shown with dotted arrows in **Figure 34**, including superoxide uncoupling, peroxide uncoupling, and oxidase uncoupling^[143]. “Coupling efficiency” which describes the ratio between produced product amount and transferred electrons is an important issue in biocatalysis and a high coupling efficiency in P450s requires a stoichiometric equilibrium between NAD(P)H, molecular oxygen and generated product^[217].

Cytochrome P450 BM3 (CYP102A1) from the gram positive bacterium *Bacillus megaterium* is a self-sufficient monooxygenase with a length of 1049 amino acids which contains its heme domain and reductase on one polypeptide strand, and often regards as “gold standard” in P450 catalysis^[143, 146]. The nature substrate of P450 BM3 is long chain saturated fatty acids and mono-unsaturated fatty acids with the highest turnover rate among P450 mono-oxygenase ($> 15000 \text{ min}^{-1}$, arachidonic acid)^[143]. Until now, P450 BM3 is known to hydroxylate a broad spectrum of substrates, including fatty acids, alkanes, phenols, and steroids^[145].

3.2.3 Protein engineering of P450 BM3

A possible solution for the cost-effective production of bolaform surfactants could be the use of cytochrome P450 monooxygenases^[214]. Oliver *et al.*^[218] reported firstly that alkyl-trimethylammonium compounds are poor substrate for P450 BM3, and generated the P450 BM3 variant R47E which mono-hydroxylate CTAB at the ω -1, ω -2 or ω -3 positions in approximately equal amounts (as confirmed for dodecyl-trimethyl ammonium by 600 MHz ¹H NMR^[218]). To our best knowledge, no double hydroxylation of CTAB has been reported.

Many P450 BM3 variants with altered substrate specificity have been reported^[143, 219], and prominent positions comprise R47, Y51, L75, A82, F87, L188, A328, A330, and I401^[220-224]. Based on the findings of Oliver *et al.*^[218] and computational analysis by YASARA (www.yasara.org) of P450 BM3 structure, positions 47, 51, 87, and 188 were considered essential for CTAB hydroxylation (see **Figure 35**, PDB code 4ZFA). Position 47 is located at the entrance of the substrate access channel and in combination with Y51 is important for binding and orienting the natural fatty acid substrate^[218, 219]. Position 87 is located directly above the catalytic heme center and often responsible for the regioselectivity of substrate oxidation^[225, 226]. L188 is located at the C-terminus of α -helix F and was reported to influence regioselectivity of myristic acid conversion^[222]. Beneficial substitutions can be recombined in an iterative or simultaneous manner with a number of different techniques, e.g. the highly successful CASTing method, which is based on iterative recombination using QuikChange experiments^[227, 228], and is the method of choice when screening capabilities are limited (e.g. three iterative SSMs generated $20+20+20 = 60$ different enzyme variants). Simultaneous site saturation mutagenesis can generate a significantly higher diversity than CASTing ($20^3 = 8000$ different variants) and is more suited when the selected positions are in close proximity (cooperative effects) which maximizes property improvements. OmniChange is a focused multi-site mutagenesis method, which enables simultaneous and efficient mutagenesis of up to five independent codons^[59, 229]. It has already been used in several campaigns as part of the protein engineering strategy termed KnowVolution^[62, 230-232].

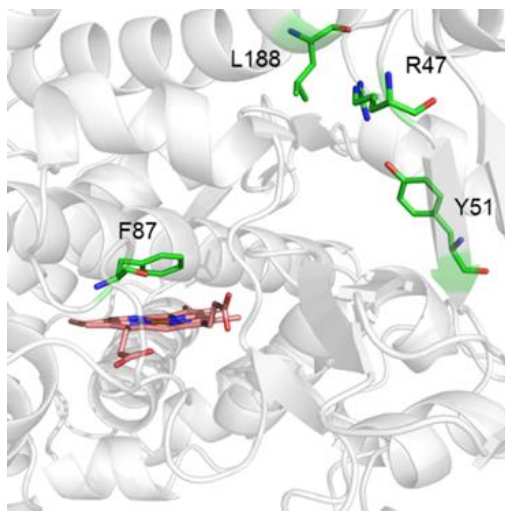


Figure 35. Crystal structure of wild-type P450 BM3 heme domain with highlighted positions used in the OmniChange library generation R47/Y51/F87/L188. [PDB code 4ZF8] Position 47 and 51 located at the entrance of the substrate access channel responsible for substrate binding and orienting; Position 87 located above the catalytic heme center and is important for regioselective hydroxylations; Position 188 located at the C-terminus of α -helix F and was reported to influence regioselectivity of myristic acid conversion. YASARA was used for P450 BM3 visualization.

3.2.4 Objectives

The main goal of this chapter was the engineering of P450 BM3 towards CTAB hydroxylation for bolaform surfactant production. This project is divided into four working packages (WPs): (1) establishment of suitable analytical methods for the identification of hydroxylated CTAB products; (2) establishment of a reliable screening system for the identification of P450 BM3 variants with improved hydroxylation activity; (3) generation and screening of mutant libraries of P450 BM3 towards improved hydroxylation activity; and (4) purification and kinetic characterization of identified variants.

3.3 Material and Methods

3.3.1 Chemicals and reagents

All chemicals were of analytical grade or higher quality and purchased from Sigma-Aldrich (Steinheim, Germany), AppliChem (Darmstadt, Germany), abcr (Karlsruhe, Germany), and Carl Roth (Karlsruhe, Germany). Phusion DNA polymerase, DpnI, and dNTPs were obtained from New England Biolabs (Frankfurt, Germany); *Taq* DNA polymerase was produced in-house. PCRs were performed in 0.2 mL thin-walled PCR tubes (Sarstedt Multiply[®]-Pro cup, Nuembrecht, Germany) using a thermal cycler (Eppendorf Mastercycler proS, Hamburg, Germany). DNA was quantified with a NanoDrop photometer (ND-1000, NanoDrop Technologies, Wilmington, DE, USA). Plasmid extraction was achieved by using a commercial kit (QIAGEN QIAprep Spin Miniprep Kit, Hilden, Germany). DNA sequencing was performed at GATC Biotech (Konstanz, Germany) and Eurofins MWG-Operon (Ebersberg, Germany). Analysis of obtained sequencing data was performed using the Clone Manager 9 Professional Edition Software (Scientific & Educational Software, Cary, NC, USA). GDH from *Pseudomonas* sp. and catalase from bovine liver were obtained from Sigma-Aldrich (Steinheim, Germany).

3.3.2 OmniChange library generation

An OmniChange library was generated by assembling gene fragments (A, B) with vector fragment C as reported before^[229]. All phosphothioate oligonucleotide (PTO) primers were synthesized in-house with a DNA/RNA Synthesizer (H-8, K&A Laborgeraete, Schaaheim, Germany) using micropure purification columns (Biosearch technology, Petaluma, USA) and subsequently purified by liquid chromatography (LC-20AD, Shimadzu GmbH, Duisburg, Germany) equipped with a C₁₈ column (125×8 mm; CS Chromatographie, Langerwehe, Germany). All synthesized primers are summarized in **Table 17**.

Table 17. Sequences and T_m value of primers used for the OmniChange library generation.

PTO primer	Sequence (5'→3')	T _m (°C)*
R47/Y51Fw	ttcgaggcgcctGGTGANGTAACGCGCNYNTTATCAAGTC	69.4
R47/Y51Rv	accgctctcctgCAAAATCACGTACAAATT	61.9
F87Fw	caggagacgggtTAGNNACAAGCTGGACGCATG	63.6
F87Rv	cttggtcattgcTTCATCCAGTG	54.6
L188Fw	gcaatgaacaagNNKCAGCGAGCAAATCCAGAC	64.7
L188Rv	aggcgcctcgaaTTTAAAGATTTCTCCTAATTCATCC	62.2

* T_m for degenerate primers have been reported as minimum, mean and maximum value; capital letter: normal nucleotide, small letter: phosphorothioated nucleotide.

For fragment A amplification targeting position R47/Y51, PTO primers (R47/Y51Fw and R47/Y51Rv, 0.1 μM each) together with *Taq*/Phusion DNA polymerase (1:2, 5 U), dNTP mix (0.2 mM), plasmid template (pALXtreme-1a plasmid, 20 ng) were used and PCR was performed (96°C for 3 min, one cycle; 96°C for 30 s, 61°C for 30 s, 72°C for 30 s, 25 cycles; 72°C, 5 min, one cycle). PTO primers (F87Fw and F87Rv, 0.1 μM each) together with Phusion DNA polymerase (5 U), dNTP mix (0.2 mM), plasmid template (pALXtreme-1a plasmid, 20 ng) were used for amplification of fragment B and the corresponding PCR program was 98°C for 3 min (1 cycle); 98°C for 30 s, 53°C for 1 min, 72°C for 1 min (30 cycles); 72°C for 5 min (1 cycle). The L188 site was included in vector backbone and it was amplified using PTO primers (L188Fw and L188Rv, 0.1 μM each) in combination with Phusion DNA polymerase (5 U), dNTP mix (0.2 mM), plasmid template (pALXtreme-1a plasmid, 20 ng) by PCR (98°C for 3 min, 1 cycle; 98°C for 30 s, 63°C for 1 min, 72°C for 5 min, 30 cycles; 72°C for 5 min, 1 cycle). The template plasmid DNA was digested by adding DpnI (20 U; 37°C, 12 h) to PCR products. PCR products were purified using the Nucleospin Extract II kit (Macherey Nagel, Dueren, Germany). Purified vector backbone fragment C was diluted to 0.04 pmol μL⁻¹ and fragments A, B were diluted to 0.11 pmol μL⁻¹ using distilled deionized water. subsequently, all fragments were cleaved by iodine-ethanol at alkaline conditions as reported before^[229]. All cleaved fragments were assembled by hybridization using a temperature gradient (70°C, 5 min; -1°C/10 s, 50 cycles; 20°C, 3 min; 4°C, 5 min) and transformed into 100 μL chemically competent *E. coli* BL21-Gold (DE3) lacI^{Q1} cells for expression and subsequent screening of P450 BM3 variants. Verification of the correct assembly was performed by colony PCR and sequencing of the clones.

3.3.3 Screening of OmniChange library

Preparation of micro titer plates (MTPs), P450 BM3 expression, and lysate preparation for screening in MTP format were carried out as described previously by Nazor *et al.* (Figure 36)^[233].

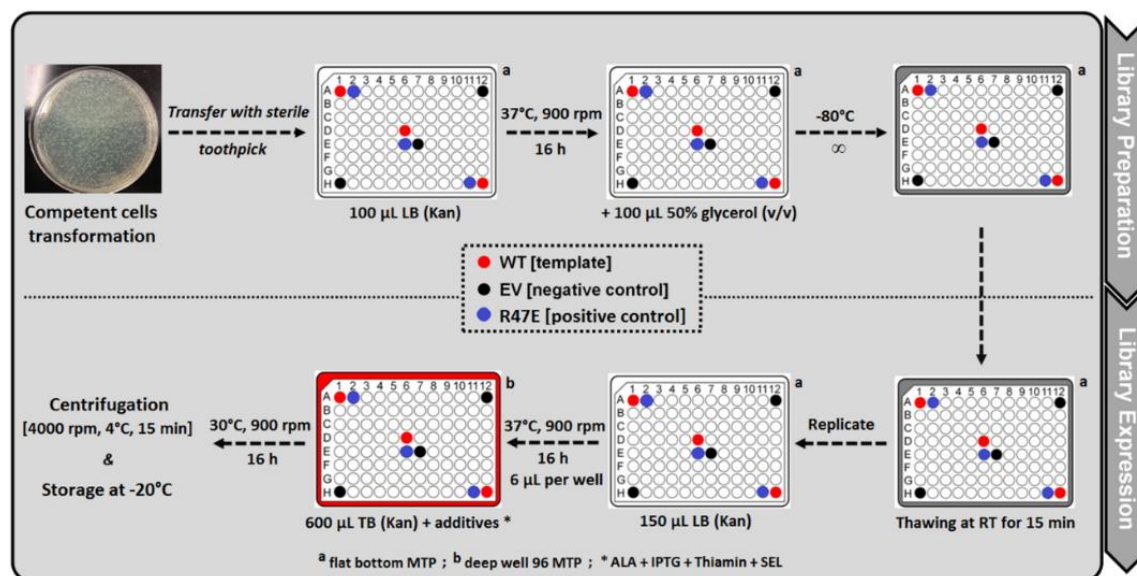


Figure 36. P450BM3 OmniChange library preparation and expression.

The OmniChange library was screened using CTAB as a substrate to identify P450 BM3 variants that are able to hydroxylate alkyl trimethylammonium compounds. Due to so called shunt reactions (e.g. peroxide shunt) in the catalytic cycle of P450s, uncoupled NADPH may lead to hydrogen peroxide (H_2O_2) production^[234] that could inhibit monooxygenases^[235]. To avoid selection of highly uncoupled P450 BM3 variants, a combination of a frequently used NADPH depletion assay and an Ampliflu™ Red/horseradish peroxidase (HRP) based hydrogen peroxide detection assay was developed to select P450 BM3 variants with high coupling efficiency (Figure 37)^[144, 236]. Thus, a total of twenty 96-well MTPs (1740 clones) were screened by measuring the NADPH oxidation rate; 8 MTPs (696 clones) were rescreened by monitoring the depletion of NADPH in combination with determining H_2O_2 formation. In the first screening step, each of the 96-MTPs contained cell lysate (35 μ L), potassium phosphate buffer (155 μ L, 100 mM, pH 7.5), and CTAB (10 μ L, final conc. 50 μ M). MTPs were incubated for 5 min before supplementation of NADPH (50 μ L, final conc. 50 μ M). NADPH consumption of P450BM3 variants and wild-type P450 BM3 recorded with a Tecan MTP reader (340 nm with interval of 15 s for 15 min; Tecan Sunrise MTP reader, Crailsheim, Germany). The initial NADPH consumption (first 90 s; 6 measuring points) was used to calculate initial

oxidation activity and P450 BM3 variants with ≥ 1.5 -fold consumption rate were selected for rescreening in 96-well MTPs. In the second step, each of the 96-MTPs contained cell lysate (10 μ L), potassium phosphate buffer (70 μ L, 100 mM, pH 7.5), and CTAB (10 μ L, final conc. 50 μ M). MTPs were incubated for 5 min before supplementation of NADPH (10 μ L, final conc. 50 μ M). NADPH consumption of P450 BM3 variants and wild-type P450 BM3 recorded with a Tecan MTP reader (excitation wavelength: 340 nm; emission wavelength: 460 nm; intervals of 15 s for 15 min; Tecan Infinite M1000 MTP reader, Crailsheim, Germany). Hydrogen peroxide formation was correlated to NADPH consumption in the rescreening experiment by adding quenching buffer (25 μ L acetonitrile), HRP/Amplex Red™ stock solution (125 μ L, final conc. 1 U HRP, 4 μ M Amplex Red™ dye) to 100 μ L fully depleted NADPH wells. Hydrogen peroxide production was monitored with a Tecan MTP reader (excitation wavelength: 535 nm; emission wavelength: 590 nm; intervals of 30 s for 30 min; Tecan Infinite M1000 MTP reader, Crailsheim, Germany).

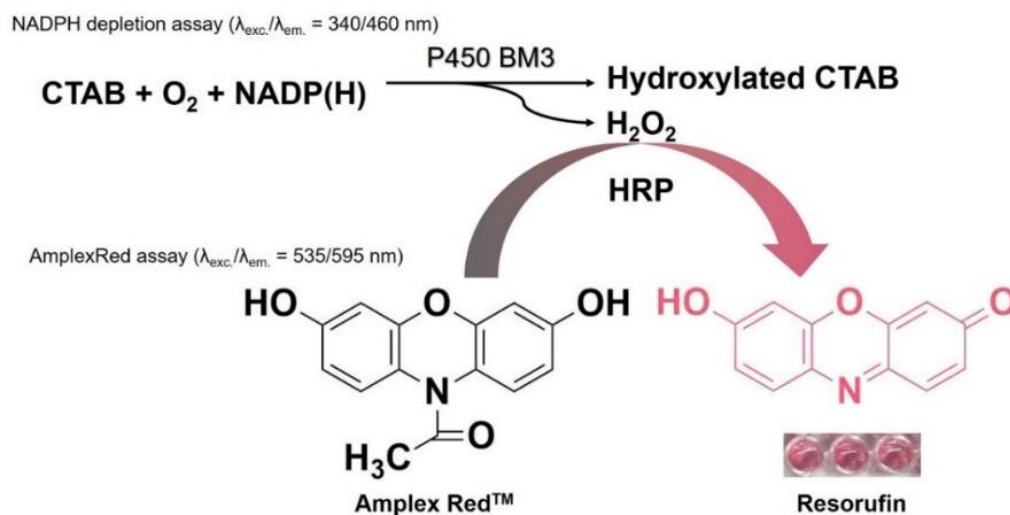


Figure 37. Two-step screening assay for P450 BM3 (NADPH depletion assay and Ampliflu™ Red/horseradish peroxidase (HRP) based hydrogen peroxide detection assay).

3.3.4 Long-term conversion in presence of a cofactor regeneration system

Productivity and regioselectivity of P450 BM3 variants (P2E7, P3A8, P5A3, P5C6, P6A4, P8G6, P10H11, P11H11, P12F3, P19G5) and wild-type P450 BM3 towards CTAB hydroxylation were determined in long-term reactions with a glucose dehydrogenase (GDH) regeneration system. A reaction mixture of 3 mL KPi buffer (100 mM, pH 7.5) containing P450 BM3 variants and wild-type P450 BM3 (2 μ M, lysate or purified enzyme), GDH (5 U

mL⁻¹), glucose (20 mM), catalase (1200 U mL⁻¹), and CTAB (1 mM) was pre-incubated in 9 mL glass tubes, sealed with lids and incubated on an Eppendorf Mix Mate (300 rpm, room temperature; Sigma-Aldrich, Steinheim, Germany) for 5 min. CTAB conversion by P450 BM3 was induced by adding NADPH (100 μM). The reactions were performed in triplicates and for 16 h for each variant. 0.5 mL samples were taken from the flask at different times (0 min, 15 min, 30 min, 1 h, 3 h, 16 h) and pipetted into a tube containing 0.5 mL acetonitrile. The reaction mixture was vortexed thoroughly, centrifuged (13000 g; 5 min; Eppendorf 5415R centrifuge, Hamburg, Germany) and the precipitate was discarded. Subsequently, the samples were dried by nitrogen and dissolved by 0.5 mL acetonitrile, then pooled in liquid chromatography vials.

3.3.5 HPLC-MS/MS analysis

A high-performance liquid chromatography (HPLC, Agilent® HP1100, Waldbronn, Germany) and an ion trap mass analyzer (Thermo LTQ-Orbitrap™, Waltham, MA, USA) equipped with an electrospray ion source were used for the analysis of CTAB derivatives in this study. CTAB and its reaction products were separated with an C₁₈ column (Phenomenex® Synergi™ Hydro RP C₁₈, 250×2 mm, 4 μm; Aschaffenburg, Germany) with gradient elution using solvent A (20:80 acetonitrile: water with 1 % acetic acid) and solvent B (95:5 ACN: water with 10 mM ammonium acetate) at a flow rate of 0.4 mL min⁻¹ (Table 18) within 16 min using 5 μL injection volume at room temperature. Ionization was conducted in the positive mode of electrospray (ESI⁺) at a capillary voltage of 3.5 V and a capillary temperature of 350°C. CTAB and products were identified by using accurate full scan mode MS. To improve the sensitivity for detection of CTAB, multiple-reaction monitoring (MRM) mode was applied for CTAB quantification. The collision energy was optimized (55 V) and daughter ion $m/z= 85.0$, $m/z= 268.0$ were selected for MRM mode. A calibration curve of CTAB was established (from 1 μM to 1 mM) with a correlation coefficient of 0.996. Processing of data was done using Xcalibur Qual Browser (Thermo Electron, San Jose, CA).

Table 18. The gradient elution mode of HPLC for substrate and product separation.

Time [min]	Flow rate [mL min ⁻¹]	Solvent A [%]	Solvent B [%]
0	0.40	100	0
1.0	0.40	100	0
5.0	0.40	0	100
12.0	0.40	0	100
13.0	0.40	100	0
16.0	0.40	100	0

3.3.6 NMR measurement

A reaction mixture of 3 mL KPi buffer (100 mM, pH 7.5) containing P450 BM3 variant P2E7/P450 BM3 variant P3A8/wild-type P450 BM3 (20 μ M, purified enzyme), GDH (50 U mL⁻¹), glucose (200 mM), catalase (12000 U mL⁻¹), and CTAB (10 mM) was pre-incubated in 9 mL glass tube, sealed with lid and incubated on an Eppendorf Mix Mate (300 rpm, room temperature; Sigma-Aldrich, Steinheim, Germany) for 5 min. CTAB conversion by P450 BM3 was induced by adding NADPH (1 mM). The reactions were performed overnight. After performing long-term conversion, 3 mL acetonitrile was added and mixed thoroughly, centrifuged (13000 g; 5 min; Eppendorf 5415R centrifuge, Hamburg, Germany) and the sediment was discarded. Subsequently, the samples were shock-frozen in liquid nitrogen and lyophilized for 8 h in a Christ ALPHA 1-2LD plus freeze-dryer (Christ, Osterode am Harz, Germany). Bruker Av ¹H NMR spectra of each sample were recorded on a Bruker Avance III 400 NMR spectrometer. Chemical shifts are reported in ppm relative to the residual solvent resonances^[237].

3.3.7 Protein purification of P450 BM3 variants

P450 BM3 variants (P2E7, P3A8, P11H11, P12F3) and wild-type P450 BM3 were expressed in shaking flasks and purified by anion exchange chromatography using a two-step elution method as described before^[238]. An ÄKTA PrimePlus FPLC system (GE Healthcare, München, Germany) equipped with a Kronlab TAC 15/125PE5-AB-2 column (YMC Europe, Dinslaken, Germany) packed with Toyo Pearl 650 S-DEAE Sepharose Matrix (Tosoh bioscience, Tokyo, Japan) was used for purification. Eluted protein samples were collected and analyzed on 10 % sodium dodecyl sulfate-polyacrylamide gel electrophoresis (SDS-PAGE) gels to assess protein purity. P450 BM3 monooxygenase fractions of high purity (around 90 %) were combined and concentrated by Amicon

Centrifugal Filters (100 kDa cut-off; Millipore, Schwalbach, Germany). Desalting of the purified BM3 variants and wild-type P450 BM3 was performed using PD-10 gel-filtration columns (GE Healthcare, Freiburg, Germany) equilibrated in KPi buffer (100 mM, pH 7.5). Protein samples were shock-frozen in liquid nitrogen and lyophilized for 16 h in a Christ ALPHA 1-2LD plus freeze-dryer (Christ, Osterode am Harz, Germany).

3.3.8 Kinetic Characterization of P450 BM3 variants

Kinetic characterizations (K_M , k_{cat}) of P450 BM3 variants (P2E7, P3A8, P11H11, P12F3) and wild-type P450 BM3 were performed by using purified P450 BM3 (concentration determined with a CO-binding assay^[212]). A mixture of 1 mL KPi buffer (100 mM, pH 7.5) containing CTAB (1 to 40 μ M), and P450 BM3 monooxygenase (0.1 μ M) was pre-incubated for 5 min. CTAB conversion by P450 BM3 was induced by addition of NADPH (100 μ M). NADPH oxidation activities of P450 BM3 variants and wild-type P450 BM3 were measured using initial NADPH consumption rate at 340 nm in a Varian Cary 50 UV spectrophotometer (Agilent Technologies, Darmstadt, Germany). Fitting of kinetic parameters was achieved by non-linear fitting model (Michaelis-Menten equation) using Origin Pro 8.6 software (OriginLab Corporation, Northampton, MA, USA).

Coupling efficiency of variants (P2E7, P3A8, P11H11, P12F3) was evaluated through the addition of NADPH (100 μ M) to the mixture (1 mL KPi buffer (100 mM, pH 7.5), CTAB (100 μ M), and P450 BM3 monooxygenase (0.5 μ M)). After full depletion of NADPH, samples were mixed with 1 mL acetonitrile containing 100 μ M dodecyl-trimethylammonium bromide as internal standard. Sample preparation and CTAB/products detection procedure were performed as described above (Long-term conversion in presence of a cofactor regeneration system). Coupling efficiency was calculated based on the consumed amount of NADPH and CTAB. All reactions were performed in triplicates with a coefficient of variation less than 10 %.

3.3.9 Surface contact angle measurements

A reaction mixture of 3 mL KPi buffer (100 mM, pH 7.5) containing P450 BM3 variant P2E7/P450 BM3 variant P3A8 (2 μ M, purified enzyme), GDH (5 U mL⁻¹), glucose (20 mM), catalase (1200 U mL⁻¹), and CTAB (1 mM) was pre-incubated in 9 mL glass tube, sealed with lid and incubated on an Eppendorf Mix Mate (300 rpm, room temperature; Sigma-Aldrich, Steinheim, Germany) for 5 min. CTAB conversion by P450 BM3 was

induced by adding NADPH (100 μ M). The reactions were performed overnight. After performing long-term conversion, 3 mL acetonitrile was added and mixed thoroughly, centrifuged (13000 g; 5 min; Eppendorf 5415R centrifuge, Hamburg, Germany) and the sediment was discarded. The mono-hydroxylated CTAB and di-hydroxylated CTAB are separated and purified by HPLC (NextEra X2, Shimadzu Deutschland GmbH, Duisburg, Germany) using CS RPC column (125 \times 8 mm, Langerwehe, Germany). By injecting 15 times reaction mixture (each injection volume: 200 μ L) in HPLC, purified fractions are collected in plastic tubes separately and dried in a vacuum concentrator. Silicon wafers (p-Typ, CrysTec GmbH, Berlin, Germany) were individually coated with 100 μ L 10 mM CTAB/mono-hydroxylated CTAB (10 mM)/di-hydroxylated CTAB. Contact angle was measured with a G40 goniometer (Krüss GmbH, Hamburg, Germany) using Millipore water. The contact angle was evaluated by the sessile drop method. Briefly, a drop of water of defined volume was placed on the solid surface with a microsyringe and contact angle was determined by light microscopy. Presented data represents the mean values of three measurements.

3.4 Result and discussion

3.4.1 OmniChange library generation and diversity estimation

Simultaneous site mutation of positions R47 (2 amino acids; GAN), Y51 (9 amino acids; NYN), F87 (5 amino acids; GNN), and L188 (20 amino acids; NNK) encodes up to 1800 different P450 BM3 variants (**Figure 35**; N: any nucleotide; K: G or T; Y: T or C). In detail, position 47 was restricted to two negatively charged amino acids (D and E) which were reported to be important for CTAB conversion before^[218]. Position 51 was limited to hydrophobic (A, V, I, L, M, F) and uncharged amino acids (S and T) to ensure a strong ionic interaction of positively charged CTAB to the negatively charged amino acid at position 47^[239]. Molecular dynamics (MD) simulations and quantum-mechanical/molecular mechanics (QM/MM) calculations of P450 BM3 towards N-palmitoylglycine reported that F87 orients the substrate toward the catalytic heme center therefore sterically differing amino acids (A, V, D, E, G) were selected^[240]. Position 188 was subjected to the full diversity as it has been reported that neither of the 19 mutants of L188 did display an obvious preference towards palmitic acid^[222]. The quality level of the OmniChange mutant library was confirmed by sequencing 15 randomly picked clones (see **Table 19**). All picked and sequenced P450 BM3 variants were unique and only a single variant exhibited an undesired substitution R47M (CGT → ATG; see **Table 20**).

Table 19. Sequencing results of 15 randomly picked clones from the OmniChange library in which four positions (R47, Y51, F87, and L188) were simultaneously mutated.

Position	Used mutational codon	Number of theoretically codons	Number of found codons	Number of theoretically amino acids	Number of found amino acid substitutions
R47	GAN	4	5	2	3
Y51	NYN	32	13	9	6
F87	GNN	16	9	5	4
L188	NNK	32	10	20	8

Table 20. Sequences result of 15 randomly picked clones from the P450BM3 OmniChange library.

	R47	Y51	F87	L188
Clone 1	D (CGT→GAT)	L (TAC→CTA)	A (TTT→GCT)	G (CTG→GGT)
Clone 2	D (CGT→GAC)	L (TAC→CTA)	G (TTT→GGG)	L (CTG→TTG)
Clone 3	D (CGT→GAT)	L (TAC→CTT)	G (TTT→GGA)	F (CTG→TTT)
Clone 4	E (CGT→GAG)	S (TAC→TCC)	V (TTT ⇒ GTG)	V (CTG→GTT)
Clone 5	D (CGT→GAT)	A (TAC→GCA)	V (TTT→GTT)	G (CTG→GGT)
Clone 6	M (CGT→ATG)	M (TAC→ATG)	F (TTT→TTT)	L (CTG→CTG)
Clone 7	D (CGT→GAC)	L (TAC→TTG)	F (TTT→TTT)	D (CTG→GAT)
Clone 8	STOP (CGT→TAG)	L (TAC→TTA)	A (TTT→GCG)	F (CTG→TTT)
Clone 9	E (CGT→GAA)	V (TAC→GTC)	A (TTT→GCG)	V (CTG→GTG)
Clone 10	E (CGT→GAG)	A (TAC→GCG)	A (TTT→GCA)	S (CTG→TCT)
Clone 11	E (CGT→GAA)	A (TAC→GCT)	G (TTT→GGA)	R (CTG→AGG)
Clone 12	E (CGT→GAG)	I (TAC→ATT)	V (TTT→GTT)	A (CTG→GCT)
Clone 13	D (CGT→GAC)	V (TAC→GTT)	V (TTT→GTT)	F (CTG→TTT)
Clone 14	E (CGT→GAG)	S (TAC→TCC)	V (TTT→GTG)	V (CTG→GTT)
Clone 15	E (CGT→GAA)	S (TAC→TCG)	E (TTT→GAG)	L (CTG→CTG)

3.4.2 P450 BM3 variants for CTAB hydroxylation through screening of OmniChange library

Among the 1740 clones with detectable NADPH consumption activity in the OmniChange library, 696 were rescreened to determine coupling efficiency. Amino acid substitutions of the 12 P450 BM3 variants with high activity and/or high coupling efficiency are shown in **Figure 38** and **Table 21**.

Substitutions in position 47 showed no preference in respect to the two negatively charged amino acids (6×D; 6×E) which is in agreement with a previous study^[218]. At position 51 a strong preference toward the aromatic amino acid F was observed (e.g. four times). At position 87 a strong preference toward a substitution to valine (11×V) was observed. The F87V substitution led to a high improvement of CTAB hydroxylation. Position L188 showed no preference in respect to chemical properties of side chains (e.g. 3×G, 2×D, 1×R, 1×W, 1×Q).

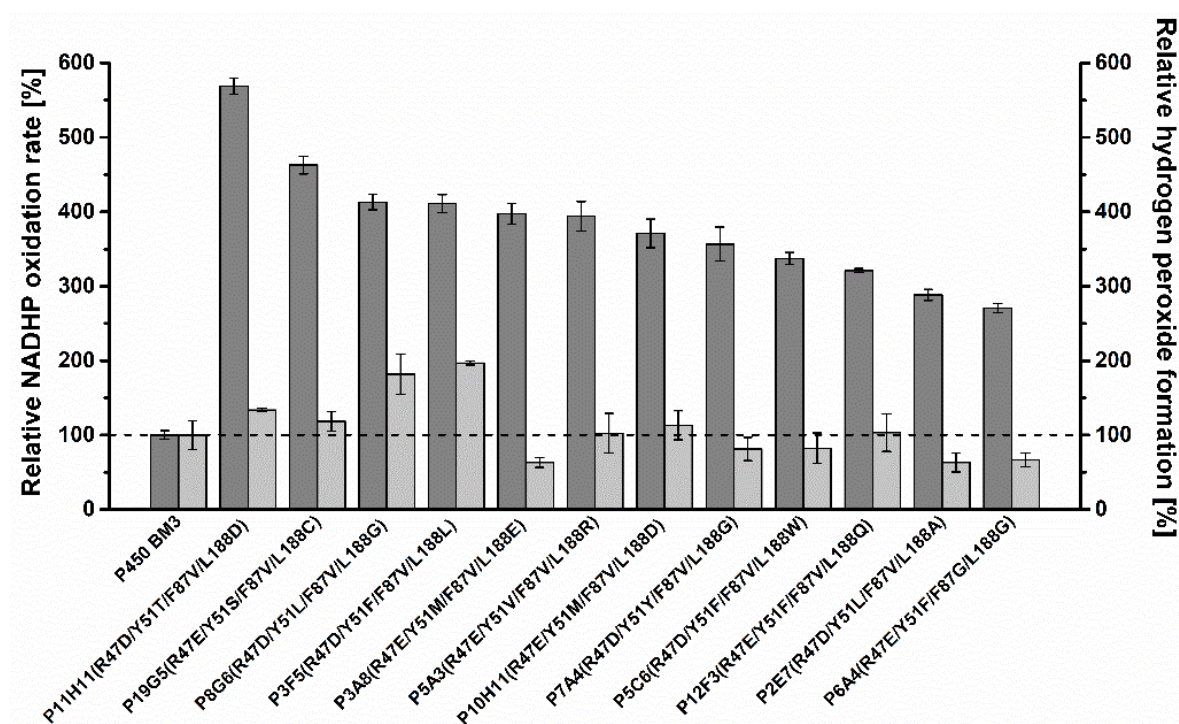


Figure 38. Rescreening results of twelve P450 BM3 variants from the OmniChange library using NADPH consumption assay and H₂O₂ detection assay (in descending order of NADPH consumption rates). The relative NADPH oxidation rate (dark grey) and relative H₂O₂ formation rate (light grey) of wild-type P450 BM3 was set to 100.

Table 21. Amino acid substitutions of 12 selected P450 BM3 variants.

P450 BM3 variant	R47	Y51	F87	L188
P2E7	D (CGT→GAC)	L (TAC→TTG)	V (TTT→GTG)	A (CTG→GCT)
P3A8	E (CGT→GAG)	M (TAC→ATG)	V (TTT→GTT)	E (CTG→GAG)
P3F5	D (CGT→GAT)	F (TAC→TTT)	V (TTT→GTG)	L (CTG→CTG)
P5A3	E (CGT→GAG)	V (TAC→GTG)	V (TTT→GTT)	R (CTG→AGG)
P5C6	D (CGT→GAT)	F (TAC→TTC)	V (TTT→GTT)	W (CTG→TGG)
P6A4	E (CGT→GAG)	F (TAC→TTT)	G (TTT→GGT)	G (CTG→GGG)
P7A4	D (CGT→GAT)	Y (TAC→TAC)	V (TTT→GTG)	G (CTG→GGG)
P8G6	D (CGT→GAT)	L (TAC→TTG)	V (TTT→GTG)	G (CTG→GGG)
P10H11	E (CGT→GAG)	M (TAC→ATG)	V (TTT→GTT)	D (CTG→GAT)
P11H11	D (CGT→GAT)	T (TAC→ACG)	V (TTT→GTG)	D (CTG→GAT)
P12F3	E (CGT→GAA)	F (TAC→TTC)	V (TTT→GTC)	Q (CTG→CAG)
P19G5	E (CGT→GAG)	S (TAC→TCA)	V (TTT→GTC)	C (CTG→TGT)

Interestingly, substitution L188W resulted in significantly reduced hydrogen peroxide formation (see comparison P3F5 (R47D/Y51F/F87V/L188L) and P5C6 (R47D/Y51F/F87V/L188W) in **Figure 38**). The latter results indicate an important role of position 188 in modulating coupling efficiency. A further confirmation for the role of position 188 was obtained by comparing the substitutions in P8G6 (R47D/Y51L/F87V/L188G) and P2E7 (R47D/Y51L/F87V/L188A) (see **Figure 38**). Notably, the P11H11 (R47D/Y51T/F87V/L188D) variant has the highest NADPH oxidation rate of all enzyme variants, while P3A8 (R47E/Y51M/F87V/L188E) exhibits the lowest H₂O₂ production rate. Based on the catalytic performance and coupling efficiency,

variants P2E7, P3A8, P5A3, P5C6, P6A4, P8G6, P10H11, P11H11, P12F3, and P19G5 were selected for detailed studies.

3.4.3 Product identification of CTAB hydroxylation

Products of CTAB hydroxylation were determined for ten P450 BM3 variants (P2E7, P3A8, P5A3, P5C6, P6A4, P8G6, P10H11, P11H11, P12F3, and P19G5) and wild-type P450 BM3 through long-term conversion (16 h, room temperature; see Material and Methods) and HPLC-MS/MS analysis. Wild-type P450 BM3 hydroxylates CTAB with slow rate as documented by a very small product peak at 6.9 min (mono-hydroxylated CTAB) and the large CTAB peak at 9.0 min with $m/z=284.3$ (see **Figure 39a&c**). The engineered P3A8 showed an efficient CTAB hydroxylation (mono- and di-hydroxylated products) and a remaining small substrate peak (CTAB; **Figure 39b&c**). In detail, the peaks at 6.1 and 6.3 min with $m/z=316.3$ (**Figure 39b&c**) correspond to two di-hydroxylated CTAB products^[218].

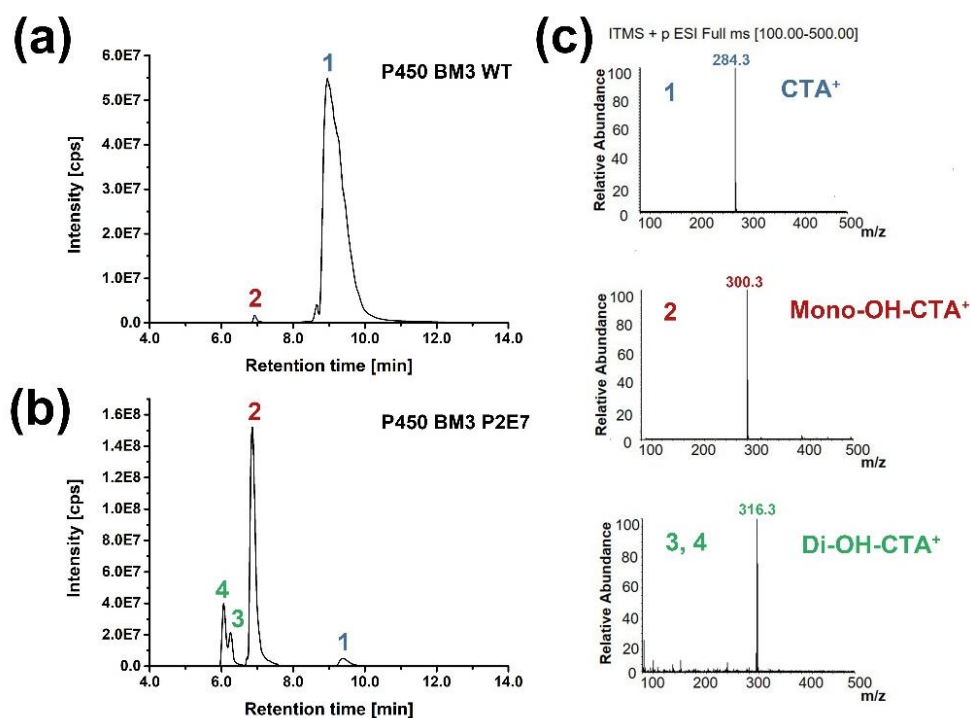


Figure 39. Exemplary HPLC chromatograms of CTAB conversion by (a) wild-type P450 BM3, (b) P450 BM3 variant P3A8. (c) MS spectrometry of products and CTAB.

The regioselectivity of CTAB hydroxylation was determined by NMR analysis (see **Figure 40& Figure 41**). After 16 h conversion, P2E7 hydroxylates for the mono-hydroxylation mainly at the $\omega-1$ position (**Figure 40& Figure 42**). P3A8 yields after 16 h conversion di-hydroxylated CTAB products (yield 77 %) at the $\omega-1/\omega-2$ and $\omega-1/\omega-3$ position (**Figure 41**). Variant P3A8 gave predominantly 2,4-OH-CTAB (55 %), along with

2,3-OH-CTAB (33 %) and 2-OH-CTAB (12 %) (**Table 22**). Variants P2E7, P10H11, P11H11, P12F3, by contrast, yielded mainly 2-OH-CTAB (55-64 %), along with 2,4-OH-CTAB (24-29 %), 2,3-OH-CTAB (12-17 %). Furthermore, variants P5A3, P5C6, P6A4, P8G6, P19G5, yielded even higher ratio of 2-OH-CTAB (87-97 %) and small quantities of 2,3-OH-CTAB (1-8 %), 2,4-OH-CTAB (2-7 %).

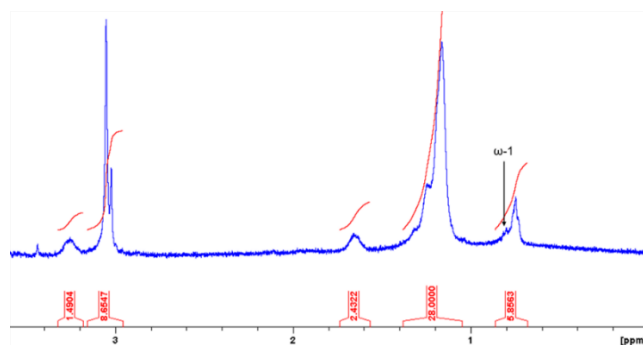


Figure 40. ^1H NMR spectra (400 MHz, 23 °C, D_2O) of and the reaction mixture catalyzed by P2E7.

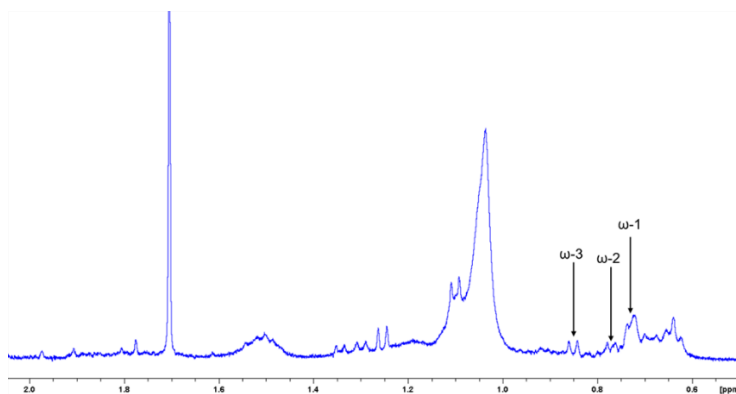


Figure 41. ^1H NMR spectra (400 MHz, 23 °C, D_2O) of the reaction mixture catalyzed by P3A8.

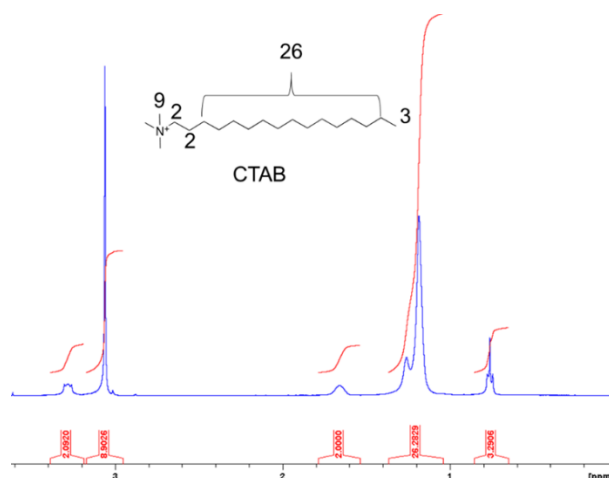


Figure 42. ^1H NMR spectrum (400 MHz, 23 °C, D_2O) of CTAB.

Table 22. Regioselectivity of P450 BM3 variants after 16 h for the hydroxylation of CTAB.

P450 BM3 catalyst	Conversion [%]	Product distribution*		
		2-OH-CTAB [%]	2,3-OH-CTAB [%]	2,4-OH-CTAB [%]
WT	0.2	100	-	-
P2E7	59.0	61	13	26
P3A8	90.0	12	33	55
P5A3	9.2	89	8	3
P5C6	8.1	88	5	7
P6A4	7.5	91	5	4
P8G6	0.7	87	8	5
P10H11	23.2	58	17	25
P11H11	27.9	64	12	24
P12F3	30.7	55	16	29
P19G5	1.7	97	1	2

*Selectivity was determined by peak area of products in HPLC-MS. Reaction conditions contained 2 μ M CFEs, 1 mM CTAB, 100 μ M NADPH, 5 U mL⁻¹ GDH, 20 mM glucose, 1200 U mL⁻¹ catalase, and potassium phosphate buffer (100 mM, pH 7.5) in a final volume of 3 mL. The reactions were allowed to proceed 16 h. All reactions were performed in triplicate.

3.4.4 Kinetic characterization of improved enzyme variants

Four P450 BM3 variants P2E7 (R47D/Y51L/F87V/L188A), P3A8 (R47E/Y51M/F87V/L188E), P11H11 (R47D/Y51T/F87V/L188D) and P12F3 (R47E/Y51F/F87V/L188Q)) were selected and purified for kinetic characterization (**Table 23**). Kinetic parameters such as k_{cat} and K_{M} values were calculated on the basis of initial NADPH depletion speed at different substrate concentrations and correlation to actually consumed NADPH. Due to turbidity formation in the assay^[241-243], up to 40 μ M CTAB and hydroxylated products were applied for k_{cat} and K_{M} determination to avoid formation of micelles. The kinetic constants of P450 BM3 variants and wild-type P450 BM3 for hydroxylation of CTAB are shown in **Table 23**. All four P450 BM3 variants had enhanced k_{cat} for CTAB hydroxylations. For instance, P3A8 reached an initial k_{cat} value of 64.9 s⁻¹ per P450 molecule which is 13 times higher than k_{cat} value of wild-type P450 BM3 (4.8 s⁻¹). As a general trend, one could observe that the coupling efficiency is in all four variants (P12F3, P11H11, P2E7, P3A8) significantly improved in comparison to wild-type P450 BM3 (0.5 %). Coupling efficiencies increased to 24.0 % (P11H11), 24.4 % (P12F3), 43.9 % (P2E7), and 92.5 % (P3A8). Coupling efficiencies in the range of 10-40 % are reported for some P450 BM3 variants for non-natural compounds^[244, 245]. A coupling efficiency of

92.5 % is exceptional high which is comparable to those measured for wild-type in the hydroxylation of C₁₂-C₁₄ fatty acids (88-96 %)^[246].

Table 23. Kinetic constants of P450 BM3 variants and WT P450 BM3 for hydroxylation of CTAB.

P450 BM3 variant	K_M [μM]	k_{cat} [s^{-1}]	k_{cat}/K_M [$\text{M}^{-1} \text{s}^{-1}$]	Coupling efficiency [%]	TTN*
WT	23.7 ± 3.3	4.8 ± 0.4	2.0×10^5	0.5 ± 0.02	1
P2E7	12.6 ± 2.5	51.2 ± 4.0	4.1×10^6	43.9 ± 3.4	295
P3A8	11.7 ± 2.2	64.9 ± 4.8	5.6×10^6	92.5 ± 6.1	450
P11H11	13.7 ± 2.0	54.4 ± 3.5	4.0×10^6	24.0 ± 0.3	139
P12F3	10.8 ± 1.2	52.6 ± 2.3	4.9×10^6	24.4 ± 2.8	153

* Total turnover numbers are reported as nmol product/nmol protein. Reaction conditions contained 0.1 μM purified P450 BM3 WT/variants, 1-40 μM CTAB, 100 μM NADPH, and potassium phosphate buffer (100 mM, pH 7.5) in a final volume of 1 mL. All reactions were performed in triplicate.

The productivities of CTAB hydroxylation were investigated in CERTAN glass tubes (9 mL; 3 mL reaction volume) over a course of three hours and production formations were determined by HPLC-MS. In accordance with **Figure 39**, **Figure 43** exemplarily shows the timescale of CTAB conversion and mono- and di-hydroxylated product formation on the example of P450 BM3 P3A8. The productivity of CTAB hydroxylation products by variant P2E7, P3A8, P11H11, P12F3 is up to 100, 108, 200, 292 $\text{mg L}^{-1} \text{h}^{-1}$ separately.

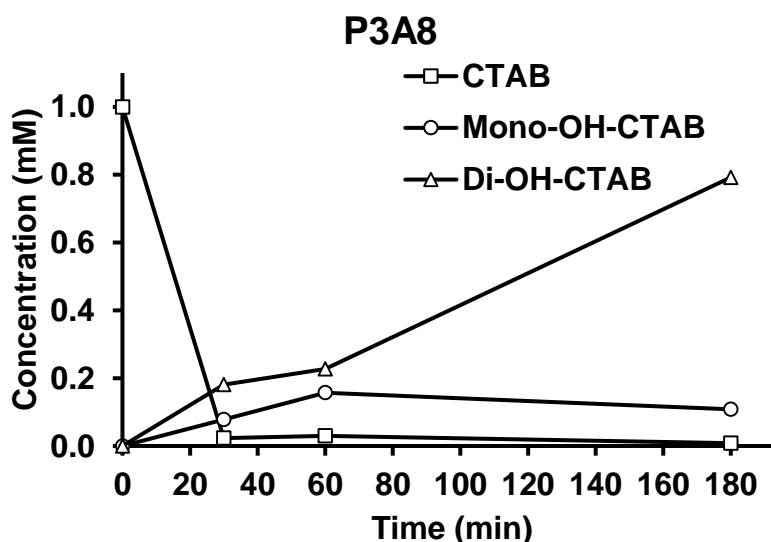


Figure 43. Exemplary timescale of CTAB conversion and mono- and di-hydroxylated product formation on the example of P450 BM3 P3A8. P3A8 was selected in order to be consisted to the reported HPLC-MS/MS results.

3.4.5 Surface contact angle measurements

Mono- and di-hydroxylated CTAB were separated using HPLC. Surface properties of mono- and di-hydroxylated CTAB were determined by sessile drop contact angle measurement on silicon wafers (**Figure 44**). As expected one could observe that with an increased number of hydroxyl-groups the contact angle is reduced (di-hydroxylated CTAB: $\theta = 16.7^\circ$; mono-hydroxylated CTAB: $\theta = 27.5^\circ$; CTAB layer with water: $\theta = 36.8^\circ$). The low contact angle for the di-hydroxylated CTAB is excellent for a cationic surfactant^[196, 200].

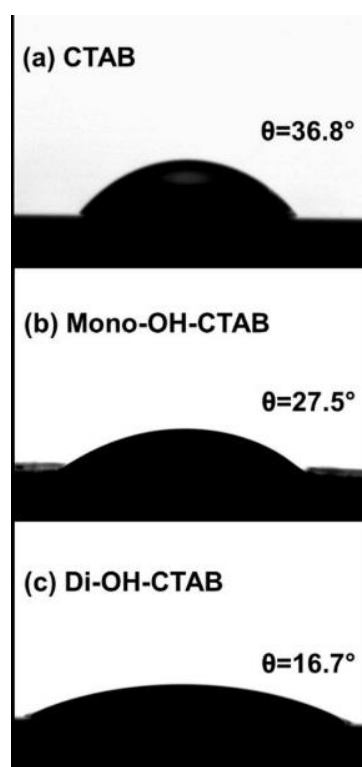


Figure 44. Surface contact angle measurement. a) A droplet of water on a CTAB surface; b) a droplet of water on a mono hydroxylated CTAB surface; c) a droplet of water on a di-hydroxylated CTAB surface.

3.5 Conclusions

P450 BM3 substrate specificity was altered by simultaneous site mutation in four relevant positions (R47, Y51, F87, and L188) using the OmniChange method. Improved variants were identified in a two-step screening system (first: NADPH depletion assay (1740 clones)// second: NADPH depletion assay followed by determining the coupling efficiency of active clones through H_2O_2 quantification (696 clones). Then 10 promising P450 BM3 variants were analyzed by HPLC-MS/MS. The P450 BM3 variants (P2E7,

P3A8, P11H11, P12F3) had significantly improved productivities and were kinetically characterized after purification. Interestingly all four variants were capable of dihydroxylating CTAB and coupling efficiency up to 92.5 % were obtained. The P450 BM3 variant P3A8 (R47E/Y51M/F87V/L188E) displayed an initial activity ($64.9 \pm 4.8 \text{ s}^{-1}$, 13.5-fold improvement) which matches the specific activity for its natural fatty acid substrate (palmitic acid, $32\text{-}122 \text{ s}^{-1}$). Notably, variant P2E7 (R47D/Y51L/F87V/L188A) forms 35 times more 2-hydroxylated CTAB than P450 BM3-WT.

4 Summary and conclusion

Catechols are considered as primary pollutants in wastewater due to high toxicity and low biodegradability. Sulfation is an important way to detoxify harmful catechols and the resulting products (catechol sulfates) with potential anti-inflammatory activity are used as biomarkers for disease surveillance (e.g. Parkinson's disease, cardiovascular diseases). Enzymatic sulfation by aryl sulfotransferases as a sustainable technology is an attractive alternative to chemical methods for sulfation. Therefore, the main focus of the first part was the engineering of aryl sulfotransferase B towards catechols for improved chemo- and regioselective sulfation.

In this work, the first product-based two-step *p*-NPS-4-AAP screening system for directed ASTB evolution towards catechol and catechol derivatives was established. Increased transfer efficiency and improved sulfation stoichiometry were achieved through the two-step screening procedure in a one-pot reaction. In the first step, the *p*-NPS assay was used (detection of the colorimetric by-product, *p*-nitrophenol) to determine the apparent ASTB activity. The sulfated product was quantified by the 4-AAP assay in the second step. A comparison of product formation to *p*-NPS consumption ensures successful directed evolution campaigns of ASTB. By using 3-chlorocatechol as a reference substrate, the two-step screening system was optimized step-by-step and a true CV below 15 % was obtained. This two-step screening system was validated by a random mutagenesis library (SeSaM library) and enable some unreported variants including variant ASTB-M5 (V430A) with up to 2.4-fold improved k_{cat} value toward 3-chlorocatechol. HPLC/MS analysis confirmed ASTB-M5's improved sulfate stoichiometry (29 %) compared to ASTB-WT (58 %) for the "screening compound" (3-chlorocatechol). This was the first synthetic access to chemo- and regioselectively sulfate catechols through the aryl sulfotransferase ASTB from *D. hafniense*. The novel *p*-NPS-4-AAP assay enables directed evolution campaigns for aryl sulfotransferases, allows direct product detection without any substrate modification, and eliminates less productive variants. Furthermore, the product-based screening system can likely be combined with non-colorimetric sulfate donors such as "green" or more cost-effective sulfate donors (e.g., *N*-hydroxysuccinimide-sulfate^[128]). In addition, attractive aryl sulfotransferases for instance from well-studied *Eubacterium A-44*, *E. coli CCFT073* can be evolved for the latter sulfate donors and the substrate profile can be expanded to other 4-AAP detectable compounds with a "free" *para*-position (e.g., cyclic trichrysobactin).

Based on the established screening system, further engineering of ASTB was conducted by KnowVolution campaign for improved sulfate transfer efficiency towards catechol and catechol derivatives. Four regions (positions in loop region; positions close to the catalytic center; positions in loop22 and loop24 regions; positions in the dimer interface) with different roles were eluted in ASTB by one round of random mutagenesis. The combination of computational analysis (based on homology model) and multi-site saturation (using OmniChange method) of the four positions (Q191, V199, Y218, and L225) in loop region (loop12& loop13) close to catalytic site H220 boosted the k_{cat} from 6.1 to 13.6-fold for catechols with minimal experimental effort. Regioselective and highly efficient sulfation of substituted catechols with sulfate transfer efficiency up to 94 % has been achieved. Final variant ASTB-OM2 (Q191Y/Y218W/L225V) also enables the improved sulfation activity towards different classes of pharmaceutically important compounds (dopamine, tanshinol, taxfolin, and quercetin) with up to 10-fold improved conversion. Therefore, the activity modulation of ASTB for a broad range of catecholic compounds was successfully accomplished by KnowVolution strategy. Taken together, we regard ASTB-OM2 as robust catalysts and novel green synthesis route to start process developments for the production of valuable sulfated catechol derivatives and structurally related compounds such as mycamine, sodium picosulfate, and minoxidil sulfate.

Bolaform surfactants are a novel class of compounds with a wide range of industrial and technical applications by forming very small micelles that are more effective than contemporary surfactants. They are biodegradable and sustainable surfactants that offer excellent solubility properties and novel possibilities for drug delivery and/or compound formulations. However, their production is expensive and involves the use of strong acids and large amounts of solvents. An alternative green synthesis route is direct hydroxylation through monooxygenase P450 BM3 as performed in nature which was the second focus of this thesis.

Simultaneous site mutagenesis using the OmniChange method at four P450BM3 positions (R47, Y51, F87, and L188) with degenerated codon yielded P450BM3 variants with excellent catalytic (35-fold improved productivity; P450 BM3-P2E7) and excellent coupling efficiency (up to 92.5 %; P450 BM3-P3A8). Improved variants were identified in a two-step screening system (first: determination of NADPH depletion; second: identification of H₂O₂ generation). Notably, di-hydroxylation products of CTAB with bolaform surfactant properties have for the first time been produced. To meet the industrial application scale, biocatalyst P450 BM3-P3A8 (TTN = 450) has to reach another 20-fold

improvement for bolaform surfactant production. Additionally, the two-step screening system proved to be efficient to boost coupling efficiency and can likely be used in many other P450 evolution campaigns to generate robust P450 catalysts.

To sum up, this thesis covers the successful protein engineering of two different classes of enzymes (aryl sulfotransferase B and P450 BM3 monooxygenase) using different evolution strategies for sustainable synthesis of biodegradable high-value chemicals catechol sulfates (> 600 €/kg) and bolaform surfactants (> 200 €/kg), respectively. To the best of our knowledge, new biocatalyst ASTB-OM2 generated in this thesis is up to now the best enzymatic catalyst for the production catechol monosulfates. Last but not least, new biocatalysts P450 BM3-P3A8/P450 BM3-P2E7 are the best biocatalysts for bolaform surfactants mono-hydroxylated CTAB/di-hydroxylated CTAB production.

5 Appendix

5.1 List of abbreviations

4-AAP	4-aminoantipyrine
ACN	Acetonitrile
ASST	Aryl(sulfate) sulfotransferase
ASTA	Aryl sulfotransferase A
ASTB	Aryl sulfotransferase B
ASST_ <i>Eu</i>	Aryl(sulfate) sulfotransferase from <i>Eubacterium A-44</i>
ASST_ <i>E. coli</i>	Aryl(sulfate) sulfotransferase from <i>E. coli</i>
ASST_ <i>Pseudo</i>	Aryl(sulfate) sulfotransferase from <i>Pseudomonas sp.</i>
ASST_ <i>Strepto</i>	Aryl(sulfate) sulfotransferase from <i>Streptomyces sp.</i>
ATP	adenosine triphosphate
BCA	Bicinchoninic acid
BVMO	Bayer-Villiger monooxygenase
bp	Base pair
CTAB	Cetyl-trimethylammonium bromide
CFE	Cell free extract
CPR	NADPH dependent Cytochrome P450 reductase
3CyC	3-Cyano-7-hydroxycoumarin
CYP	Cytochrome P450 Monooxygenase
DCC	dicyclohexylcarbodiimide
ddH ₂ O	Deionized water
<i>D. hafniense</i>	<i>Desulfitobacterium hafniense</i>
DMF	Dimethylformamide
DMSO	Dimethylsulfoxide
DNA	Deoxyribonucleic acid
dNTPs	Deoxynucleotide triphosphate
epPCR	error-prone polymer chain reaction
<i>E. coli</i>	<i>Escherichia coli</i>
ESI	Electrospray ionization
EV	Empty vector
GAN	G: Guanine; A: Adenine; N: Any nucleotide
GDH	Glucose dehydrogenase
GNN	G: Guanine; N: Any nucleotide
GO _x	Glucose oxidase
His	Histidine
HNLs	Hydroxynitrile lyases
HPLC-MS	High performance liquid chromatography-mass spectrometry
HRP	Horse radish peroxidase

HTS	High-throughput screening
IPTG	Isopropyl- β -D-thiogalactopyranoside
IUBMB	International Union of Biochemistry and Molecular Biology
kb	Kilobase
kDa	Kilodalton
KPi	Potassium phosphate
MTP	Microtiter plate
NADPH	Nicotinamide adenine dinucleotide phosphate
NMR	Nuclear magnetic resonance
NNK	N: Any nucleotide; K: Guanine or Thymine (keto)
NYN	N: Any nucleotide; Y: Thymine or Cytosine (Pyrimidine)
OD ₆₀₀	Optical density at 600 nm
P450 BM3	Cytochrome P450 from <i>Bacillus megaterium</i> 3
PAPS	3'-phosphoadenosine-5'-phosphosulfate
PCR	Polymerase chain reaction
PDA	Photometric Diode Array
PLICing	Phosphorothioate-based ligase-independent gene cloning
<i>p</i> -NP	<i>para</i> -nitrophenolate
<i>p</i> -NPS	<i>para</i> -nitrophenyl sulfate
ppm	parts per million
PTO	Phosphorothiolated oligonucleotides
Py	Pyridine
rpm	Revolutions per minute
RT	Room temperature
SDS-PAGE	Sodium dodecyl sulfate polyacrylamide gel electrophoresis
SeSaM	Sequence saturation mutagenesis
SDM	Site directed mutagenesis
ssDNA	Single-stranded DNA
SSM	Site saturation mutagenesis
U	(Enzyme) Unit
WT	Wild type
WP	working package
YASARA	Yet Another Scientific Artificial Reality Application

5.2 List of DNA and protein sequences

Gene sequence of ASTA (Wildtype):

ATGAACCCGATCAAAAAGCGAACAAATCCCCGCACATTATCCACCGTCAAAAAGACCTGGAAGA
 AGCGTTTCTGGCTGAATTTAGCGCCGGCCATTACACCCTGGAAAACCCGCTGGTGAAACTGAA
 TCCGTATGATATTTGCCCGCTGACCGCAATGGTCCTGTTTGAAACGCCGGTGGCAACCGAAGC
 TACGATTATCGTTCGTGGCAAAGAACATCCGGGTGATATTCGCCACACCTTCCCGGCTGACAA
 AAAACATATCCTGCCGGTCTATGGCCTGTACGCGGATTACGAAAACAAAATCGAAATCGTTCT
 GGCGAACGGCCAGAAAAACACCATTACGCTGAAAACCGAACCGCTGCACCCGGATGTTCCGG
 TCGCAACGTCCATCAAAACCACGCCGGAATATATGGGTAACAATCTGATGTTTCTGACCGCGG
 CCATGAAAGCAATGCCGGTTGGCTATGATTACGCTGGTGAAGTCCGTTGGTATGCGACCCGCA
 ACTTTGCCTTCGACCTGAAACGTATGCCGAACGGCCATATTCTGATCGGTACGGAACGCCTGG
 TGAAACTGCCGTACTTTACCACGGGCCTGTATGAAATGGCCTTCTCTGGTAAAATCTTCAAAG
 AATACCGTCTGAGTGGCGGTTATCATCACGATCAGTTCGTGATGGAAGACGGCAATATCCTGG
 TTCTGACCTTTGATTTCTACTCGGGTACGGTTGAAGATATGTGCGTCCTGCTGGACGCCATTAC
 CGGCGAAATCCTGAAAAGCTGGGATTATAAACGTGTGCTGCCGCAGGACGTTGCAGGTAGCG
 GTTCTCAAGATGCCCATGACTGGTTTCACAACAATGCAGTGTGGTACGATAAGAAAACCCATA
 GTCTGTCCTTCTCAGGCCGCCACCAGGACGTGGTTATTAACCTGGATTATGACACGGGTGAAC
 TGAATTGGATTATCGGCGATCCGGAAGGTTGGCCGCAAGATATGGTCGACAAATACTTTTTCA
 CCCCAGTGGGCGAGGGTGAATTTGATTGGCAGTATGAACAACATGCGTGTGTCGTGCTGCCGG
 ATGGCGACATCATGCTGTTTGATAACGGTCACTTCCGTGCGAAGAAAAAAGAAAATTACCTCG
 CGAACGGCCGTAATTTAGCCGCGGTGTGCGTTATCGCATTGATACCGAAAAAATGACGATCG
 AACAGGTTTGGCAATACGGCAAAGAACGCGGTGCGGAATTTTTCTCCCCGATATTTGCAACG
 TTGAATACTACAACGAAGGCCATTACCTGGTCCACTCAGGCGGTATCGGCTATGAAAACGGTG
 AAACCTGTGAGGGTATGGCCGTGATGAAAGTTCTGCAGCCGGAATTTAAAGATTCTGGTGTTTA
 CCTTCAACAGCATTACGTGCGAACTGAAAGATGACGTCCTGATGTACGAACTGCAAGTGCCGG
 CAAATTGTTATCGCGCTGAAAAACTGCCGCTGTATTACGCACATGAAACCGCTGAACTGGGCG
 CGGGTGAAATTCTGGGCAATCTGATCGAAACCCAGGAAACGAAAATGAAAATCAAAGCAGTT
 GAAACCGGTGAACGTGTCCCGGATCACTATGAAGCTTCTATTACGGAAGAAGAAGATCGCGTT
 CTGTTTAAACGCCATCTTCAAGCAGGCGAAATGGCTCAGCTGCTGCTGGTTGATGGTGACGGC
 GGTGTTAAACGTTATCCGGTCAATACCGTGCCGCAGGCGTTTCAAGCCATGTGTGTGGGCACG
 TTCCAGAAAGCGGATCCGCGCAACATTGACGTTTATATCAATAAAAACCGGCCTGTCAGGTA
 TACCAGGTGAAACTGATTGCTGAAGAAAAACTGTATGAAACGGGTGTGTCCATTACCGCAGAG
 CTCTCTGCATGGAGCCATCCGCAGTTCGAAAAG

Protein sequence of ASTA (Wildtype):

MNPIKSEQIPHIHRQKDLLEAFLAEFSAGHYTLENPLVKLNPHYDICPLTAMVLFETPVATEATIIVRG
 KEHPGDIRHTFPADKKHILPVYGLYADYENKIEIVLANGQKNTITLKTEPLHPDVPVATSIKTTPEY
 MGNLMLFLTAAMKAMPVGYDYAGEVRWYATRNFAFDLKRMPNGHILIGTERLVKLPYFTTGLY
 EMAFSGKIFKEYRLSGGYHHDQFVMEDGNILVLTDFYSGTVEDMCVLLDAITGEILKSWDYKRV
 LPQDVAGSGSQDAHDWFHNAVWYDKKTHLSFSGRHQDVVINLDYDTGELNWIIGDPEGWPQD
 MVDKYFFTPVGEFEFDWQYEQHACVVLDPGDIMLFDNGHFRAKKKENYLPNGRNFSRQVRYRID
 TEKMTIEQVWQYGKERGAEFFSPYICNVEYYNEGHYLVHSGGIGYENGETCEGMAVMKVLQPEF
 KDSVFTFNSITCELKDDVLMYELQVPANCYRAEKLPLYAHETAELGAGEILGNLIETQETKMKIK
 AVETGERVPDHYEASITEEDRVLFNAIFEAGEMAQLLLVDGDGGVKRYPVNTVPQAFQAMCVGT
 FQKADPRNIDVYINKTGLSGKYQVKLIAEEKLYETGVSITAELSAWVSHPPQFEK

Gene sequence of ASTB (Wildtype):

ATGCGTACCTACCTGAATACCGAAAAACATCTGATTACCCTGCAAGCTGAATCTGAAGAACGT
 TTCCTGGCCGAACCTGCGTGCTGGTAACTACACCGCCGAATCACCGCTGGTTGTGAAAAACCCG
 TATATTATCAATCCGCTGGCGGCCGTTATTTGCTTTAATACGGATGAAGAAACCACGGCCGAA
 ATTACCGTCAAAGGCAAAGCAATCGAAGGTGACCTGTCTCATACTTCGCAGCTGCGAAAGAA
 CACGTTCTGCCGGTCTATGGCCTGTACGATGACTATGTGAACACGGTCGTGATCAAACCTGAGT
 AATGGTAAAACCAGCGAAGTGAAAATTGAAGTGGAAGAAGTGAACGTTAATAAAGCCCTGTA
 CTGCCGACCCACGCCGGAATACTTCGGCAAAGATTTTCATGCTGATCTCAACCACGACCCCGCT
 GATCGAATCGGCTCGTACGGCAGGCTTTGATTACGCAGGTGACCTGCGTTGGTGTATTACCAA

CCTGCAGTCATGGGATATCAAAAACTGGAAAATGGTCGCCTGCTGTATACGTCGCATCGTAC
 CGTGCAGAAACCGTATTACAACGTGGGCGTTATGGAAATGGATTTCTGTGGTAAAATCTACAA
 AGAATACCGTCTGCCGGGCGGTTATCATCACGACGCGGTTGAACTGGAAAACGGCAATATTCT
 GGCCGCAAGTGATAACGACTTTAATGATTCCGTGGAAAGACTTCGTTGTGCGAAATTGAACGCGC
 CACCGGCGCAGTTATCAAAGTTGGGATCTGCAGAAAATTCTGCCGCGCGGCCAGGGTAAAG
 CTGGTGATTGGAACCATCACGACTGGTTTCATAACAATGCGGTGTGGTACGATAAACCGACGA
 ATAGCATCACCATGTCTGGCCGCCACATGGACGCTGTTATTAACCTTCGATTATGACAGCGGTG
 CGCTGAATTGGATCCTGGGCGATCCGGAAGGTTGGTCTGAAGAATGGCAGAAAATACTTTTTCA
 AAAACGTGACCAAAGGCGATTTTGACTGGCAGTATGAACAACATGCTGCGCGTATTCTGCCGA
 ATGGCGATGTTTTCTGTTTCGACAACGGCACGTATCGCAGTAAAAATGAAGCTACCCGTGTGG
 ATCCGGAACAGAATTTTTCCCGCGGTGTTATTTACCGTATCGATACCGACAAAATGGAAATCG
 AACAAAGTGTGGCAATATGGCAAAGAACGCGGTGCCGAATTCTACAGCCCGTATATCTGCAACG
 TCGATTATTACGCGAAGGTCATTACATGGTGCACCTCTGGCGGTATTGCCACGTATCGTGGCA
 AACACCCGATGGCTGGGTGCAATGCTGTGAACAAATACAAAGACGAACATATCCACCTG
 ACGTGGAAATCAATCACCGTCGAAGTGCAGAACGATCAACTGAAATACGAACTGAAAGTGCA
 GGGCGGTAATTATTACCGCGCACGTCCGTTTCGCCGTATGATGAAAAACCAACCTGGTCTCT
 GGGCAAAGGTGAACTGCTGGGCGGTTTTGGTGTACGCCGAATTTATGAAAGTCAATTTCAA
 AGATGCGGAAACCGAACTGAGCGAAAAACATAACCTGAATGTCATCCTGGAAGAAGACCGTC
 TGGCTATTCGCGCGTCATTTCTGTAAGGCTCGCAGGTTTTCTGGAAGTGAAGGGTGCAGAAC
 AAAGTAAATTTTATAACATTCGACGGAAGTGCACGATGTTACCGCCGCATGTGTCTCTTCG
 AAGAACAGAACGATAATGACTTTCAATTCTATGTGAGCCGTGAAGGCCTGTCTGGTGAATTCG
 GCATCTACCTGAACATTGATAGCAAACGCTACGATACGCATCTGTCTGTGAACTGGAGCTCT
 CTGCATGGAGCCATCCGCAGTTCGAAAAG

Protein sequence of ASTB (Wildtype):

MRTYLNTEKHLITLQAESEERFLAELRAGNYTAESPLVVKNPYIINPLAAVICFNTDEETTAEITVKG
 KAIEGDLSHTFAAAKEHVLVPVYGLYDDYVNTVVIKLSNGKTSEVKIEVEELNVNKALYCRTTPEYF
 GKDFMLISTTTPLIESARTAGFDYAGDLRWCITNLQSWDIKKLENGRLLYTSHRTVQKPYYNVGV
 MEMDFCGKIYKEYRPLPGGYHHDAVELENGNILAASDNDFNDSVEDFVVEIERATGAVIKSWDLQK
 ILPRGQKAGDWNHHDWFHNNAVWYDKPTNSITMSGRHMDAVINFDYDSGALNWILGDPEGWS
 EEWQKYFFKNVTKGDFDWQYEQHAARILPNGDVFLFDNGTYRSKNEATRVDPEQNFSGVIYRID
 TDKMEIEQVWQYGKERGAEFYSPYICNVDYYGEGHYMVHSGGIATYRGKHTDGLGAMLLNKYK
 DEHIHLTLESITVEVQNDQLKYELKVQGGNYRARRVSPYDEKTNLVLGKGELGGFGVTPEFMK
 VNFKDAETELSEKHNLVILEEDRLAIRASFREGSQVFLELKGAEQSKFYNIPTVHDVTAACVSFE
 EQNDNDFQFYVSREGLSGEFGIYLNIDSKRYDTHLSVKLELSAWSHPQFEK

Gene sequence of ASST *Strepto* (Wildtype):

ATGTTTCGACAAATACCGTAAAACCCCTGGTTGCAGGCACCGTTGCAATTACCTGGGTCTGAGC
 GCAAGCGGTGTTATGGCAATGACCGTCTGGTTCGTCGTCGTACCCGTGCAGCAAGCCGTCGT
 AGCACCAGCGCAGTTCGTCTGATGGCACTGCTGGTTACCGCAGTTCGTGACCCTGGCACTGGGT
 AGCGCACCGGGTCTGGCAGCACAGAGCCCGAGTGGTCTGCCTGGTTCATCCGCTGAGCCTGGTT
 ACCCGTCCGGATCTGCTGCCTCCGGCAATTGATGTTCTGTGAAAGTGCACCGGGTACAAGTCCG
 GGTTATGTTTTCTGGCACCGAAAACCGGTGATGTTCTGCAGGGTCCGGGTACTGTCAGAGC
 GGTCGGATGATTGTTGATAATGAAGGTGAACCGGTTGGTTTCTGCCTCGTGGTATTGGTGCAC
 TGAATTATGTTACCGCATTTACAGCGTCAGACCTATCGTGGCGAACCGGTGCTGACCTGGTGGG
 AAGGTGCACCGCTGCCGACCGGTGTTGGTGGTGGTTATTGGGTTGTTATGGATCAGAGCTATC
 GCGAAATTGCACGTATTCGTGCAGGTAAGGTCATGCCGGTGCCGATCTGCACGATATGCAGA
 TTACACCGGATAAATACCGCACTGGTTCTG
 ATTGCAGAACCGCAGCTGCATCGTGTGATGGTTCATGCACGTCTGGTTATGAATAACATTGTG
 CAAGAAATTGATATTGCCAGCGCACCGTCTGCATGAATGGGATAGCCTGCGTCATGTTGAT
 GTTGATGAAAGCTATCTGAGCAGCATTCCGCTGCTGCCGTATGATTATGTTTCATATTAACAGCA
 TGAGCGTGGATACCGATGGTAATCTGCTGCTGAGCGGTGTAATACCCATGCAGTTTATAAAG
 TTGATCGTCACAGCGGTGATATCATTGGCGTCTGGGTGGCAAAAAAACGATTTACCATGG
 AAAAAGGTGCAAGCTTTGCATGGCAGCATGATGTTAGCCGTGAAGGTGATGGCACCCTGAGC
 GTTTTTGATAATGCAGCAGCAGGTAGCATTGAAACCGGTGGTGGCGCACCGCCTGGCACCCTG
 AGTCGTGCACTGTTTCTGAGTGTGATACCGAAGCACGTACCGCACGTGTTGATCGTAGCTATA
 CCAGTCCGGATGGTCTGCTGAGCACCAGGGTAGCATGCAACTGCTGCCGAATGGCAATG
 TTCTGGTTGGTTGGGGTAGCCATGGTTATTACACCGAATATGCCGATAGCGGTGAAGTGCTGA

TGAATGCCAGCTTTAAAGATCCGCTGGTTAATAGCTATCGTGCCCTGCGTTTTCCGTGGCATGG
TCGTCCGACCGATAGTCCGGCAGTTGCAGGTCGTGCGGGTGCACATGGTATGACCGTGCATGC
CAGCTGGAATGGTGCAACCGAAGTTGCAAGCTGGCGTATTCTGGCAGGCGATACACCGCAGA
GCCTGAGCGGTGTGAAAGAAGTTCCGAAAGACGCATTTGAAACCAGCGCAACCGTTGCACAT
ACCAGCAGCTATGTTGCAGTTCAGGCACTGGATAGCACCGGTCGTGTTCTGGGCACCAGCAAA
GCCAGCCGTGTTCTAGCGCATGGTCACATCCGCAGTTTGAAAAATGATAA

Protein sequence of ASST *Strepto* (Wildtype):

MFDKYRKTLLVAGTVAITLGLSASGVMAMTVLVRRTTRAASRRSTSAVRLMALLVTAVLTLALGS
APGLAAQSPSGLPGHPLSLVTRPDLLPPAIDVRESAPGTSFGYVFLAPKTGDVQLQPGTLQSGPMIV
DNEGEPVWFLPRGIGALNYVTAQRQTYRGEPLVTTWEGAPLPTGVGVGYWVVMQDSYREIARI
RAGKGHAGADLHDMQITPDNTALVLIAPQLHRVDGHARLVMNNIVQEIDIASGTVLHEWDSLRLH
VDVDESYLSSIPLLPYDYVHINSMSVDTDGNLLSGRNTH
AVYKVDHRHSGDIWRLGGKKNDFTEKGFASFAWQHDSREGDGTLSVFDNAAAGSIETGGGAPP
GTVSRALFSLVDTEARTARVDRSYTSPDGLLSTSQGSMQLLPNGNVLVWGWSHGYYTEYADSGEV
LMNASFKDPLVNSYRALRFPWHGRPTDSPAVAGRAGAHGMTVHASWNGATEVASWRILAGDTP
QSLSGVKEVPKDAFETSATVAHTSSYVAVQALDSTGRVLGTSKASRVRSASWHPQFEK

Gene sequence of ASST *Pseudo* (Wildtype):

ATGTTTCGACAAATACCGTAAAACCCTGGTTGCAGGCACCGTTGCAATTACCCTGGGTCTGAGC
GCAAGCGGTGTTATGGCAATGAATGCAAAAACCCAGCCGCATGATCTGCCGGAAGGTGCATG
TCTGACCGCAAAAGTCCGGATCGTGATGAAGCACTGCTGGGTGATGTTGTTGTTAATCCGTAT
CGTCTGGCACCCTGACCGCCATTATTCGTGATGGTGGTCTGACCGTACCGTACCGTACCGTACCGT
GTGTTCTGGGTCTGGTGAACCGTGGTATTGATATTGTTTATGATGTTAGCGATCGTAGCCTGTG
GACCTATGGTGGTATTCCGGTTTTTGGTCTGTATCCGGATCATGTGAATCAGATTGAAGTGAAC
TATAAAGTGGATGGTGAACCGCATTCGTGAACACTATGAAATTTATGCACCGGCAGTCTGCTG
CCGTTGTTGCAAAACAGACCGCAGCACTGCCTGAAGTTGAACCGGTTAAAGTTGCACCGGGT
TTTGAACAGCGTCTGTACCTGTTAATCATCTGCTGGCAGAAATTCCGGGTGGTCTGCTGCTTA
AATGGAATGGTCTGGGTGGTGCAGCAGAATGGGATAGCGTTGGTAATAATTGGATTGCAGATA
GCAATGGTGATGTGCGTTGGTATCTG
GATATTGAGCAGATTCATGATAGCAATCATCGTGATGGCCTGGGTGGCACCATGGGTTTTTCAT
CAGACCCGTGATGGTAAACTGATTTGGGGTCAGGGTCAGACCTATAGCAAATATGATCTGCTG
GGTCGTCGATTTGGCAGCGTAACCTGCCGGATAAATTTGCAGATTTTAGCCATGAAATTCGC
GAAACCCCGAATGGCACCTATCTGCTGCGTGTGGCACCAGCGATTATCGTCGTCGGGATGGC
AAACGTGTTCTCAATTCGTGATCATATCATCGAACTGAATGAAGCCGGTGTGTTCTGGATT
TTTGGGATCTGAACCAGATTCTGGATCCTTATCGCGGTGAAGTCTGGAAACCCTGGGTAAAG
CAGCAATTCAGCTGCCGATGGTGTTCAGAAACAGGATGAACGTCTGGCAAATGAAGTGGCA
GAAGGCGATCTGCCGTTTGGTGATACACCGGGTGTGGTACAGGTCGTAATTGGGCACATGTT
AATGCCATTGATTATGATGCAGATGACGACAGCATTATTGTTAGCGCACGTCATCAGGGTGT
GTTAAAATTGGTCTGATAAAACAGGTGAAATGGATTCTGGCAGCACCGCAGGGTTGGCCTGCA
CGTCTGCAGGATAAAGTTCTGAAACCGGTTGGTGAAGGTTTTGAATGGTTCATGGACCCAGCAT
ACCGCATGGCTGACCGGTCGTGGTACACTGACCGTTTTTGGATAATGGTTGGGGTCTGATTTTG
GTCCGACAAAAGTGGCAGGTAATTATAGCCGTGCAGTGGAAATACAAAATCGATGAAGCAAAA
GGTACAGTTGAACAGGTTTGGCAGTATGGTAAAGAACGTGGTGTGATGAATGGTATAGCCCGATT
ACCAGCGTTGTTGCATATCGTGCAGATACCGATACCCAGTTTATCTATAGCGCCAGCGTTAATT
TTCTGACACCGCAGAAACTGACCACAGTGTCTGAACGAAGTTCGTCTGGCACCCAAGAAG
TTGCAGTTGAACTGAAAGTTCATAGCCGTGAGCCTGGTAGCGTGGGTTATCGTGCACCTGGTTAT
TGATCTGGATAAAGCATTAGCGCATGGTCACATCCGCAGTTTGAAAAATGATAA

Protein sequence of ASST *Pseudo* (Wildtype):

MFDKYRKTLLVAGTVAITLGLSASGVMAMNAKTQPHDLPEGACLTAKVPDRDEALLGDVVVNPY
RLAPLTAIIRDGGRTLSAAHVRVLGRGERGIDIVYDVSDRSLWYGGIPVFLYDPHVNQIEVSYKL
DGERIREHYEYIYAPAVRLPVVAKQTAALPEVEPVKVAPGFQRLYLFNHLLAEIPGGRAFKNWNLG
GAAEWDVSGNNWIADSNVDVRYLDIEQIHDSNHRDGLGTMGFHQTRDGKLIWGGQQTYSKY
DLLGRRIRWQRNLPDKFADFSHEIRETPNGTYLLRVGTSDYRRPDGKRVRISRDHIIELNEAGDVLDF
WDLNQILDOPYRGELLETLGKAAIQLPDGVQKQDERLANELAEGDLPFGDTPGVGTGRNWAHVNAI

DYDADDDSIIVSARHQGVVVKIGRDKQVKWILAAPQGWPARLQDKVLKPVGEGFEWSWTQHTAW
 LTGRGTLTVFDNGWGRDFGPTKLAGNYSRAVEYKIDEAKGTVEQVWQYGKERGDEWYSPITSVV
 AYRADTDTQFIYSASVNFLTPQKLTTSVLNEVRRGTQEVAVELKVHSRQPGSVGYRALVIDLDKAF
 SAWSHPQFEK

Gene sequence of ASST *E.coli* (Wildtype):

ATGTTTCGACAAATACCGTAAAACCCTGGTTGCAGGCACCGTTGCAATTACCTGGGTCTGAGC
 GCAAGCGGTGTTATGGCAGCAGGTTTTAAACCGGCACCGCTGCAGGTCAGCTGGGTGCAGTT
 ATTGTTGATCCGTATGGTAATGCACCGCTGACCGCACTGGTTGATCTGGATAGCCATGTTATTA
 GTGATGTTAAAGTTACGGTGCATGGCAAAGGTGAAAAAGGTGTTGAAATTAGCTATCCGGTTG
 GTC AAGAAAGCCTGAAAACCTATGATGGTGTTCGGATTTTTGGCCTGTATCAGAAATTTGCCA
 ATAAAGTTACCGTCGAATGGAAAGAAAATGGCAAAGTGATGAAAGATGATTACGTTGTTTCAT
 ACCAGCGCCATCGTGAATAACTATATGGATAATCGTAGCATCAGCGATCTGCAGCAGACCAAA
 GTTATTAAGTTGCACCGGGTTTTGAAGATCGTCTGTATCTGGTTAATACCCATACCTTTACCG
 CACAGGGTAGTGATCTGCATTGGCATGGCGAAAAAGATAAAAATGCAGGTATTCTGGATGCA
 GGTCCGGCAACCGGTGCACTGCCGTTTGATATTGCACCGTTTACCTTTATTGTGGATACCGAAG
 GTGAATATCGTTGGTGGCTGGATCAGGATACCTTTTATGATGGTCTGTGATCGCGATATTAACA
 AACGTGGTTATCTGATGGGTATTTCGTGAAACACCGCGTGGTACATTTACCGCAGTTCAGGGTC
 AGCATTGGTATGAATTTGATATGATGGGTGAGGTGCTGGAAGATCATAAACTGCCTCGTGGTT
 TTGCAGATGCAACCCATGAAAGCATTGAAACCCCGAATGGCACCCTGCTGCTGCCTGTTGGTA
 AAAGCAATTATCGTCTGTGATGATGGCGTTCATGTTACCACCATTCGTGATCATATTCTGGAAGT
 TGATAAAAGCGGTCGTGTTGTTGATGTTTGGGATCTGACCAAATTCGGATCCGAAACGTGA
 TGC ACTGCTGGGTGCCCTGGATGCCGGTGCAGTTTGTGTTAATGTGGATCTGGCACATGCCGGT
 CAGCAGGCAAAACTGGAACCGGATACCCCGTTTGGTGATGCCCTGGGTGTTGGTCCGGGTCGT
 AATTGGGCACATGTTAATAGCATTGCATATGATGCCAAAGACGATAGCATTATTCTGAGCAGC
 CGTCATCAGGGTGTGTTGTTAAAATTGGTCGCGATAAACAGGTGAAATGGATTCTGGCACCGAGC
 AAAGGTTGGGAAAAACCGCTGGCAAGCAAACCTGCTGAAACCGGTTGATGCAAATGGTAAACC
 GATTACCTGTAATGAAAATGGCCTGTGCGAAAACAGCGATTTTCGATTTTACCTATACCCAGCA
 TACCGCATGGATTAGCAGCAAAGGCACCCTGACCATTTTTGATAATGGTGTGATGGTCCCATCT
 GGAACAGCCTGCCCTGCCGACCATGAAATATAGCCGTTTTGTTGAGTATAAAATCGATGAAAA
 AAAAGGCACCGTGCAGCAGGTATGGGAATATGGTAAAGAACGCGGTTATGATTTCTATAGCCC
 GATTACCAGCATCATTGAATATCAGGCAGATCGCAATACCATGTTTGGTTTTGGTGGTAGCATC
 CACCTGTTTGATGTTGGTCAGCCGACCGTTGGTAAACTGAATGAAATTGACTACAAAACGAAA
 GAAGTGAAAGTCGAGATTGATGTGCTGAGCGATAAACCGAATCAGACCCATTATCGTGCCCTG
 CTGGTTCGTCCGCAGCAGATGTTTAAAAGCGCATGGTCACATCCGCAGTTTGAGAAATAATGA

Protein sequence of ASST *E.coli* (Wildtype):

MFDKYRRTLVAAGTVAITLGLSASGVMAAGFKPAPPAGQLGAVIVDPYGNAPLTALVDLDSHVISD
 VKVTVHGKGEKGVESISYPVGQESLKYTDGVPIFLYQKFANKVTVEWKENGKVMKDDYVVHTS
 AIVNNYMDNRSISDLQQTQKVIKVPGFEDRLYL VNTHTFTAQGS DLHWHGEKDKNAGILDAGPAT
 GALPFDIAPFTFIVDTEGEYRWLWDQDTFYDGRDRDINKRGYLMGIRETPRGFTFAVQQQHWYEF
 DMMGQVLEDHKLPRGFADATHESIETPNGTVLLRVGKSNYRR
 DDGVHVTTIRDHILEVDKSGRVVDVWDLTKILDPKRDALLGALDAGAVCVNVDLAHAGQQAKLE
 PDTPFGDALGVGPGRNWAHVNSIAYDAKDDSIILSSRHQGVVVKIGRDKQVKWILAPSKGWKPLA
 SKLLKPDANGKPITCNENGLCENSDFDFTYTQHTAWISSKGLTIFDNGDGRHLEQPALPTMKYS
 RFVEYKIDEKKGTVQVWEYGKERGYDFYSPITSIIIEYQADRNTMFGFGGSIHLFDVQGPTVGLKN
 EIDYKTKVEKVEIDVLSKPNQTHYRALLVRPQQMFKSAWSHPQFEK

Gene sequence of ASST *Eu* (Wildtype):

ATGAGCGTGAAATATAGCTTCGAGGATCATATTATCAACCGCCAGTATGAAGCAGAACAGGC
 AATGCTGGCAAAATTTGAAGCAGGCAATTACACCATTGCAAATCCGCTGGTTACCTATAATGC
 CTATCTGGTTAATCCGCTGAGCGCAGTTGTTTGTTTTAAACCCGAAAAAGAAACCGCAGTTAC
 CGTTACCGTTCTGGGTAAAACACCGCAGGGTAATATTAGCCATACCTTTCCGAAAGCCAAAAA
 ACATGTTCTGCCGATTGTTGGTCTGTATAGCGATTATCAGAACCGCATTGAAATTCGTGCATAT
 CGTGGTGAAAGCAACATTATTACCATTGATGTTCCGGATGTGTTTCGATGGCAAAGAAGTGATT
 TATAGCATGGATACCACACCGGAATATCTGCAGGATAACATTATTCTGGTTAGTCCGGCAGGC

GAAGATCTGGCAGTTGGTTTTGATTATGCCGGTGATGCACGTTGGCATATGACCGTTCCGTGTG
TTTTTATGTTAAACGCCTGAAAAATGGCAACCTGATTATGGGTAGCCATCGTGTATTTCAGAT
GCCGTATTATATGAGCGGTCTGTATGAAATTAGCCCGTGCGGTAAAATCTACAAAGAATTTCCG
TCTGCCTGGTGGCTATCATCACGATGAA
TTTGAAATGGAAGATGGCAATCTGCTGAGCCTGACCGATGATCTGACCAGCGAAACCGTTGAA
GATATGTGTGTTCTGATTGATCGTAACACCGGTGAAATTCTGAAAACCTGGGACTACAAAAAA
TTCTGGATCCGAAAACCGTTAGCCGTAGCGGTAGTTGGAGCGATCATGATTGGTTTTCATAAT
AATGCCGTGTGGTACGACAAAAATACCAATAGCCTGACCTTTAGCGGTGTCATATTGATAGC
ATTGTGAACATTGATTACGAAACCGGTGATCTGAATTGGATTATTGGTGATCCGGAAGGTTGG
CCTGAAGAAATGCAGAAATACTTTTTCAAACCGGTGGGCAATAACTTTGGTTGGCAGTATGAA
CAGCATGCCTGTGTTATTACACCGGATGGTGATGTTATGTGCTTTGATAATCATCACTACGGCA
GCAAAAACAAGAGAATTATCTGGCAGCCAAAGACAATTATAGCCGTGGTGTTCGCTATAAA
ATCAACACAGATGATGACGATTGAACAGGTTTGGCAGTACGGTAAAGATCGTGGTGCAGA
ATTTTTCAGCCCGTATATTTGTAACGTGCAGTATTATAACGAGGGCCATTATATGGTTCATAGC
GGTGGTATTGCATATGATAGCGAAGGTAATCCGAGCGAAGCACTGGGTGCATTTGCAAAAGAT
CAGGGTGGTCTGCTGGAAAGCATTACCGTTGAAATTTGCGATAACAAAAAAATGCTGGACCTG
CATGTTCCGGGTAACCTATTATCGCGGTGAAAAACTGAAACTGTACAGCGACGGTATTAATCTG
GAACTGGGTAAAGGCCAGATTCTGGGTGAAATGGGTGTTACCAAAGAGTTTGATACCGAAATT
CCGCTGGATCCGTCAGGTGAAATGCTGCCGGAAAGCTGTAATGCACGTATTGAAGATGAAATC
GATCGCTTTACCTTTTTTAGCCGCTTTGAGAAAGGTCAGCTGGTTATGCTGCTGCTGGAACAGG
GTGAAGAAGTTCATCGTTATTTTCATTAGCACACCAGTCCGCTTTCTGGCAATGTGTTGTGG
CACCTTTCTGGATTCAGATGATCGTAATACCCGCACCAATATTAACAAAGCAGGTCTGAAAGG
CACCTATGATGTTTCGTGTGATTATCGATGACAAAAAATACGAAACGGGTGTGACCATTAGCTG
TAGCGCATGGTCACATCCGCAGTTTGAGAAATAATGA

Protein sequence of ASST *E.coli* (Wildtype):

MSVKYSFEDHIINRQYEAQAMLAKEAGNYTIANPLVTYNAYLVNPLSAVVCFNTEKETAVTVT
VLGKTPQGNISHTFPKAKKHVLPVGLYSYQNRIEIRAYRGESNIITIDVPDVFDFGKEVIYSMDTTP
EYLQDNILVSPAGEDLAVGFDYAGDARWHMTVPCVFDVKRLKNGNLMGSHRVIQMPYYMSGL
YEISPCGKIYKEFRLPGGYHHDEFEMEDGNLLSLTDDLSETVEDMCVLIDRNTGEILKTWDYKKF
LDPKTVSRSGSWSDHDFHNNNAVWYDKNTNSLTFSGRHIDSIVNIDYETGDLNWIIGDPEGWPEE
MQKYFFKPVGNFNGWQYEQHACVITPDGDVMCFDNHHYGSKNKENYLAAKDNYSRGVRYKINT
DDMTIEQVWQYKDRGAEFFSPYICNVQYYNEGHYMVHSGGIAYDSEGNPSEALGAFKADQGG
LESITVEICDNKMLDLHVPGNYYRGEKLLYSDGINLELKGQILGEMGVTKFDTEIPLDPSGE
MLPESCNAIEDEIDRFTFFSRFEKQLVMLLLEQGEEVHRYFISTTAVPFLAMCCGTFLDSDDRNT
RTNINKAGLKGTYDVRVIIDDKKYETGVTISCSAWSHPQFEK

5.3 List of Figures

<i>Figure 1. Overview of enzyme classes and industrial relevant enzymes.</i>	4
<i>Figure 2. Principles of directed enzyme evolution.</i>	5
<i>Figure 3. The 4-step strategy for the simultaneous saturation of five independent codons by OmniChange.</i>	7
<i>Figure 4. Overview of the KnowVolution strategy which comprises four phases.</i>	8
<i>Figure 5. Engineering of aryl sulfotransferase B for chemo- and/or regio sulfation of catechols.</i>	9
<i>Figure 6. Engineering of P450 BM3 for bolaform surfactants synthesis.</i>	10
<i>Figure 7. Scheme of sulfation vs. sulfonation.</i>	11
<i>Figure 8. Scheme of PAPS-dependent sulfotransferases and ASST-catalyzed reaction.</i>	14
<i>Figure 9. ASST from Escherichia coli CFT073 shows a ping-pong bi-bi reaction mechanism.</i>	14
<i>Figure 10. SDS-PAGE analysis of six sulfotransferases and activity comparison.</i>	27
<i>Figure 11. Sulfation efficiency of 4 different aryl sulfotransferases identified by HPLC.</i>	28
<i>Figure 12. Theoretical sulfation of 3-chlorocatechol catalyzed by aryl sulfotransferase ASTB.</i>	29
<i>Figure 13. Electrospray ionization mass spectroscopic analysis (negative mode) of enzymatic conversion of 3-chlorocatechol by ASTB.</i>	29
<i>Figure 14. Nuclear magnetic resonance (NMR) spectrum of enzymatic conversion of 3-chlorocatechol by ASTB.</i>	29
<i>Figure 15. Principle of the two-step p-NPS-4-AAP screening system.</i>	31
<i>Figure 16. Sulfation of catechols and phenol catalyzed by ASTB-WT followed by treating with 4-AAP.</i>	31
<i>Figure 17. Optimization of important parameters and the coefficient of variation determination.</i>	33
<i>Figure 18. Kinetic curves of ASTB-WT and ASTB-M5.</i>	36
<i>Figure 19. HPLC chromatography of 3-chlorocatechol conversion after 12 h.</i>	37
<i>Figure 20. Electrospray ionization mass spectroscopic analysis of 3-chlorocatechol.</i>	37
<i>Figure 21. Electrospray ionization mass spectroscopic analysis.</i>	39
<i>Figure 22. Overview of ASTB engineering strategy.</i>	41
<i>Figure 23. ASTB secondary structure prediction.</i>	41
<i>Figure 24. Molecular docking study and conservation analysis.</i>	43
<i>Figure 25. Agarose gel analysis of DNA fragments for ASTB OmniChange library generation.</i>	44
<i>Figure 26. Hammett plots for the sulfation reaction of meta- substituted catechol.</i>	47
<i>Figure 27. HPLC-MS analysis of enzymatic sulfation of catechols.</i>	48
<i>Figure 28. Chemical structure of 7 selected compounds for sulfation study.</i>	51
<i>Figure 29. Electrospray ionization mass spectroscopic analysis of enzymatic conversion of other compounds.</i>	52

Figure 30. Six potential beneficial positions (I398, V430, A448, E542, N612, and L622) close to the catalytic center H350.	53
Figure 31. Activity comparison of four ASTB variants (I398V, A448V, I398V/A448V, and I398V/A448V/E542G).	54
Figure 32. A 3D-structural alignment of ASTB-WT (white cartoon) and the improved ASTB-M5 variant (magenta cartoon).	57
Figure 33. Micelle model formed by the bolaform surfactant	62
Figure 34. Cytochrome P450 monooxygenases catalytic cycle.	64
Figure 35. Crystal structure of wild-type P450 BM3 heme domain with highlighted positions used in the OmniChange library generation R47/Y51/F87/L188.	66
Figure 36. P450BM3 OmniChange library preparation and expression.	69
Figure 37. Two-step screening assay for P450 BM3 (NADPH depletion assay and Ampliflu™ Red/horseradish peroxidase (HRP) based hydrogen peroxide detection assay).	70
Figure 38. Rescreening results of twelve P450 BM3 variants from the OmniChange library using NADPH consumption assay and H ₂ O ₂ detection assay	77
Figure 39. Exemplary HPLC chromatograms of CTAB conversion by (a) wild-type P450 BM3, (b) P450 BM3 variant P3A8. (c) MS spectrometry of products and CTAB.	79
Figure 40. ¹ H NMR spectra (400 MHz, 23 °C, D ₂ O) of and the reaction mixture catalyzed by P2E7.	80
Figure 41. ¹ H NMR spectra (400 MHz, 23 °C, D ₂ O) of the reaction mixture catalyzed by P3A8.	80
Figure 42. ¹ H NMR spectrum (400 MHz, 23 °C, D ₂ O) of CTAB.	80
Figure 43. Exemplary timescale of CTAB conversion and mono- and di-hydroxylated product formation on the example of P450 BM3 P3A8.	82
Figure 44. Surface contact angle measurement.	83

5.4 List of Tables

<i>Table 1. Sequences and T_m value of primers used for the OmniChange library generation.</i>	21
<i>Table 2. Sequencing results of beneficial ASTB variants from Phase 1.</i>	35
<i>Table 3. Substrate profile and kinetic characterization of six converted catechols by ASTB-WT and ASTB-M5.</i>	38
<i>Table 4. ASTB-WT and ASTB-M5 catalyzed conversions of six catechols.</i>	38
<i>Table 5. Sequencing results of beneficial ASTB variants from Phase 1.</i>	40
<i>Table 6. Beneficial positions and substitutions with improved sulfation activity.</i>	42
<i>Table 7. Sequencing results of nine randomly picked clones from the ASTB OmniChange library.</i>	44
<i>Table 8. Sequencing results of the ten most beneficial ASTB variants found after rescreening of the OmniChange library.</i>	45
<i>Table 9. Kinetic characterization of 3-chlorocatechol by ASTB-WT and variants.</i>	46
<i>Table 10. Kinetic characterization of ASTB-WT and ASTB-OM2 for six converted catechols to explore their substrate profile and general importance of the identified substitutions.</i>	47
<i>Table 11. Results on sulfation stoichiometry of ASTB-WT and ASTB-OM2 for six catechols.</i>	49
<i>Table 12. Binding energies determined by molecular docking of all six catechol substrates within the binding pocket of ASTB-WT and ASTB-OM2.</i>	50
<i>Table 13. Results on sulfation stoichiometry of ASTB-WT and ASTB-OM2 for dopamine, tanshinol, taxfolin, and quercetin after 24 h.</i>	53
<i>Table 14. Kinetic characterization of ASTB-WT and ASTB-OM2 for dopamine.</i>	53
<i>Table 15. $\Delta\Delta G$ calculation of recombination of beneficial substitutions.</i>	54
<i>Table 16. Coupling efficiency determined from ASTB-WT and ASTB-M5.</i>	57
<i>Table 17. Sequences and T_m value of primers used for the OmniChange library generation.</i>	68
<i>Table 18. The gradient elution mode of HPLC for substrate and product separation.</i>	72
<i>Table 19. Sequencing results of 15 randomly picked clones from the OmniChange library in which four positions (R47, Y51, F87, and L188) were simultaneously mutated.</i>	75
<i>Table 20. Sequences result of 15 randomly picked clones from the P450BM3 OmniChange library.</i>	76
<i>Table 21. Amino acid substitutions of 12 selected P450 BM3 variants.</i>	78
<i>Table 22. Regioselectivity of P450 BM3 variants after 16 h for the hydroxylation of CTAB.</i>	81
<i>Table 23. Kinetic constants of P450 BM3 variants and WT P450 BM3 for hydroxylation of CTAB.</i>	82

6 References

- [1] Hughes, G., and Lewis, J. C. (2018) Introduction: biocatalysis in industry, pp 1-3, ACS Publications.
- [2] Illanes, A. (2008). Enzyme biocatalysis. *Principles and Applications. Editorial Springer-Verlag New York Inc., United States.*
- [3] Sheldon, R. A., and Pereira, P. C. (2017). Biocatalysis engineering: the big picture. *Chemical Society Reviews*, 46, 2678-2691.
- [4] Goodwin, N. C., Morrison, J. P., Fuerst, D. E., and Hadi, T. (2019) Biocatalysis in Medicinal Chemistry: Challenges to Access and Drivers for Adoption, ACS Publications.
- [5] Buchner, E. (1897). Alkoholische gahrung ohne hefezellen. *Berichte der deutschen chemischen Gesellschaft*, 30, 117-124.
- [6] Zaks, A., and Klibanov, A. M. (1984). Enzymatic catalysis in organic media at 100 degrees C. *Science*, 224, 1249-1251.
- [7] Choi, J.-M., Han, S.-S., and Kim, H.-S. (2015). Industrial applications of enzyme biocatalysis: Current status and future aspects. *Biotechnology advances*, 33, 1443-1454.
- [8] Schulze, B., and Wubbolts, M. G. (1999). Biocatalysis for industrial production of fine chemicals. *Current Opinion in Biotechnology*, 10, 609-615.
- [9] Akoh, C. C., Chang, S.-W., Lee, G.-C., and Shaw, J.-F. (2008). Biocatalysis for the production of industrial products and functional foods from rice and other agricultural produce. *Journal of agricultural and food chemistry*, 56, 10445-10451.
- [10] Forti, L., Di Mauro, S., Cramarossa, M. R., Filippucci, S., Turchetti, B., and Buzzini, P. (2015). Non-conventional yeasts whole cells as efficient biocatalysts for the production of flavors and fragrances. *Molecules*, 20, 10377-10398.
- [11] Thanikaivelan, P., Rao, J. R., Nair, B. U., and Ramasami, T. (2004). Progress and recent trends in biotechnological methods for leather processing. *Trends in Biotechnology*, 22, 181-188.
- [12] Cavaco-Paulo, A., and Gubitz, G. (2003) *Textile processing with enzymes*, Elsevier.
- [13] Robledo-Narvez, P. N., Montes-Horcasitas, M., Ponce-Noyola, M., and Poggi-Varaldo, H. (2006). Production of biocatalysts of trametes versicolor for the treatment of recalcitrant effluents of the pulp and paper industry. *Battelle ISBN*, 1-57477.
- [14] Sheldon, R. A., and Woodley, J. M. (2017). Role of biocatalysis in sustainable chemistry. *Chemical reviews*, 118, 801-838.
- [15] Woodley, J. M. (2006). Microbial biocatalytic processes and their development. *Advances in applied microbiology*, 60, 1-15.
- [16] Schmid, A., Dordick, J., Hauer, B., Kiener, A., Wubbolts, M., and Witholt, B. (2001). Industrial biocatalysis today and tomorrow. *Nature*, 409, 258.
- [17] Goldberg, K., Schroer, K., Lutz, S., and Liese, A. (2007). Biocatalytic ketone reduction-a powerful tool for the production of chiral alcohols-part I: processes with isolated enzymes. *Applied microbiology and biotechnology*, 76, 237.
- [18] Rubsam, K., Weber, L., Jakob, F., and Schwaneberg, U. (2018). Directed evolution of polypropylene and polystyrene binding peptides. *Biotechnology and bioengineering*, 115, 321-330.
- [19] Mohamad, N. R., Marzuki, N. H. C., Buang, N. A., Huyop, F., and Wahab, R. A. (2015). An overview of technologies for immobilization of enzymes and surface analysis techniques for immobilized enzymes. *Biotechnology & Biotechnological Equipment*, 29, 205-220.

- [20] Sheldon, R. A., and van Pelt, S. (2013). Enzyme immobilisation in biocatalysis: why, what and how. *Chemical Society Reviews*, 42, 6223-6235.
- [21] Fischer, E. (1894). Einfluss der Configuration auf die Wirkung der Enzyme. *Berichte der deutschen chemischen Gesellschaft*, 27, 2985-2993.
- [22] Koshland Jr, D. E. (1995). The key-lock theory and the induced fit theory. *Angewandte Chemie International Edition*, 33, 2375-2378.
- [23] Koshland, D. E. (1958). Application of a theory of enzyme specificity to protein synthesis. *Proceedings of the National Academy of Sciences*, 44, 98-104.
- [24] Monod, J., Wyman, J., and Changeux, J.-P. (1965). On the nature of allosteric transitions: a plausible model. *Journal of Molecular Biology*, 12, 88-118.
- [25] Changeux, J.-P., Thiéry, J., Tung, Y., and Kittel, C. (1967). On the cooperativity of biological membranes. *Proceedings of the National Academy of Sciences* 57, 335.
- [26] Martí, S., Roca, M., Andrés, J., Moliner, V., Silla, E., Tuñón, I., and Bertrán, J. (2004). Theoretical insights in enzyme catalysis. *Chemical Society Reviews*, 33, 98-107.
- [27] Changeux, J.-P., and Edelstein, S. (2011). Conformational selection or induced fit? 50 years of debate resolved. *F1000 biology reports*, 3.
- [28] Cornish-Bowden, A. (2014). Current IUBMB recommendations on enzyme nomenclature and kinetics. *Perspectives in Science*, 1, 74-87.
- [29] Singhania, R. R., Patel, A. K., Thomas, L., Goswami, M., Giri, B. S., and Pandey, A. (2015) Industrial enzymes, In *Industrial Biorefineries & White Biotechnology*, pp 473-497, Elsevier.
- [30] Wong, C. M., Wong, K. H., and Chen, X. D. (2008). Glucose oxidase: natural occurrence, function, properties and industrial applications. *Applied microbiology and biotechnology*, 78, 927-938.
- [31] Herga, M., Gasparič, A., Bitenc, M., Pohar, A., and Likozar, B. (2019). Development, optimization and scale-up of stereo-selective enzymatic Baeyer-Villiger oxidation of pyrimetazole to esomeprazole active ingredient in an industrial-scale slurry reactor. *Journal of Industrial and Engineering Chemistry*, 72, 214-221.
- [32] Kiener, A. (1992). Enzymatic oxidation of methyl groups on aromatic heterocycles: a versatile method for the preparation of heteroaromatic carboxylic acids. *Angewandte Chemie International Edition* 31, 774-775.
- [33] Ghislieri, D., Green, A. P., Pontini, M., Willies, S. C., Rowles, I., Frank, A., Grogan, G., and Turner, N. J. (2013). Engineering an enantioselective amine oxidase for the synthesis of pharmaceutical building blocks and alkaloid natural products. *Journal of the American Chemical Society*, 135, 10863-10869.
- [34] Savile, C. K., Janey, J. M., Mundorff, E. C., Moore, J. C., Tam, S., Jarvis, W. R., Colbeck, J. C., Krebber, A., Fleitz, F. J., and Brands, J. (2010). Biocatalytic asymmetric synthesis of chiral amines from ketones applied to sitagliptin manufacture. *Science*, 329, 305-309.
- [35] Kuraishi, C., Yamazaki, K., and Susa, Y. (2001). Transglutaminase: its utilization in the food industry. *Food reviews international*, 17, 221-246.
- [36] Vandamme, E., and Voets, J. (1974) Microbial penicillin acylases, In *Advances in applied microbiology*, pp 311-369, Elsevier.
- [37] Arroyo, M., De la Mata, I., Acebal, C., and Castellón, M. P. (2003). Biotechnological applications of penicillin acylases: state-of-the-art. *Applied microbiology and biotechnology*, 60, 507-514.
- [38] Broxterman, R., Sonke, T., Worries, H., and van den Tweel, W. (2000). Biocatalytic production of unnatural amino acids. *Pharm. Manuf. Int*, 61.
- [39] Li, Q., Yi, L., Marek, P., and Iverson, B. L. (2013). Commercial proteases: present and future. *FEBS letters*, 587, 1155-1163.

- [40] Lanfranchi, E., Steiner, K., Glieder, A., Hajnal, I., A Sheldon, R., van Pelt, S., and Winkler, M. (2013). Mini-review: recent developments in hydroxynitrile lyases for industrial biotechnology. *Recent patents on biotechnology*, 7, 197-206.
- [41] Jensen, V. J., and Rugh, S. (1987) [33] Industrial-scale production and application of immobilized glucose isomerase, In *Methods in enzymology*, pp 356-370, Elsevier.
- [42] Li, Y., Wei, G., and Chen, J. (2004). Glutathione: a review on biotechnological production. *Applied microbiology and biotechnology*, 66, 233-242.
- [43] Arnold, F. H. (2018). Directed evolution: bringing new chemistry to life. *Angewandte Chemie International Edition*, 57, 4143-4148.
- [44] Bornscheuer, U. T., Hauer, B., Jaeger, K. E., and Schwaneberg, U. (2019). Directed evolution empowered redesign of natural proteins for the sustainable production of chemicals and pharmaceuticals. *Angewandte Chemie International Edition*, 58, 36-40.
- [45] Martínez, R., and Schwaneberg, U. (2013). A roadmap to directed enzyme evolution and screening systems for biotechnological applications. *Biological research*, 46, 395-405.
- [46] Amar, D., Berger, I., Amara, N., Tafa, G., Meijler, M. M., and Aharoni, A. (2012). The transition of human estrogen sulfotransferase from generalist to specialist using directed enzyme evolution. *Journal of molecular biology*, 416, 21-32.
- [47] Francis, J., and Hansche, P. (1972). Directed evolution of metabolic pathways in microbial populations. I. Modification of the acid phosphatase pH optimum in *S. cerevisiae*. *Genetics*, 70, 59-73.
- [48] Cadwell, R. C., and Joyce, G. F. (1994). Mutagenic PCR. *Genome Research*, 3, S136-S140.
- [49] Robertson, D. L., and Joyce, G. F. (1990). Selection in vitro of an RNA enzyme that specifically cleaves single-stranded DNA. *Nature*, 344, 467-468.
- [50] Beaudry, A. A., and Joyce, G. F. (1992). Directed evolution of an RNA enzyme. *Science*, 257, 635-641.
- [51] Tindall, K. R., and Kunkel, T. A. (1988). Fidelity of DNA synthesis by the *Thermus aquaticus* DNA polymerase. *Biochemistry*, 27, 6008-6013.
- [52] Chen, K., Robinson, A. C., Van Dam, M. E., Martinez, P., Economou, C., and Arnold, F. H. (1991). Enzyme engineering for nonaqueous solvents. II. Additive effects of mutations on the stability and activity of subtilisin E in polar organic media. *Biotechnology progress*, 7, 125-129.
- [53] You, L., and Arnold, F. (1996). Directed evolution of subtilisin E in *Bacillus subtilis* to enhance total activity in aqueous dimethylformamide. *Protein Engineering, Design and Selection*, 9, 77-83.
- [54] Zhao, H., and Arnold, F. H. (1999). Directed evolution converts subtilisin E into a functional equivalent of thermitase. *Protein Engineering*, 12, 47-53.
- [55] Giver, L., Gershenson, A., Freskgard, P.-O., and Arnold, F. H. (1998). Directed evolution of a thermostable esterase. *Proceedings of the National Academy of Sciences*, 95, 12809-12813.
- [56] Reetz, M. T., Zonta, A., Schimossek, K., Jaeger, K. E., and Liebeton, K. (1997). Creation of enantioselective biocatalysts for organic chemistry by in vitro evolution. *Angewandte Chemie International Edition* 36, 2830-2832.
- [57] Zhao, J., Kardashliev, T., Joëlle Ruff, A., Bocola, M., and Schwaneberg, U. (2014). Lessons from diversity of directed evolution experiments by an analysis of 3,000 mutations. *Biotechnology and bioengineering*, 111, 2380-2389.
- [58] Wong, T. S., Roccatano, D., Loakes, D., Tee, K. L., Schenk, A., Hauer, B., and Schwaneberg, U. (2008). Transversion-enriched sequence saturation mutagenesis

- (SeSaM-Tv+): a random mutagenesis method with consecutive nucleotide exchanges that complements the bias of error-prone PCR. *Biotechnology journal*, *3*, 74-82.
- [59] Dennig, A., Shivange, A. V., Marienhagen, J., and Schwaneberg, U. (2011). OmniChange: the sequence independent method for simultaneous site-saturation of five codons. *PloS one*, *6*, e26222.
- [60] Martinez, R., Jakob, F., Tu, R., Siegert, P., Maurer, K. H., and Schwaneberg, U. (2013). Increasing activity and thermal resistance of *Bacillus gibsonii* alkaline protease (BgAP) by directed evolution. *Biotechnology and bioengineering*, *110*, 711-720.
- [61] Körfer, G., Novoa, C., Kern, J., Balla, E., Grütering, C., Davari, M. D., Martinez, R., Vojcic, L., and Schwaneberg, U. (2018). Directed evolution of an acid *Yersinia mollaretii* phytase for broadened activity at neutral pH. *Applied microbiology and biotechnology*, *102*, 9607-9620.
- [62] Cheng, F., Zhu, L., and Schwaneberg, U. (2015). Directed evolution 2.0: improving and deciphering enzyme properties. *Chemical Communications*, *51*, 9760-9772.
- [63] Islam, S., Laaf, D., Infanzón, B., Pelantová, H., Davari, M. D., Jakob, F., Křen, V., Elling, L., and Schwaneberg, U. (2018). KnowVolution campaign of an aryl sulfotransferase increases activity toward cellobiose. *Chemistry—A European Journal*, *24*, 17117-17124.
- [64] Mandawe, J., Infanzon, B., Eisele, A., Zaun, H., Kuballa, J., Davari, M. D., Jakob, F., Elling, L., and Schwaneberg, U. (2018). Directed Evolution of Hyaluronic Acid Synthase from *Pasteurella multocida* towards High-Molecular-Weight Hyaluronic Acid. *ChemBioChem*, *19*, 1414-1423.
- [65] Rübsam, K., Davari, M., Jakob, F., and Schwaneberg, U. (2018). KnowVolution of the Polymer-Binding Peptide LCI for Improved Polypropylene Binding. *Polymers*, *10*, 423.
- [66] Ji, Y., Islam, S., Mertens, A. M., Sauer, D. F., Dhoke, G. V., Jakob, F., and Schwaneberg, U. (2019). Directed aryl sulfotransferase evolution toward improved sulfation stoichiometry on the example of catechols. *Applied microbiology and biotechnology*, *103*, 3761-3771.
- [67] Garg, B., Bisht, T., and Ling, Y.-C. (2014). Graphene-based nanomaterials as heterogeneous acid catalysts: a comprehensive perspective. *Molecules*, *19*, 14582-14614.
- [68] Chapman, E., Best, M. D., Hanson, S. R., and Wong, C.-H. (2004). Sulfotransferases: Structure, Mechanism, Biological Activity, Inhibition, and Synthetic Utility. *Angewandte Chemie International Edition*, *43*, 3526-3548.
- [69] Dado, G., and Bernhardt, R. (2017) Sulfonation and Sulfation, In *Kirk-Othmer Encyclopedia of Chemical Technology*, pp 1-30.
- [70] Al-Horani, R. A., and Desai, U. R. (2010). Chemical Sulfation of Small Molecules - Advances and Challenges. *Tetrahedron*, *66*, 2907-2918.
- [71] Farn, R. J. (2008) *Chemistry and technology of surfactants*, John Wiley & Sons.
- [72] Desoky, A. Y., Hendel, J., Ingram, L., and Taylor, S. D. (2011). Preparation of trifluoroethyl- and phenyl-protected sulfates using sulfonyl imidazolium salts. *Tetrahedron*, *67*, 1281-1287.
- [73] Purchartová, K., Valentová, K., Pelantová, H., Marhol, P., Cvačka, J., Havlíček, L., Křenková, A., Vavříková, E., Biedermann, D., Chambers, C. S., and Křen, V. (2015). Prokaryotic and Eukaryotic Aryl Sulfotransferases: Sulfation of Quercetin and Its Derivatives. *ChemCatChem*, *7*, 3152-3162.
- [74] Sperry, S., and Crews, P. (1997). Haliclostanoone sulfate and halistanol sulfate from an Indo-Pacific Haliclona sponge. *Journal of natural products*, *60*, 29-32.

- [75] Barrett, D. (2002). From natural products to clinically useful antifungals. *Biochimica et Biophysica Acta (BBA)-Molecular Basis of Disease*, 1587, 224-233.
- [76] Hashimoto, S. (2009). Micafungin: a sulfated echinocandin. *The Journal of antibiotics*, 62, 27.
- [77] Gilbert, E. E. (1965) *Sulfonation and related reactions*, Interscience Publishers.
- [78] Deno, N., and Newman, M. S. (1950). Mechanism of sulfation of alcohols1, 2. *Journal of the American Chemical Society*, 72, 3852-3856.
- [79] Gilbert, E. E. (1962). The Reactions of Sulfur Trioxide, and Its Adducts, with Organic Compounds. *Chemical Reviews*, 62, 549-589.
- [80] Takano, R., Matsuo, M., Kamei-Hayashi, K., Hara, S., and Hirase, S. (1992). A novel regioselective desulfation method specific to carbohydrate 6-sulfate using silylating reagents. *Bioscience, biotechnology, and biochemistry*, 56, 1577-1580.
- [81] Kitagawa, K., Aida, C., Fujiwara, H., Yagami, T., Futaki, S., Kogire, M., Ida, J., and Inoue, K. (2001). Facile Solid-Phase Synthesis of Sulfated Tyrosine-Containing Peptides: Total Synthesis of Human Big Gastrin-II and Cholecystokinin (CCK)-391, 2. *The Journal of organic chemistry*, 66, 1-10.
- [82] Lee, J.-C., Lu, X.-A., Kulkarni, S. S., Wen, Y.-S., and Hung, S.-C. (2004). Synthesis of heparin oligosaccharides. *Journal of the American Chemical Society*, 126, 476-477.
- [83] Tully, S. E., Mabon, R., Gama, C. I., Tsai, S. M., Liu, X., and Hsieh-Wilson, L. C. (2004). A chondroitin sulfate small molecule that stimulates neuronal growth. *Journal of the American Chemical Society*, 126, 7736-7737.
- [84] Young, T., and Kiessling, L. L. (2002). A strategy for the synthesis of sulfated peptides. *Angewandte Chemie International Edition*, 41, 3449-3451.
- [85] Popek, T., and Lis, T. (2002). Synthesis and X-ray structures of sulfate esters of fructose and its isopropylidene derivatives. Part 1: 2, 3: 4, 5-di-O-isopropylidene- β -d-fructopyranose 1-sulfate and 4, 5-O-isopropylidene- β -d-fructopyranose 1-sulfate. *Carbohydrate research*, 337, 787-801.
- [86] Al-Horani, R. A., Karuturi, R., Verespy, S., 3rd, and Desai, U. R. (2015). Synthesis of glycosaminoglycan mimetics through sulfation of polyphenols. *Methods Mol Biol*, 1229, 49-67.
- [87] Marhol, P., Hartog, A. F., van der Horst, M. A., Wever, R., Purchartová, K., Fuksová, K., Kuzma, M., Cvačka, J., and Křen, V. (2013). Preparation of silybin and isosilybin sulfates by sulfotransferase from *Desulfitobacterium hafniense*. *Journal of Molecular Catalysis B: Enzymatic*, 89, 24-27.
- [88] Dusza, J. P., Joseph, J. P., and Bernstein, S. (1985). A fusion method for the preparation of steroid sulfates. *Steroids*, 45, 317-323.
- [89] van der Horst, M. A., Hartog, A. F., El Morabet, R., Marais, A., Kircz, M., and Wever, R. (2015). Enzymatic sulfation of phenolic hydroxy groups of various plant metabolites by an arylsulfotransferase. *European Journal of Organic Chemistry*, 2015, 534-541.
- [90] Penney, C. L., and Perlin, A. S. (1981). A method for the sulfation of sugars, employing a stable, aryl sulfate intermediate. *Carbohydrate Research*, 93, 241-246.
- [91] Proud, A. D., Prodger, J. C., and Flitsch, S. L. (1997). Development of a protecting group for sulfate esters. *Tetrahedron letters*, 38, 7243-7246.
- [92] Liu, Y., Lien, I.-F. F., Ruttgaizer, S., Dove, P., and Taylor, S. D. (2004). Synthesis and protection of aryl sulfates using the 2, 2, 2-trichloroethyl moiety. *Organic letters*, 6, 209-212.

- [93] Ali, A. M., and Taylor, S. D. (2009). Efficient solid-phase synthesis of sulfotyrosine peptides using a sulfate protecting-group strategy. *Angewandte Chemie International Edition*, 48, 2024-2026.
- [94] Simpson, L. S., and Widlanski, T. S. (2006). A comprehensive approach to the synthesis of sulfate esters. *Journal of the American Chemical Society*, 128, 1605-1610.
- [95] Hungerford, N. L., McKinney, A. R., Stenhouse, A. M., and McLeod, M. D. (2006). Selective manipulation of steroid hydroxyl groups with boronate esters: efficient access to antigenic C-3 linked steroid-protein conjugates and steroid sulfate standards for drug detection. *Organic & biomolecular chemistry*, 4, 3951-3959.
- [96] Richter, A., and Klemm, D. (2003). Regioselective sulfation of trimethylsilyl cellulose using different SO₃-complexes. *Cellulose*, 10, 133-138.
- [97] Gavard, O., Hersant, Y., Alais, J., Duverger, V., Dilhas, A., Bascou, A., and Bonnaffé, D. (2003). Efficient preparation of three building blocks for the synthesis of heparan sulfate fragments: Towards the combinatorial synthesis of oligosaccharides from hypervariable regions. *European Journal of Organic Chemistry*, 2003, 3603-3620.
- [98] Spillane, W., and Malaubier, J. B. (2014). Sulfamic acid and its N- and O-substituted derivatives. *Chemical reviews*, 114, 2507-2586.
- [99] Malojčić, G., and Glockshuber, R. (2010). The PAPS-independent aryl sulfotransferase and the alternative disulfide bond formation system in pathogenic bacteria. *Antioxidants & redox signaling*, 13, 1247-1259.
- [100] Ayuso-Fernández, I., Galmés, M. A., Bastida, A., and García-Junceda, E. (2014). Aryl sulfotransferase from *Haliangium ochraceum*: A versatile tool for the sulfation of small molecules. *ChemCatChem*, 6, 1059-1065.
- [101] Blanchard, R. L., Freimuth, R. R., Buck, J., Weinshilboum, R. M., and Coughtrie, M. W. (2004). A proposed nomenclature system for the cytosolic sulfotransferase (SULT) superfamily. *Pharmacogenetics and Genomics*, 14, 199-211.
- [102] Falany, C. N. (1997). Enzymology of human cytosolic sulfotransferases. *The FASEB Journal*, 11, 206-216.
- [103] Malojčić, G., Owen, R. L., and Glockshuber, R. (2014). Structural and mechanistic insights into the PAPS-independent sulfotransferase catalyzed by bacterial aryl sulfotransferase and the role of the DsbL/DsbI system in its folding. *Biochemistry*, 53, 1870-1877.
- [104] Kim, D.-H., Yoon, H.-K., Koizumi, M., and Kobashi, K. (1992). Sulfation of phenolic antibiotics by sulfotransferase obtained from a human intestinal bacterium. *Chemical and pharmaceutical bulletin*, 40, 1056-1057.
- [105] van der Horst, M. A., van Lieshout, J. F., Bury, A., Hartog, A. F., and Wever, R. (2012). Sulfation of various alcoholic groups by an arylsulfate sulfotransferase from *Desulfitobacterium hafniense* and synthesis of estradiol sulfate. *Advanced Synthesis & Catalysis*, 354, 3501-3508.
- [106] Roubalová, L., Purchartová, K., Papoušková, B., Vacek, J., Křen, V., Ulrichová, J., and Vrba, J. (2015). Sulfation modulates the cell uptake, antiradical activity and biological effects of flavonoids in vitro: An examination of quercetin, isoquercitrin and taxifolin. *Bioorganic & medicinal chemistry*, 23, 5402-5409.
- [107] Islam, S., Mate, D. M., Martínez, R., Jakob, F., and Schwaneberg, U. (2018). A robust protocol for directed aryl sulfotransferase evolution toward the carbohydrate building block GlcNAc. *Biotechnology and bioengineering*, 115, 1106-1115.
- [108] Hartog, A. F., and Wever, R. (2015). Substrate engineering and its synthetic utility in the sulfation of primary aliphatic alcohol groups by a bacterial arylsulfotransferase. *Advanced Synthesis & Catalysis*, 357, 2629-2632.

- [109] Valentová, K., Káňová, K., Di Meo, F., Pelantová, H., Chambers, C., Rydlová, L., Petrásková, L., Křenková, A., Cvačka, J., and Trouillas, P. (2017). Chemoenzymatic preparation and biophysical properties of sulfated quercetin metabolites. *International journal of molecular sciences*, *18*, 2231.
- [110] Kim, D. H., and Kobashi, K. (1991). Kinetic studies on a novel sulfotransferase from *Eubacterium A-44*, a human intestinal bacterium. *The Journal of Biochemistry*, *109*, 45-48.
- [111] de Macedo-Ribeiro, S., Renirie, R., Wever, R., and Messerschmidt, A. (2008). Crystal structure of a trapped phosphate intermediate in vanadium apochloroperoxidase catalyzing a dephosphorylation reaction. *Biochemistry*, *47*, 929-934.
- [112] Sterner, E., Li, L., Paul, P., Beaudet, J. M., Liu, J., Linhardt, R. J., and Dordick, J. S. (2014). Assays for determining heparan sulfate and heparin O-sulfotransferase activity and specificity. *Analytical and bioanalytical chemistry*, *406*, 525-536.
- [113] Sun, Y. G., Cui, H., Li, Y. H., and Lin, X. Q. (2000). Determination of some catechol derivatives by a flow injection electrochemiluminescent inhibition method. *Talanta*, *53*, 661-666.
- [114] Han, S., Liu, B., Liu, Y., and Fan, Z. (2016). Silver nanoparticle induced chemiluminescence of the hexacyanoferrate-fluorescein system, and its application to the determination of catechol. *Microchimica Acta*, *183*, 917-921.
- [115] Schweigert, N., Zehnder, A. J., and Eggen, R. I. (2001). Chemical properties of catechols and their molecular modes of toxic action in cells, from microorganisms to mammals: minireview. *Environmental microbiology*, *3*, 81-91.
- [116] Ahmadi, S., Shadman, M., Hossini, H., and Hashemi, S. (2016). Catechol removal using MWCNTs from synthetic solutions: modeling, equilibrium and kinetics. *Journal of Materials and Environmental Science*, *7*, 3885-3894.
- [117] Capasso, R., Evidente, A., Schivo, L., Orru, G., Marcialis, M., and Cristinzio, G. (1995). Antibacterial polyphenols from olive oil mill waste waters. *Journal of Applied Bacteriology*, *79*, 393-398.
- [118] Bukowska, B., Michałowicz, J., and Marczak, A. (2015). The effect of catechol on human peripheral blood mononuclear cells (in vitro study). *Environmental toxicology and pharmacology*, *39*, 187-193.
- [119] Bukowska, B., Marczak, A., Michałowicz, J., and Wisniewska, K. (2009). Effects of Phenol, Catechol, Chloro- and Metylphenol on Human Erythrocyte Membrane (in vitro). *Polish Journal of Environmental Studies*, *18*.
- [120] Bukowska, B., and Kowalska, S. (2004). Phenol and catechol induce prehemolytic and hemolytic changes in human erythrocytes. *Toxicology letters*, *152*, 73-84.
- [121] Suresh, S., Srivastava, V. C., and Mishra, I. M. (2012). Adsorption of catechol, resorcinol, hydroquinone, and their derivatives: a review. *International Journal of Energy and Environmental Engineering*, *3*, 32.
- [122] Cavalieri, E. L., and Rogan, E. G. (2016). Depurinating estrogen-DNA adducts, generators of cancer initiation: their minimization leads to cancer prevention. *Clinical and translational medicine*, *5*, 12.
- [123] Hatano, T., Saiki, S., Okuzumi, A., Mohny, R. P., and Hattori, N. (2016). Identification of novel biomarkers for Parkinson's disease by metabolomic technologies. *J Neurol Neurosurg Psychiatry*, *87*, 295-301.
- [124] Pimpao, R. C., Dew, T., Figueira, M. E., McDougall, G. J., Stewart, D., Ferreira, R. B., Santos, C. N., and Williamson, G. (2014). Urinary metabolite profiling identifies novel colonic metabolites and conjugates of phenolics in healthy volunteers. *Molecular nutrition & food research*, *58*, 1414-1425.

- [125] Pimpao, R. C., Ventura, M. R., Ferreira, R. B., Williamson, G., and Santos, C. N. (2015). Phenolic sulfates as new and highly abundant metabolites in human plasma after ingestion of a mixed berry fruit purée. *British Journal of Nutrition*, *113*, 454-463.
- [126] Fang, C., Kim, H., Barnes, R. C., Talcott, S. T., and Mertens-Talcott, S. U. (2018). Obesity-Associated Diseases Biomarkers Are Differently Modulated in Lean and Obese Individuals and Inversely Correlated to Plasma Polyphenolic Metabolites After 6 Weeks of Mango (*Mangifera indica* L.) Consumption. *Molecular nutrition & food research*, *62*, 1800129.
- [127] Olson, J. A., Adler-Moore, J. P., Smith, P., and Proffitt, R. T. (2005). Treatment of *Candida glabrata* infection in immunosuppressed mice by using a combination of liposomal amphotericin B with caspofungin or micafungin. *Antimicrobial agents and chemotherapy*, *49*, 4895-4902.
- [128] Hartog, A. F., and Wever, R. (2016). Sulfation made easy: A new versatile donor for enzymatic sulfation by a bacterial arylsulfotransferase. *Journal of Molecular Catalysis B: Enzymatic*, *129*, 43-46.
- [129] Woodley, J. M. (2013). Protein engineering of enzymes for process applications. *Current opinion in chemical biology*, *17*, 310-316.
- [130] Turner, N. J. (2009). Directed evolution drives the next generation of biocatalysts. *Nature chemical biology*, *5*, 567.
- [131] Cherry, J. R., and Fidantsef, A. L. (2003). Directed evolution of industrial enzymes: an update. *Current opinion in biotechnology*, *14*, 438-443.
- [132] Powell, K. A., Ramer, S. W., del Cardayré, S. B., Stemmer, W. P., Tobin, M. B., Longchamp, P. F., and Huisman, G. W. (2001). Directed evolution and biocatalysis. *Angewandte Chemie International Edition*, *40*, 3948-3959.
- [133] Alcolombri, U., Elias, M., and Tawfik, D. S. (2011). Directed evolution of sulfotransferases and paraoxonases by ancestral libraries. *Journal of molecular biology*, *411*, 837-853.
- [134] Xu, D., Moon, A. F., Song, D., Pedersen, L. C., and Liu, J. (2008). Engineering sulfotransferases to modify heparan sulfate. *Nature chemical biology*, *4*, 200.
- [135] Brix, L. A., Barnett, A. C., Duggleby, R. G., Leggett, B., and McManus, M. E. (1999). Analysis of the substrate specificity of human sulfotransferases SULT1A1 and SULT1A3: site-directed mutagenesis and kinetic studies. *Biochemistry*, *38*, 10474-10479.
- [136] Bidwell, L. M., McManus, M. E., Gaedigk, A., Kakuta, Y., Negishi, M., Pedersen, L., and Martin, J. L. (1999). Crystal structure of human catecholamine sulfotransferase. *Journal of molecular biology*, *293*, 521-530.
- [137] Dajani, R., Cleasby, A., Neu, M., Wonacott, A. J., Jhoti, H., Hood, A. M., Modi, S., Hersey, A., Taskinen, J., and Cooke, R. M. (1999). X-ray Crystal Structure of Human Dopamine Sulfotransferase, SULT1A3. Molecular modeling and quantitative structure-activity relationship analysis demonstrate a molecular basis for sulfotransferase substrate specificity. *Journal of Biological Chemistry*, *274*, 37862-37868.
- [138] Berger, I., Guttman, C., Amar, D., Zarivach, R., and Aharoni, A. (2011). The molecular basis for the broad substrate specificity of human sulfotransferase 1A1. *PloS one*, *6*, e26794.
- [139] Yoshinari, K., Petrotchenko, E. V., Pedersen, L. C., and Negishi, M. (2001). Crystal structure-based studies of cytosolic sulfotransferase. *Journal of biochemical and molecular toxicology*, *15*, 67-75.

- [140] Lu, J. H., Li, H. T., Liu, M. C., Zhang, J. P., Li, M., An, X. M., and Chang, W. R. (2005). Crystal structure of human sulfotransferase SULT1A3 in complex with dopamine and 3'-phosphoadenosine 5'-phosphate. *Biochemical and biophysical research communications*, 335, 417-423.
- [141] Malojčić, G., Owen, R. L., Grimshaw, J. P., Brozzo, M. S., Dreher-Teo, H., and Glockshuber, R. (2008). A structural and biochemical basis for PAPS-independent sulfuryl transfer by aryl sulfotransferase from uropathogenic *Escherichia coli*. *Proceedings of the National Academy of Sciences*, 105, 19217-19222.
- [142] Liu, L., Schmid, R. D., and Urlacher, V. B. (2010). Engineering cytochrome P450 monooxygenase CYP 116B3 for high dealkylation activity. *Biotechnology letters*, 32, 841-845.
- [143] Whitehouse, C. J., Bell, S. G., and Wong, L.-L. (2012). P450 BM3 (CYP102A1): connecting the dots. *Chemical Society Reviews*, 41, 1218-1260.
- [144] Morlock, L. K., Böttcher, D., and Bornscheuer, U. T. (2018). Simultaneous detection of NADPH consumption and H₂O₂ production using the Ampliflu™ Red assay for screening of P450 activities and uncoupling. *Applied microbiology and biotechnology*, 102, 985-994.
- [145] Dennig, A., Lülldorf, N., Liu, H., and Schwaneberg, U. (2013). Regioselective o-hydroxylation of monosubstituted benzenes by P450 BM3. *Angewandte Chemie International Edition*, 52, 8459-8462.
- [146] Tee, K. L., and Schwaneberg, U. (2006). A screening system for the directed evolution of epoxygenases: importance of position 184 in P450 BM3 for stereoselective styrene epoxidation. *Angewandte Chemie International Edition*, 45, 5380-5383.
- [147] Ji, Y., Mertens, A. M., Gertler, C., Fekiri, S., Keser, M., Sauer, D. F., Smith, K. E., and Schwaneberg, U. (2018). Directed OmniChange Evolution Converts P450 BM3 into an Alkyltrimethylammonium Hydroxylase. *Chemistry—A European Journal*, 24, 16865-16872.
- [148] MJ Gillam, E., and A Hayes, M. (2013). The evolution of cytochrome P450 enzymes as biocatalysts in drug discovery and development. *Current topics in medicinal chemistry*, 13, 2254-2280.
- [149] Rivera-Marrero, C. A., Ritzenthaler, J. D., Newburn, S. A., Roman, J., and Cummings, R. D. (2002). Molecular cloning and expression of a novel glycolipid sulfotransferase in *Mycobacterium tuberculosis*. *Microbiology*, 148, 783-792.
- [150] Ettinger, M., Ruchhoft, C., and Lishka, R. (1951). Sensitive 4-aminoantipyrine method for phenolic compounds. *Analytical Chemistry*, 23, 1783-1788.
- [151] Wong, T., Wu, N., Roccatano, D., Zacharias, M., and Schwaneberg, U. (2005). Sensitive assay for laboratory evolution of hydroxylases toward aromatic and heterocyclic compounds. *Journal of biomolecular screening*, 10, 246-252.
- [152] Lülldorf, N., Vojcic, L., Hellmuth, H., Weber, T. T., Mußmann, N., Martinez, R., and Schwaneberg, U. (2015). A first continuous 4-aminoantipyrine (4-AAP)-based screening system for directed esterase evolution. *Applied microbiology and biotechnology*, 99, 5237-5246.
- [153] Lupetti, K. O., Rocha, F. R., and Fatibello-Filho, O. (2004). An improved flow system for phenols determination exploiting multicommution and long pathlength spectrophotometry. *Talanta*, 62, 463-467.
- [154] Van Durme, J., Delgado, J., Stricher, F., Serrano, L., Schymkowitz, J., and Rousseau, F. (2011). A graphical interface for the FoldX forcefield. *Bioinformatics*, 27, 1711-1712.

- [155] Guerois, R., Nielsen, J. E., and Serrano, L. (2002). Predicting changes in the stability of proteins and protein complexes: a study of more than 1000 mutations. *Journal of molecular biology*, 320, 369-387.
- [156] Duan, Y., Wu, C., Chowdhury, S., Lee, M. C., Xiong, G., Zhang, W., Yang, R., Cieplak, P., Luo, R., and Lee, T. (2003). A point-charge force field for molecular mechanics simulations of proteins based on condensed-phase quantum mechanical calculations. *Journal of computational chemistry*, 24, 1999-2012.
- [157] Wang, J., Wolf, R. M., Caldwell, J. W., Kollman, P. A., and Case, D. A. (2004). Development and testing of a general amber force field. *Journal of computational chemistry*, 25, 1157-1174.
- [158] Jakalian, A., Jack, D. B., and Bayly, C. I. (2002). Fast, efficient generation of high-quality atomic charges. AM1-BCC model: II. Parameterization and validation. *Journal of computational chemistry*, 23, 1623-1641.
- [159] Essmann, U., Perera, L., Berkowitz, M. L., Darden, T., Lee, H., and Pedersen, L. G. (1995). A smooth particle mesh Ewald method. *The Journal of chemical physics*, 103, 8577-8593.
- [160] Carmichael, A. B., and Wong, L. L. (2001). Protein engineering of *Bacillus megaterium* CYP102: the oxidation of polycyclic aromatic hydrocarbons. *European journal of biochemistry*, 268, 3117-3125.
- [161] Lee, H.-L., Chang, C.-K., Jeng, W.-Y., Wang, A. H.-J., and Liang, P.-H. (2012). Mutations in the substrate entrance region of β -glucosidase from *Trichoderma reesei* improve enzyme activity and thermostability. *Protein Engineering, Design & Selection*, 25, 733-740.
- [162] Kreß, N., Halder, J. M., Rapp, L. R., and Hauer, B. (2018). Unlocked potential of dynamic elements in protein structures: channels and loops. *Current opinion in chemical biology*, 47, 109-116.
- [163] Wallraf, A.-M., Liu, H., Zhu, L., Khalfallah, G., Simons, C., Alibiglou, H., Davari, M. D., and Schwaneberg, U. (2018). A loop engineering strategy improves laccase lcc2 activity in ionic liquid and aqueous solution. *Green chemistry*, 20, 2801-2812.
- [164] Cheng, F., Yang, J., Bocola, M., Schwaneberg, U., and Zhu, L. (2018). Loop engineering reveals the importance of active-site-decorating loops and gating residue in substrate affinity modulation of arginine deiminase (an anti-tumor enzyme). *Biochemical and biophysical research communications*, 499, 233-238.
- [165] Mayr, P., and Nidetzky, B. (2002). Catalytic reaction profile for NADH-dependent reduction of aromatic aldehydes by xylose reductase from *Candida tenuis*. *Biochemical journal*, 366, 889-899.
- [166] Boucher, G., Said, B., Ostler, E. L., Resmini, M., Brocklehurst, K., and Gallacher, G. (2007). Evidence that the mechanism of antibody-catalysed hydrolysis of arylcarbamates can be determined by the structure of the immunogen used to elicit the catalytic antibody. *Biochemical Journal*, 401, 721-726.
- [167] Ferguson, K. L., Arunrattanamook, N., and Marsh, E. N. G. (2016). Mechanism of the novel prenylated flavin-containing enzyme ferulic acid decarboxylase probed by isotope effects and linear free-energy relationships. *Biochemistry*, 55, 2857-2863.
- [168] Coughtrie, M. W. (1997) Catecholamine sulfation in health and disease, In *Advances in pharmacology*, pp 339-342, Elsevier.
- [169] Renskers, K. J., Feor, K. D., and Roth, J. A. (1980). Sulfation of dopamine and other biogenic amines by human brain phenol sulfotransferase. *Journal of neurochemistry*, 34, 1362-1368.
- [170] Itäaho, K., Alakurtti, S., Yli-Kauhaluoma, J., Taskinen, J., Coughtrie, M. W., and Kostianen, R. (2007). Regioselective sulfonation of dopamine by SULT1A3 in

- vitro provides a molecular explanation for the preponderance of dopamine-3-O-sulfate in human blood circulation. *Biochemical pharmacology*, 74, 504-510.
- [171] Lodi, F., Jimenez, R., Moreno, L., Kroon, P. A., Needs, P. W., Hughes, D. A., Santos-Buelga, C., Gonzalez-Paramas, A., Cogolludo, A., and Lopez-Sepulveda, R. (2009). Glucuronidated and sulfated metabolites of the flavonoid quercetin prevent endothelial dysfunction but lack direct vasorelaxant effects in rat aorta. *Atherosclerosis*, 204, 34-39.
- [172] Correia-da-Silva, M., Sousa, E., and Pinto, M. M. (2014). Emerging sulfated flavonoids and other polyphenols as drugs: Nature as an inspiration. *Medicinal research reviews*, 34, 223-279.
- [173] Vaidyanathan, J. B., and Walle, T. (2002). Glucuronidation and sulfation of the tea flavonoid (-)-epicatechin by the human and rat enzymes. *Drug metabolism and disposition*, 30, 897-903.
- [174] Tian, D. D., Jia, W. W., Liu, X. W., Wang, D. D., Liu, J. H., Dong, J. J., Li, L., Du, F. F., Xu, F., and Wang, F. Q. (2015). Methylation and its role in the disposition of tanshinol, a cardiovascular carboxylic catechol from *Salvia miltiorrhiza* roots (Danshen). *Acta Pharmacologica Sinica*, 36, 627.
- [175] Studer, R. A., Christin, P.-A., Williams, M. A., and Orengo, C. A. (2014). Stability-activity tradeoffs constrain the adaptive evolution of RubisCO. *Proceedings of the National Academy of Sciences*, 111, 2223-2228.
- [176] Cui, H., Cao, H., Cai, H., Karl-Erich, J., Davari, M. D., and Schwaneberg, U. (2019). Computer-assisted Recombination (CompassR) teaches us how to recombine beneficial substitutions from directed evolution campaigns. *Chemistry—A European Journal*.
- [177] Buß, O., Rudat, J., and Ochsenreither, K. (2018). FoldX as protein engineering tool: better than random based approaches? *Computational and structural biotechnology journal*, 16, 25-33.
- [178] Zhang, L., Huang, M., Blair, I. A., and Penning, T. M. (2012). Detoxication of benzo [a] pyrene-7, 8-dione by sulfotransferases (SULTs) in human lung cells. *Journal of Biological Chemistry*, 287, 29909-29920.
- [179] Mitra, P. S., Basu, N. K., and Owens, I. S. (2009). Src supports UDP-glucuronosyltransferase-2B7 detoxification of catechol estrogens associated with breast cancer. *Biochemical and biophysical research communications*, 382, 651-656.
- [180] Dias-Pedroso, D., Guerra, J., Gomes, A., Oudot, C., Brenner, C., Santos, C. N., and Vieira, H. L. (2019). Phenolic Metabolites Modulate Cardiomyocyte Beating in Response to Isoproterenol. *Cardiovascular toxicology*, 19, 156-167.
- [181] Barnes, R. C., Krenek, K. A., Meibohm, B., Mertens-Talcott, S. U., and Talcott, S. T. (2016). Urinary metabolites from mango (*Mangifera indica* L. cv. Keitt) galloyl derivatives and in vitro hydrolysis of gallotannins in physiological conditions. *Molecular nutrition & food research*, 60, 542-550.
- [182] Kang, L. T., and Schwaneberg, U. (2007). Directed Evolution of Oxygenases: Screening Systems, Success Stories and Challenges. *Combinatorial Chemistry & High Throughput Screening*, 10, 197-217.
- [183] Kakuta, Y., Petrotchenko, E. V., Pedersen, L. C., and Negishi, M. (1998). The Sulfuryl Transfer Mechanism crystal structure of a vanadate complex of estrogen sulfotransferase and mutational analysis *Journal of Biological Chemistry*, 273, 27325-27330.

- [184] Lu, L.-Y., Chiang, H.-P., Chen, W.-T., and Yang, Y.-S. (2009). Dimerization is responsible for the structural stability of human sulfotransferase 1A1. *Drug metabolism and disposition*, 37, 1083-1088.
- [185] Salager, J.-L. (2002). Surfactants types and uses. *FIRP booklet*, 300.
- [186] Nishiyama, N., Toshima, Y., and Ikeda, Y. (1995). Biodegradation of alkyltrimethylammonium salts in activated sludge. *Chemosphere*, 30, 593-603.
- [187] Keen, P. L., and Montforts, M. H. (2011) *Antimicrobial resistance in the environment*, John Wiley & Sons.
- [188] Gorelikov, I., and Matsuura, N. (2008). Single-step coating of mesoporous silica on cetyltrimethyl ammonium bromide-capped nanoparticles. *Nano letters*, 8, 369-373.
- [189] Singh, M., Briones, M., Ott, G., and O'Hagan, D. (2000). Cationic microparticles: a potent delivery system for DNA vaccines. *Proceedings of the National Academy of Sciences*, 97, 811-816.
- [190] Yang, Y. J., and Li, W. (2014). CTAB functionalized graphene oxide/multiwalled carbon nanotube composite modified electrode for the simultaneous determination of ascorbic acid, dopamine, uric acid and nitrite. *Biosensors and Bioelectronics*, 56, 300-306.
- [191] Sau, T. K., and Murphy, C. J. (2005). Self-assembly patterns formed upon solvent evaporation of aqueous cetyltrimethylammonium bromide-coated gold nanoparticles of various shapes. *Langmuir*, 21, 2923-2929.
- [192] Lu, J., Chang, Y.-X., Zhang, N.-N., Wei, Y., Li, A.-J., Tai, J., Xue, Y., Wang, Z.-Y., Yang, Y., and Zhao, L. (2017). Chiral plasmonic nanochains via the self-assembly of gold nanorods and helical glutathione oligomers facilitated by cetyltrimethylammonium bromide micelles. *ACS nano*, 11, 3463-3475.
- [193] Shikata, T., Hirata, H., and Kotaka, T. (1987). Micelle formation of detergent molecules in aqueous media: viscoelastic properties of aqueous cetyltrimethylammonium bromide solutions. *Langmuir*, 3, 1081-1086.
- [194] Fameau, A. L., Saint-Jalmes, A., Cousin, F., Houinsou Houssou, B., Novales, B., Navailles, L., Nallet, F., Gaillard, C., Boué, F., and Douliez, J. P. (2011). Smart foams: switching reversibly between ultrastable and unstable foams. *Angewandte Chemie International Edition*, 50, 8264-8269.
- [195] Borse, M. S., and Devi, S. (2006). Importance of head group polarity in controlling aggregation properties of cationic gemini surfactants. *Advances in colloid and interface science*, 123, 387-399.
- [196] Lim, J., Park, J.-m., Park, C. J., and Lee, B. M. (2013). Synthesis and surface active properties of a gemini-type surfactant linked by a quaternary ammonium group. *Colloid and Polymer Science*, 291, 855-866.
- [197] Wong, Y.-L., Hubieki, M. P., Curfman, C. L., Doncel, G. F., Dudding, T. C., Savle, P. S., and Gandour, R. D. (2002). A structure-activity study of spermicidal and anti-HIV properties of hydroxylated cationic surfactants. *Bioorganic & medicinal chemistry*, 10, 3599-3608.
- [198] Das, D., and Das, P. K. (2003). Improving the lipase activity profile in cationic water-in-oil microemulsions of hydroxylated surfactants. *Langmuir*, 19, 9114-9119.
- [199] Dasgupta, A., Das, P. K., Dias, R. S., Miguel, M. G., Lindman, B., Jadhav, V. M., Gnanamani, M., and Maiti, S. (2007). Effect of headgroup on DNA- cationic surfactant interactions. *The Journal of Physical Chemistry B*, 111, 8502-8508.
- [200] Bagshaw, S. A., and Hayman, A. R. (2001). Synthesis of novel super-microporous silicates by ω -hydroxy alkyl ammonium halide bolaform surfactant templating. *Microporous and mesoporous materials*, 44, 81-88.

- [201] Bagshaw, S. A., and Hayman, A. R. (2000). Novel super-microporous silicate templating by ω -hydroxyalkylammonium halide bolaform surfactants. *Chemical Communications*, 533-534.
- [202] Klinger, D., Wang, C. X., Connal, L. A., Audus, D. J., Jang, S. G., Kraemer, S., Killops, K. L., Fredrickson, G. H., Kramer, E. J., and Hawker, C. J. (2014). A Facile Synthesis of Dynamic, Shape-Changing Polymer Particles. *Angewandte Chemie International Edition*, 53, 7018-7022.
- [203] da Silva, M. G. A., Meneghetti, M. R., Denicourt-Nowicki, A., and Roucoux, A. (2013). New and tunable hydroxylated driving agents for the production of tailor-made gold nanorods. *RSC Advances*, 3, 18292-18295.
- [204] da Silva, M. G. A., Meneghetti, M. R., Denicourt-Nowicki, A., and Roucoux, A. (2014). Tunable hydroxylated surfactants: an efficient toolbox towards anisotropic gold nanoparticles. *RSC advances*, 4, 25875-25879.
- [205] Berchel, M., Le Gall, T., Haelters, J.-P., Lehn, P., Montier, T., and Jaffrès, P.-A. (2015). Cationic lipophosphoramidates containing a hydroxylated polar headgroup for improving gene delivery. *Molecular pharmaceuticals*, 12, 1902-1910.
- [206] Fischer, N. O., Verma, A., Goodman, C. M., Simard, J. M., and Rotello, V. M. (2003). Reversible “irreversible” inhibition of chymotrypsin using nanoparticle receptors. *Journal of the American Chemical Society*, 125, 13387-13391.
- [207] Jardak, K., Drogui, P., and Daghrir, R. (2016). Surfactants in aquatic and terrestrial environment: occurrence, behavior, and treatment processes. *Environmental Science and Pollution Research*, 23, 3195-3216.
- [208] Holder, S. J., Sriskantha, B. C., Bagshaw, S. A., and Bruce, I. J. (2012). Headgroup effects on the krafft temperatures and self-assembly of ω -hydroxy and ω -carboxy hexadecyl quaternary ammonium bromide bolaform amphiphiles: Micelles versus molecular clusters? *Journal of colloid and interface science*, 367, 293-304.
- [209] Davey, T. W., and Hayman, A. R. (1998). Synthesis of ω -hydroxy quaternary ammonium bolaform surfactants. *Australian journal of chemistry*, 51, 581-586.
- [210] Ortiz de Montellano, P. R. (2009). Hydrocarbon hydroxylation by cytochrome P450 enzymes. *Chemical reviews*, 110, 932-948.
- [211] Klingenberg, M. (1958). Pigments of rat liver microsomes. *Archives of biochemistry and biophysics*, 75, 376-386.
- [212] Omura, T., and Sato, R. (1964). The carbon monoxide-binding pigment of liver microsomes I. Evidence for its hemoprotein nature. *Journal of Biological Chemistry*, 239, 2370-2378.
- [213] U Nair, N., A Denard, C., and Zhao, H. (2010). Engineering of enzymes for selective catalysis. *Current Organic Chemistry*, 14, 1870-1882.
- [214] Meunier, B., De Visser, S. P., and Shaik, S. (2004). Mechanism of oxidation reactions catalyzed by cytochrome P450 enzymes. *Chemical reviews*, 104, 3947-3980.
- [215] Myllylä, R., Majamaa, K., Günzler, V., Hanauske-Abel, H., and Kivirikko, K. (1984). Ascorbate is consumed stoichiometrically in the uncoupled reactions catalyzed by prolyl 4-hydroxylase and lysyl hydroxylase. *Journal of Biological Chemistry*, 259, 5403-5405.
- [216] Boanca, G., Sand, A., and Barycki, J. J. (2006). Uncoupling the enzymatic and autoprocessing activities of *Helicobacter pylori* γ -glutamyltranspeptidase. *Journal of Biological Chemistry*, 281, 19029-19037.
- [217] Bernhardt, R. (2006). Cytochromes P450 as versatile biocatalysts. *Journal of biotechnology*, 124, 128-145.
- [218] Oliver, F. C., Modi, S., Prmrose, U. W., Lian, L.-Y., and Roberts, C. G. (1997). Engineering the substrate specificity of *Bacillus megaterium* cytochrome P-450

- BM3: hydroxylation of alkyl trimethylammonium compounds. *Biochemical Journal*, 327, 537-544.
- [219] Munro, A. W., Leys, D. G., McLean, K. J., Marshall, K. R., Ost, T. W., Daff, S., Miles, C. S., Chapman, S. K., Lysek, D. A., and Moser, C. C. (2002). P450 BM3: the very model of a modern flavocytochrome. *Trends in biochemical sciences*, 27, 250-257.
- [220] Li, Q.-S., Schwaneberg, U., Fischer, M., Schmitt, J., Pleiss, J., Lutz-Wahl, S., and Schmid, R. D. (2001). Rational evolution of a medium chain-specific cytochrome P-450 BM-3 variant. *Biochimica Et Biophysica Acta (BBA)-Protein Structure and Molecular Enzymology*, 1545, 114-121.
- [221] Meinhold, P., Peters, M. W., Hartwick, A., Hernandez, A. R., and Arnold, F. H. (2006). Engineering cytochrome P450 BM3 for terminal alkane hydroxylation. *Advanced Synthesis & Catalysis*, 348, 763-772.
- [222] Jang, H.-H., Shin, S.-M., Ma, S. H., Lee, G.-Y., Joung, Y. H., and Yun, C.-H. (2016). Role of Leu188 in the fatty acid hydroxylase activity of CYP102A1 from *Bacillus megaterium*. *Journal of Molecular Catalysis B: Enzymatic*, 133, 35-42.
- [223] Chen, M. M., Snow, C. D., Vizcarra, C. L., Mayo, S. L., and Arnold, F. H. (2012). Comparison of random mutagenesis and semi-rational designed libraries for improved cytochrome P450 BM3-catalyzed hydroxylation of small alkanes. *Protein Engineering, Design & Selection*, 25, 171-178.
- [224] Dennig, A., Marienhagen, J., Ruff, A. J., Guddat, L., and Schwaneberg, U. (2012). Directed Evolution of P 450 BM 3 into ap-Xylene Hydroxylase. *ChemCatChem*, 4, 771-773.
- [225] Li, Q.-S., Ogawa, J., and Shimizu, S. (2001). Critical role of the residue size at position 87 in H₂O₂-dependent substrate hydroxylation activity and H₂O₂ inactivation of cytochrome P450BM-3. *Biochemical and biophysical research communications*, 280, 1258-1261.
- [226] Graham-Lorence, S., Truan, G., Peterson, J. A., Falck, J. R., Wei, S., Helvig, C., and Capdevila, J. H. (1997). An active site substitution, F87V, converts cytochrome P450 BM-3 into a regio- and stereoselective (14S, 15R)-arachidonic acid epoxidase. *Journal of Biological Chemistry*, 272, 1127-1135.
- [227] Reetz, M. T., Bocola, M., Carballeira, J. D., Zha, D., and Vogel, A. (2005). Expanding the range of substrate acceptance of enzymes: combinatorial active-site saturation test. *Angewandte Chemie International Edition*, 44, 4192-4196.
- [228] Reetz, M. T., Wang, L. W., and Bocola, M. (2006). Directed evolution of enantioselective enzymes: iterative cycles of CASTing for probing protein-sequence space. *Angewandte Chemie International Edition*, 45, 1236-1241.
- [229] Dennig, A., Marienhagen, J., Ruff, A. J., and Schwaneberg, U. (2014) OmniChange: simultaneous site saturation of up to five codons, In *Directed Evolution Library Creation*, pp 139-149, Springer.
- [230] Shivange, A. V., Dennig, A., and Schwaneberg, U. (2014). Multi-site saturation by OmniChange yields a pH- and thermally improved phytase. *Journal of biotechnology*, 170, 68-72.
- [231] Dudek, H. M., Fink, M. J., Shivange, A. V., Dennig, A., Mihovilovic, M. D., Schwaneberg, U., and Fraaije, M. W. (2014). Extending the substrate scope of a Baeyer–Villiger monooxygenase by multiple-site mutagenesis. *Applied microbiology and biotechnology*, 98, 4009-4020.
- [232] Gutierrez, E. A., Mundhada, H., Meier, T., Duefel, H., Bocola, M., and Schwaneberg, U. (2013). Reengineered glucose oxidase for amperometric glucose determination in diabetes analytics. *Biosensors and Bioelectronics*, 50, 84-90.

- [233] Nazor, J., and Schwaneberg, U. (2006). Laboratory evolution of P450 BM3 for mediated electron transfer. *ChemBioChem*, 7, 638-644.
- [234] Denisov, I. G., Makris, T. M., Sligar, S. G., and Schlichting, I. (2005). Structure and chemistry of cytochrome P450. *Chemical reviews*, 105, 2253-2278.
- [235] Cirino, P. C., and Arnold, F. H. (2003). A self-sufficient peroxide-driven hydroxylation biocatalyst. *Angewandte Chemie International Edition*, 42, 3299-3301.
- [236] Zhou, M., Diwu, Z., Panchuk-Voloshina, N., and Haugland, R. P. (1997). A stable nonfluorescent derivative of resorufin for the fluorometric determination of trace hydrogen peroxide: applications in detecting the activity of phagocyte NADPH oxidase and other oxidases. *Analytical biochemistry*, 253, 162-168.
- [237] Fulmer, G. R., Miller, A. J., Sherden, N. H., Gottlieb, H. E., Nudelman, A., Stoltz, B. M., Bercaw, J. E., and Goldberg, K. I. (2010). NMR chemical shifts of trace impurities: common laboratory solvents, organics, and gases in deuterated solvents relevant to the organometallic chemist. *Organometallics*, 29, 2176-2179.
- [238] Schwaneberg, U., Sprauer, A., Schmidt-Dannert, C., and Schmid, R. (1999). P450 monooxygenase in biotechnology: I. Single-step, large-scale purification method for cytochrome P450 BM-3 by anion-exchange chromatography. *Journal of Chromatography A*, 848, 149-159.
- [239] Ost, T. W., Miles, C. S., Murdoch, J., Cheung, Y.-F., Reid, G. A., Chapman, S. K., and Munro, A. W. (2000). Rational re-design of the substrate binding site of flavocytochrome P450 BM3. *FEBS letters*, 486, 173-177.
- [240] Dubey, K. D., Wang, B., and Shaik, S. (2016). Molecular dynamics and QM/MM calculations predict the substrate-induced gating of cytochrome P450 BM3 and the regio- and stereoselectivity of fatty acid hydroxylation. *Journal of the American Chemical Society*, 138, 837-845.
- [241] Ray, G. B., Chakraborty, I., Ghosh, S., Moulik, S., and Palepu, R. (2005). Self-aggregation of alkyltrimethylammonium bromides (C₁₀-, C₁₂-, C₁₄-, and C₁₆TAB) and their binary mixtures in aqueous medium: a critical and comprehensive assessment of interfacial behavior and bulk properties with reference to two types of micelle formation. *Langmuir*, 21, 10958-10967.
- [242] Bahri, M. A., Hoebeke, M., Grammenos, A., Delanaye, L., Vandewalle, N., and Seret, A. (2006). Investigation of SDS, DTAB and CTAB micelle microviscosities by electron spin resonance. *Colloids and Surfaces A: Physicochemical and Engineering Aspects*, 290, 206-212.
- [243] Udit, A. K., Hagen, K. D., Goldman, P. J., Star, A., Gillan, J. M., Gray, H. B., and Hill, M. G. (2006). Spectroscopy and electrochemistry of cytochrome P450 BM3-surfactant film assemblies. *Journal of the American Chemical Society*, 128, 10320-10325.
- [244] Neufeld, K., Marienhagen, J., Schwaneberg, U., and Pietruszka, J. (2013). Benzylic hydroxylation of aromatic compounds by P450 BM3. *Green Chemistry*, 15, 2408-2421.
- [245] Sang, T. J., Lauchli, R., and Arnold, F. H. (2011). Cytochrome P450: taming a wild type enzyme. *Current opinion in biotechnology*, 22, 809-817.
- [246] Fasan, R., Chen, M. M., Crook, N. C., and Arnold, F. H. (2007). Engineered alkane-hydroxylating cytochrome P450BM3 exhibiting natively-like catalytic properties. *Angewandte Chemie International Edition*, 46, 8414-8418.

7 Declaration / Eidesstattliche Erklärung

Yu Ji

erklärt hiermit, dass diese Dissertation und die darin dargelegten Inhalte die eigenen sind und selbstständig, als Ergebnis der eigenen originären Forschung, generiert wurden.

Hiermit erkläre ich an Eides statt

1. Diese Arbeit wurde vollständig oder größtenteils in der Phase als Doktorand dieser Fakultät und Universität angefertigt;
2. Sofern irgendein Bestandteil dieser Dissertation zuvor für einen akademischen Abschluss oder eine andere Qualifikation an dieser oder einer anderen Institution verwendet wurde, wurde dies klar angezeigt;
3. Wenn immer andere eigene- oder Veröffentlichungen Dritter herangezogen wurden, wurden diese klar benannt;
4. Wenn aus anderen eigenen- oder Veröffentlichungen Dritter zitiert wurde, wurde stets die Quelle hierfür angegeben. Diese Dissertation ist vollständig meine eigene Arbeit, mit der Ausnahme solcher Zitate;
5. Alle wesentlichen Quellen von Unterstützung wurden benannt;
6. Wenn immer ein Teil dieser Dissertation auf der Zusammenarbeit mit anderen basiert, wurde von mir klar gekennzeichnet, was von anderen und was von mir selbst erarbeitet wurde;
7. Ein Teil oder Teile dieser Arbeit wurden zuvor veröffentlicht und zwar in:
Ji, Y., Mertens, A. M., Gertler, C., Fekiri, S., Keser, M., Sauer, D. F., Kilian E. C. Smith, Schwaneberg, U. (2018). Directed OmniChange evolution converts P450 BM3 into an alkyltrimethylammonium hydroxylase. *Chemistry–A European Journal*, 24(63), 16865-16872.
Ji, Y., Islam, S., Mertens, A. M., Sauer, D. F., Dhoke, G. V., Jakob, F., Schwaneberg, U. (2019). Directed aryl sulfotransferase evolution toward improved sulfation stoichiometry on the example of catechols. *Applied microbiology and biotechnology*, 103(9), 3761-3771.
Der geleistete Eigenanteil ist im Abschnitt „Author contributions“ aufgeführt.

Yu Ji

Aachen, 16. January, 2020

8 Author contributions

Ji, Y., Mertens, A. M., Gertler, C., Fekiri, S., Keser, M., Sauer, D. F., Smith, K. E. C., Schwaneberg, U. (2018). Directed OmniChange evolution converts P450 BM3 into an alkyltrimethylammonium hydroxylase. *Chemistry-A European Journal*, 24(63), 16865-16872.

Manuscript preparation and writing were performed by Yu Ji. Yu Ji performed OmniChange library generation, screening assay optimization, library screening, protein purification, hydroxylation reactions, and LC-MS analysis. Merve Keser contributed to library screening. Sallama Fekiri contributed to P450 BM3 variant's purification and hydroxylation reactions. Dr. Kilian Smith (Institute for Environmental Research, RWTH Aachen University) contributed to LC-MS/MS method development. The experimental part of NMR analysis was performed by Dr. Daniel Sauer (Institute of Biotechnology, RWTH Aachen University). Prof. Dr. Ulrich Schwaneberg (Institute of Biotechnology, RWTH Aachen University) and Dr. Alan Mertens (Institute of Biotechnology, RWTH Aachen University) gave advice to the project, participated in the experiment design and manuscript revision. Dr. Christoph Gertler (Institute of Biotechnology, RWTH Aachen University) contributed to manuscript revision.

Ji, Y., Islam, S., Mertens, A. M., Sauer, D. F., Dhoke, G. V., Jakob, F., Schwaneberg, U. (2019). Directed aryl sulfotransferase evolution toward improved sulfation stoichiometry on the example of catechols. *Applied microbiology and biotechnology*, 103(9), 3761-3771.

Manuscript preparation and writing were performed by Yu Ji. The two-step *p*-NPS-4AAP screening system development, library screening, protein purification, and sulfation product detection was performed by Yu Ji. Dr. Shohana Islam (Institute of Biotechnology, RWTH Aachen University) contributed to SeSaM library generation and manuscript revision. The experimental part of NMR analysis was performed by Dr. Daniel Sauer (Institute of Biotechnology, RWTH Aachen University). The sulfotransferase structure analysis was done by Dr. Gaurao Dhoke (Institute of Biotechnology, RWTH Aachen University). Prof. Dr. Ulrich Schwaneberg (Institute of Biotechnology, RWTH Aachen University) and Dr. Alan Mertens (Institute of Biotechnology, RWTH Aachen University) gave advice to the project, participated in the experiment design and manuscript revision.

Ji, Y., Islam, S., Cui, H., Dhoke, G. V., Davari, M. D., Mertens, A. M., Schwaneberg, U. (2020). Loop engineering of aryl sulfotransferase B for improving catalytic performance in regioselective sulfation. *Catalysis Science & Technology*, 10, 2369-2377.

Manuscript preparation and writing were performed by Yu Ji. The OmniChange library generation, screening, protein purification, and sulfation product detection was performed by Yu Ji.

Dr. Shohana Islam (Institute of Biotechnology, RWTH Aachen University) contributed to SeSaM library generation and manuscript revision. Protein structure analysis, docking study was done by Haiyang Cui, Dr. Gaurao Dhoke, and Dr. Mehdi Davari (Institute of Biotechnology, RWTH Aachen University). Prof. Dr. Ulrich Schwaneberg (Institute of Biotechnology, RWTH Aachen University) and Dr. Alan Mertens (Institute of Biotechnology, RWTH Aachen University) gave advice to the project, participated in the experiment design and manuscript revision.

Pan, J., Ji, Y., Du, Z., Zhang, J. (2016). Rapid characterization of commercial polysorbate 80 by ultra-high performance supercritical fluid chromatography combined with quadrupole time-of-flight mass spectrometry. *Journal of Chromatography A*, 1465, 190-196.

Yu Ji contributed to the UPC²-MS method development and composition analysis for 3 batches of commercial polysorbate 80. Jinheng Pan (College of Science, Beijing University of Chemical Technology) contributed to the further composition analysis and manuscript writing. Prof. Dr. Zhenxia Du (College of Science, Beijing University of Chemical Technology) and Prof. Dr. Jianwen Zhang (Institute of Fluid Flow and Heat Transfer and IGCIT, Beijing University of Chemical Technology) gave advice to the project, participated in the experiment design and manuscript revision.

Wu, X. #, Lin, Y. #, Ji, Y., Zhou, D., Liu, Z., Sun, X. (2020). Insights into the Catalytic Mechanism of Fe-doped LiCoPO₄ for oxygen evolution reaction. *ACS Applied Energy Materials*, 3, 2959-2965. (#shared first authorship).

The manuscript preparation and writing was done by Xiaochao Wu (College of Science, Beijing University of Chemical Technology) and Yangmin Lin (Max-Planck-Institut für Chemische Energiekonversion). This work focuses on the development of a series of Fe-doped LiCoPO₄ materials for oxygen evolution reaction. Yu Ji contributed to the analysis of solution composition by high performance liquid chromatography. Xiaochao Wu contributed to the synthesis and characterization of Fe-doped LiCoPO₄ materials. Yangming Lin and Daojin Zhou (College of Science, Beijing University of Chemical Technology) contributed to the electrochemical measurements in aqueous solution. Prof. Dr. Xiaoming Sun (College of Science, Beijing University of Chemical Technology) and Dr. Zigeng Liu (Department Max-Planck-Institut für Chemische Energiekonversion) gave advice to the project, participated in the experiment design and manuscript revision.

9 Acknowledgement

First of all, I would like to express my sincere gratitude to Prof. Dr. Ulrich Schwaneberg who offered me the opportunity to do research as a PhD student in Germany. He is like a doctor father that encourages me to be confident and always supervises me patiently with giving precious suggestions on my work in the last four years. He is the first person helps me correcting my paper word by word and his attitude to science influenced me deeply. Thanks for his trust that I can have the opportunity to explore more fields of biotechnology.

Besides my supervisor, I would like to appreciate Prof. Dr. Lothar Elling for being my second examiner and taking his valuable time on attending my PhD proposal defense, reading this thesis and giving valuable comments.

In the beginning hard time, without any knowledge of molecular biology, Dr. Alan Mertens, as my direct supervisor, spent lots of time explaining me fundamental knowledge and detailed experiment operation. Dear Alan, I greatly appreciate your guidance and support! Without your help, I cannot finish P450 work smoothly. I also want to thank Stephi Mertens who supervised me in the lab at the very beginning. Thanks to my bachelor student Merve and my master students Sallama and Alex for their hard-working and creative-thinking. I would like to thank Dr. Shohana Islam for her continuous support on ASTB project, paper writing, and thesis correction. Dear Shohana, you set a good model for me to do everything with high quality. I thank Dr. Kilian E. C. Smith and David Kämpfer for helping me with the MS measurement and Dr. Daniel Sauer for NMR support.

I acknowledge CSC scholarship for supporting my living in Germany during my PhD time.

Thanks to my sisters and brothers in the biotechnology institute: Dr. Leilei Zhu, Dr. Feng Cheng, Dr. Jianhua Yang, Wei Long, Dr. Zhanzhi Liu, Dr. Lingling Zhang, Dr. Zhi Zou, Haiyang Cui, Lilin Feng, Liang Gao, Yi Lu, Shuaiqi Meng. I enjoyed the happy lunch times with you and all the festival dinner together.

In addition, I want to thank all the coworkers in Schwaneberg group.

Thanks to my father Zhenggui Ji and mother Shouqin Shi for their endless love. They treasure me a lot and always relieve my pressure and encourage me. I am so lucky to be born in such a harmonious family. At last, thanks to beloved my husband Xiaochao Wu

who always stands behind me and accompanies me in the last eight years. I am so lucky to have him in my life. Without you, I cannot finish my PhD.

I cannot remember how many days I worked until midnight and I cannot remember how many nights I was anxious and hardly got asleep. In the last four years, I finished two projects and published three first-author papers. I was involved in three proposal writing, practical course teaching, and exam supervision. I want to thank myself for the courage of cross-major PhD study in a foreign country and hard-working to overcome all the difficulties. I survived and matured.

10 Curriculum vitae

Personal data

Name	Yu Ji
Gender	Female
Date of birth	2 nd June, 1991
Place of birth	Jiangsu, China
Nationality	Chinese

Education

2015.10 – Present	Ph.D. fellow in Biotechnology, RWTH Aachen University, Aachen, Germany
2012.09 – 2015.06	Master of Science in Chemistry, Beijing University of Chemical Technology (BUCT), Beijing, China
2008.09 – 2012.06	Bachelor of Science in Applied Chemistry, Beijing University of Chemical Technology (BUCT), Beijing, China
2002.09 – 2008.06	Hanjiang High School of Jiangsu Province (HJZX), Yangzhou, Jiangsu, China